FACULTEIT GENEESKUNDE EN GEZONDHEIDSWETENSCHAPPEN

Investigation of novel treatment methods to overcome early embryonic developmental arrest due to *PADI6* mutations

Silke De Norre
Student number: 01709117

Promotor: Prof. Dr. Björn Heindryckx
Co-Promotor/Mentor: Dr. ir. Annekatrien Boel

Ghent-Fertility And Stem cell Team (G-FaST), Department for Reproductive Medicine, Ghent University Hospital, Corneel Heymanslaan 10, 9000 Ghent, Belgium

A dissertation submitted to Ghent University in partial fulfilment of the requirements for the degree of Master of Science in the Biomedical Sciences

Academic year: 2021-2022

UNIVERSITEIT GENT

Preface

Five years of university teaches you a lot of new things. It challenges you to become the best version of yourself, but it is not all sunshine and rainbows. University also gives you many frustrations and meltdowns. Luckily, a lot of people were always there to help me out and to support me to achieve the bigger goals.

I would like to thank my promotor, Prof. Björn Heindryckx, for the opportunity to work on this interesting topic.

The G-FaST group as a whole also deserves a special thanks. Thank you for always being supportive and always wanting to help where needed, even though they had a lot of work their selves. The salsa nights with or without a drink I won't forget soon.

A special thanks to the person who made it possible for me to write this thesis, Dr. ir. Annekatrien Boel. Thank you for the guidance throughout these past two years, for learning me the different techniques, reading and providing feedback on my dissertation and answering my many questions.

Lasty, I want to thank all my friends and family who accompanied and supported me, but also kept the student life going during these wonderful five years. To the students who worked in the same lab, enormous thank you for all your support, ideas and proof reading of my thesis. Now this chapter can be closed, I wish you all the best writing your new ones.

Table of abbreviations

A	
A	Adenosine
Ab	Antibody
$ADAR_2$	Adenosine Deaminase Acting on RNA
$ADAR_{2DD}$	$ADAR_2$ Deaminase Domain
Ala	Alanine
AMP	Ampicillin
AOA	Assisted Oocyte Activation
aPKC	Atypical PKC
Arg	Arginine
ART	Assisted Reproductive Technology
Asn	Asparagine
B	
bp	Base pairs
BSA	Bovine Serum Albumin
BWS	Beckwith-Wiedemann Syndrome
C	
C	Cytidine
Ca^{2+}	Calcium
cDNA	Complementary DNA
Cit	Citrulline
COC	Cumulus Oocyte Complex
CPL	Cytoplasmatic Lattice
cRNA	Complementary RNA
crRNA	CRISPR RNA
Cys	Cysteine
D	
dCas13	Dead Cas13
ddH_2O	Distillated water
ddNTPs	Dideoxynucleotide triphosphates
DEL	Deletion
DMSO	Dimethyl sulfoxide
DNA	Deoxyribonucleic Acid
dNTPs	Deoxyribonucleotide triphosphate
dsDNA	Double-stranded DNA
DSB	Double-Strand Break
E	
E	Embryonic day
EB	Elution Buffer
EDA	Embryo Developmental Arrest
EGA	Embryonic Genome Activation
EPI	Epiblast
ET	Embryo Transfer
G	
G	Guanosine
Gln	Glutamine
Gly	Glycine
gRNA	Guide RNA
GV	Germinal Vesical
H	
hCG	human Chorionic Gonadotrophin
His	Histidine

HM	Hydatidiform Moles
HDR	Homologous directed recombination
H&E	Hematoxylin and eosin

I

I	Inosine
ICM	Inner Cell Mass
ICSI	Intracytoplasmic Sperm Injection
IDT	Integrated DNA Technologies
Ile	Isoleucine
INS	Insertion
IUI	Intra Uterine Insemination
IVF	*In Vitro* Fertilization
IVT	*In Vitro* Transcription

K

KAN	Kanamycin
kb	Kilobase
KO	Knock-Out
KLD	Kinase-Ligase-DpnI

L

LB	Lysogeny Broth
LR-PCR	Long Range PCR

M

MII	Metaphase II
MEG	Maternal Effect Gene
MET	Maternal-to-embryonic
mNEST	Non-Surgical Embryo Transfer device for mice
mRNA	Messenger RNA
MT	Microtubules
MZT	Maternal to Zygote Transition

N

N3	Neutralization buffer
NEB	New England Biolabs
NGS	Next Generation Sequencing
NHEJ	Nonhomologous End-Joining
nt	Nucleotide

P

P1	Resuspension buffer
P2	Lyse buffer
PAD	Peptidylarginine deiminase
PAM	Protospacer Adjacent Motif
PARD3	Par-3 Family Cell Polarity Regulator
PARD6B	Par-6 Family Cell Polarity Regulator Beta
PB	Washing buffer
PBS	Phosphate Buffer Saline
PBT	PBS with a low-concentration of Triton™
PCR	Polymerase Chain Reaction
PE (Embryo)	Primitive Endoderm
PE (DNA extraction)	Purification buffer containing Ethanol
PFA	Paraformaldehyde
PLK	Polo-like Kinase
PMSG	Pregnant Mare’s Serum Gonadotrophin
Pro	Proline

Q

QG	Binding buffer

R

REPAIR	RNA Editing for Programmable A to I Replacement
RNA	Ribonucleic Acid
RNP	Ribonucleoprotein
RT	Room Temperature

S

SCMC	Subcortical Maternal Complex
Ser	Serine
SOC	Super Optimal broth with Catabolite repression
ssDNA	Single-stranded DNA

T

T	Thymine
TAE	Tris-acetate-EDTA
TALENs	Transcription Activator-Like Effectors
TE	Trophectoderm
TF	Transcription Factor
Thr	Threonine
tracrRNA	Transactivating crRNA

W

WT	Wild-Type

Z

ZNF	Zinc Finger

Table of contents

1. Summary

Embryo Developmental Arrest (EDA) is an infertility phenotype, characterized by developmental arrest during the early cleavage stages or lower blastocyst formation rates. Defects in a number of maternal genes have been associated with EDA, one of them being *PADI6*. Besides oocyte donation, treatment options for these patients are limited. Therefore, we aimed to develop a relevant mouse model, harboring a disease-causing *Padi6* point mutation, to compare three future strategies to restore PADI6 function: nuclear transfer for defective ooplasm replacement, CRISPR/Cas13 mRNA base editing to correct the defective *Padi6* mRNA and *Padi6* complementary RNA (cRNA) injection, to complement defective *Padi6* mRNA.

The generation of the relevant mouse model consisted of electroporation-mediated delivery of CRISPR/Cas9 components into mouse zygotes, after which good quality blastocysts were transferred to pseudo-pregnant female mice. The resulting offspring was genotyped by next-generation sequencing. Only *Padi6* knock-out mice were encountered to date, which were selected for further breeding and exploratory phenotyping, which included zygote collection and embryonic developmental assessment, immunostaining and histology. From these preliminary data, it was shown that both fertilization and the first cleavages were compromised. Next, ready-to-use cRNA was already prepared by ligating *Padi6* cDNA into an expression vector, followed by its *in vitro* transcription.

In conclusion, additional electroporation and embryo transfer attempts should be undertaken to obtain a mouse model with the desired point mutation, however both cRNA administration and nuclear transfer can already be evaluated in the currently produced *Padi6* knock out model.

2. Societal impact

PADI6 mRNA transcripts are exclusively expressed in oocytes and early embryos, making them responsible for the first cleavage stages of development. When mutations in *PADI6* occur, embryo arrest takes place during the early developmental stages, usually before the onset of embryo genome activation. Since treatment options for EDA are rather limited, most of these patients have to seek oocyte donation to fulfill their child wish. As a lot of people want to obtain a genetically related child, other possible treatment options are being investigated. During this research, three potential future treatment options to overcome EDA will be assessed, making use of a *Padi6* mouse model.

Once one or more of these methods are proven to be efficient and safe by evaluation in a mouse model, they will be further validated in subfertile human couples diagnosed with EDA, in a preclinical research setting.

3. Introduction

3.1. Embryonic development

3.1.1. Preimplantation embryo

The preimplantation embryonic development is made up of several stages: fertilization, cell cleavage, morula development and blastocyst formation. The late blastocyst will later implant in the uterine wall[1,2].

Preimplantation development starts with fertilization, which is an essential step in the whole reproducibility process[3]. Fertilization is a complex process, which is believed to be conserved across mammalian species, and consists of different steps to make the emergence of a zygote happen **(Figure 1)**.

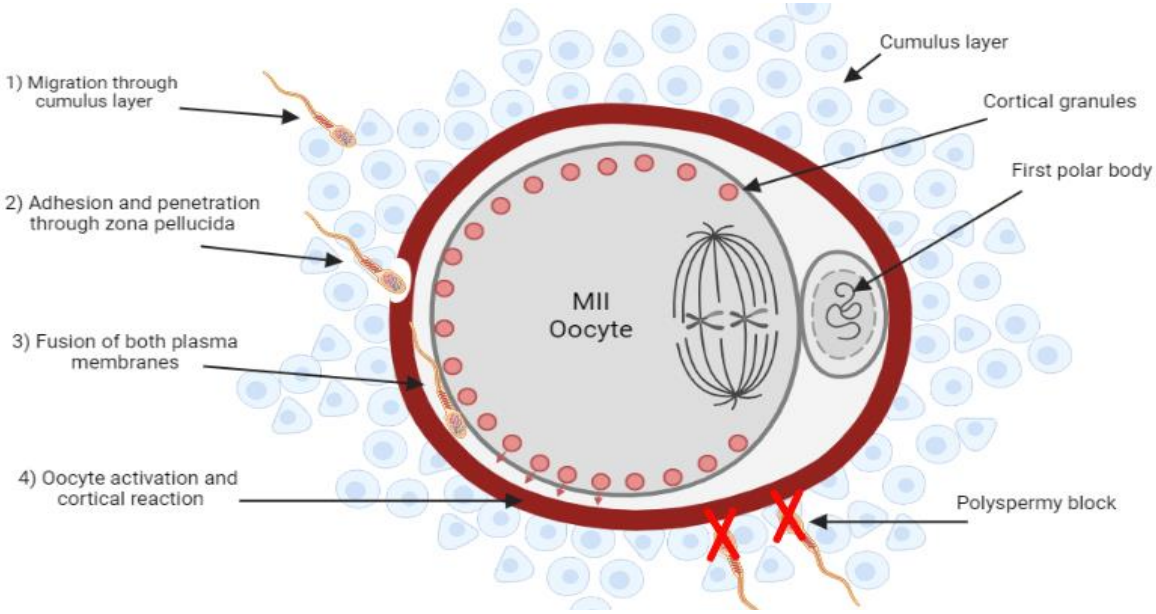

***Figure 1**: Graphical overview of the four big steps during the fertilization process: 1) migration of the spermatozoa through the cumulus layer, 2) adhesion and penetration through the zona pellucida, 3) fusion of the oocyte's and spermatozoa's plasma membrane and 4) oocyte activation and cortical reaction. The fifth step, fusion of the male and female pronuclei, is not shown in this figure.*

First, migration of a spermatozoon through the cumulus layer, which is the protective layer surrounding the haploid matured oocyte, is possible due to a hyaluronic reaction[4]. Due to the presence of a hyaluronic enzyme on the sperm cell and its mechanical function, digestion of the protective layer can take place. Once the sperm has passed the first barrier, it needs to adhere and penetrate through the second surrounding layer, the zona pellucida[3–8]. Attachment and penetration through the zona pellucida is mediated by the incorporated glycoproteins and the sperms acrosome reaction. Next, fusion of the oocyte's and spermatozoon's plasma membranes takes place, followed by oocyte activation, during which the arrested MII oocyte resumes meiosis, and polyspermy block[9]. The fertilization process ends with fusion of the male and female pronucleus. In this way a diploid and totipotent zygote is formed.

Following fertilization, mitotic cleavages in the embryo take place[10]**(Figure 2)**. These symmetrical cleavages divide the zygote into more and progressively smaller cells, called blastomeres, without causing any change in its overall volume. Once the embryo consists out of eight to sixteen cells, which is at embryonic day (E) 3.5 in human embryos and E2.5 in mouse embryos, it undergoes compaction. This process is characterized by flattening of the blastomeres and the increased occurrence of tight junctions, which causes more cell adhesion. At the end of this process the morula is formed. Concurrent with compaction, polarization takes place, causing the formation of an apical-basal axis. Moreover, polarization is possible due to the localization of different elements inside the blastomeres. For example the nucleus, cell adhesion structures and acetylated microtubes are located at the basal side, whereas actin

filaments, microtubes and microvilli can be found apically. Molecularly, two systems lay at the basis of the polarization process; the Par-aPCK system, containing Par-6 Family Cell Polarity Regulator Beta (PARD6B), Par-3 Family Cell Polarity Regulator (PARD3) and atypical PKC (aPKC), and the Par1. The Par-aPCK system coordinates the formation of the apical domain, and the Par1 is responsible for the assembly of the basolateral domain.

Also at the eight to sixteen cell stage, the first lineage segregation takes place, blastomeres become part of the inner cell mass (ICM) or the trophectoderm (TE)[11]. Together with a cavitation by fluid accumulation, this decision is leading to the formation of the early blastocyst, at E3.5 in mice and E5 in human. The internally positioned blastomeres are forming the ICM, whereas the external cells surrounding the blastocoel cavity become the TE **(Figure 2)**. While the ICM cells contain a pluripotent character, mainly forming all fetal tissues, the cells from the TE play an important role in the implantation process and contribute to the fetal part of the placenta.

At E4.5 in mice and E6 in humans, just before the blastocyst implants in the uterine wall, the second cell fate decision or lineage segregation takes place, this time only occurring in the ICM[10,11]. The ICM changes to a two-layered structure, existing out of a primitive endoderm (PE) and an epiblast (EPI). These two layers later form the yolk sac and the embryo proper, respectively **(Figure 2)**. This time, the cell fate decision is provoked by the timing of blastomere internalization. Cells becoming the EPI are most likely internalized during the first round of division and those internalizing in the second round will become part of the PE. Further in the process, the two-layered structure becomes a three-layered structure, consisting of the ectoderm, endoderm and the mesoderm in between. At E5 and E7 of the developmental process in respectively mouse and human, the blastocyst hatches, meaning the embryo is released from the zona pellucida. Without hatching, implantation of the embryo cannot take place, which is required for further proper embryonic development.

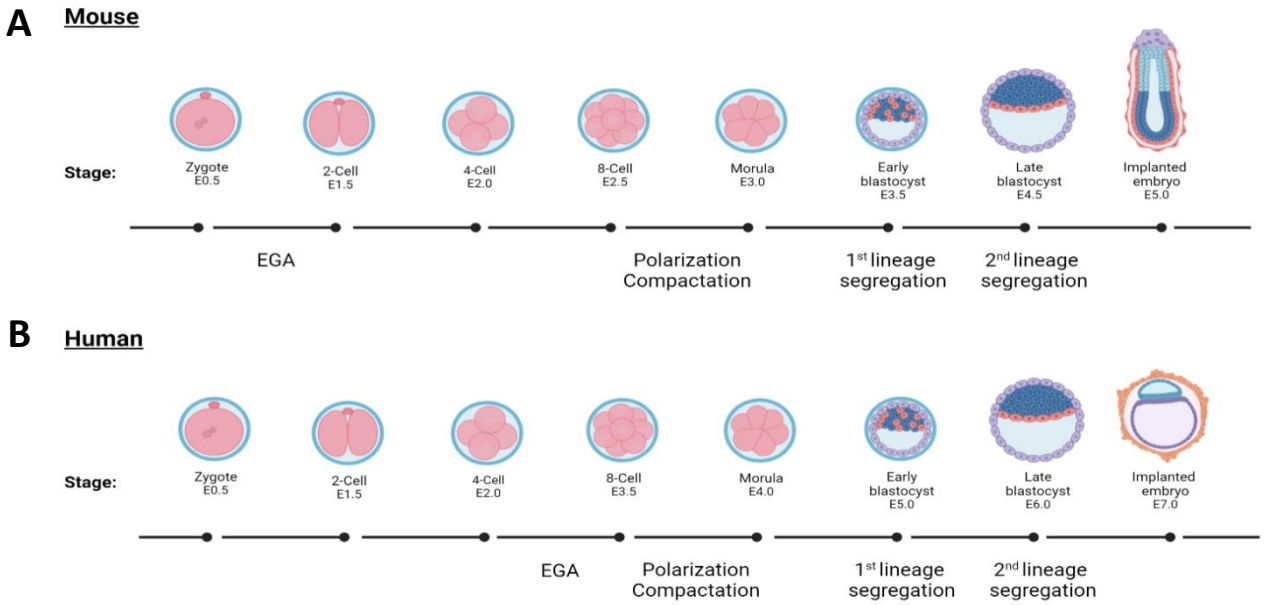

***Figure 2**: Overview of the embryonic developmental process from zygote formation to implantation in mouse (A) and human (B).*

3.2. Subfertility

Subfertility can be defined as a prolonged time of unwanted non-conception. There is a worldwide subfertility rate of 10 to 15 percent[12]. Subfertility can be caused by male or female factors or even a combination of them. This can occur due to a variety of reasons such as damage of the reproductive organs, genetic defects, health problems, overexposure to certain environmental factors, structural problems, etc.

To help patients with fertility problems, assisted reproductive technology (ART) procedures have been applied with increasing success during the past years. The used techniques in the clinic are ovulation induction together with timed coitus, intra-uterine insemination (IUI), *in vitro* fertilization (IVF) and the most commonly applied technique is intracytoplasmic sperm injection (ICSI), first introduced in 1992[13]. During this procedure, a single sperm is injected into the cytoplasm of an oocyte. The procedure consists out of different steps: stimulation of the ovaries, followed by collection of the oocytes (egg retrieval), next the matured oocytes are injected with a sperm cell into the cytoplasm and the resulting embryos are cultured *in vitro* until the blastocyst stage, after which good quality embryos are transferred back to the patient or cryopreserved.

3.2.1. Embryo Arrest

The ICSI technique has an overall good success rate, showing high fertilization rates, however for some patients, no high-quality blastocysts can be obtained. Ten percent of human embryos generated by IVF or ICSI arrests during the early cleavages[14]. On top of this, 40% of these patients have at least one arrested embryo per treatment cycle. These two findings indicate that embryo developmental arrest (EDA) is a common phenomenon in humans. When EDA recurrently takes place for the same individual, it is seen that the embryos generally stop developing before or at the onset of embryonic genome activation (EGA), which takes place between the second and third day in human, when the embryo consists out of four to eight cells, and around the two-cell stage in mice. Since the embryo's survival shortly after the fertilization is completely dependent on the maternal factors already present in the zygote, the cause of recurrent EDA is therefore believed to be mainly maternally related[10,15].

3.2.1.1. Genetic developmental phases

The first stages of embryo development are fully controlled by the maternal transcriptome[10,16]. During oocyte growth, maternal macromolecules (messenger RNA (mRNA) and proteins) are formed and deposited in the ooplasm. These factors stay present and active until the embryonic genome is activated, between the one- and two-cell stage in mice and between the four- and eight-cell stage in humans. The maternal factors are responsible for three major actions. Firstly, combining the paternal and maternal DNA to from the genome of the embryo, meaning that the maternal as well as the paternal genomic contributions are reprogrammed. Directly after fertilization, histones coming from the mother replace the paternal protamines, extensively erasing almost all DNA methylation from the father. Secondly, the degradation of the maternal proteins and RNA, and lastly, transcription activation of the embryonic genome. This embryonic genome activation does not only change gene expression, but also the metabolism; meaning a more active metabolism occurs due to the high energy demand of the further developmental stages (a more rapid cell division, blastocyst stage formation and the mass increasement of the embryo).

The different maternal factors present in the oocyte are transcribed from the so-called maternal effect genes (MEGs). These encoded maternal factors are RNA, proteins, subcellular organelles and macromolecules [16,17]. A group of these MEGs contributes to the formation of a multi-protein complex, the subcortical maternal complex (SCMC), consisting of the following protein members: KHDC3 (or FILIA), NLRP2, NLRP5 (or MATER), NLRP7, TLE6, OOEP (or FLOPED) and PADI6. However, not all components are identified yet (**Figure 3**). In both mice and humans, the complex is situated in the subcortex of the oocyte and the embryo. Important is that the ICM is completely free of the complex, due to the fact that the SCMC is only segregated in the outer cells of the morula and blastocyst. The exact function of the complex has not been fully unraveled yet. However, valuable information on its functionality has been already obtained in mouse, employing knock-out models. In mouse, it has been shown that a knockout of different SCMC members results in embryos that are not able to develop beyond the first cleavage stage. Lately, by identifying causal mutations in a number of these genes in

patients showing embryo developmental arrest, their importance in embryo development has also been confirmed in human.

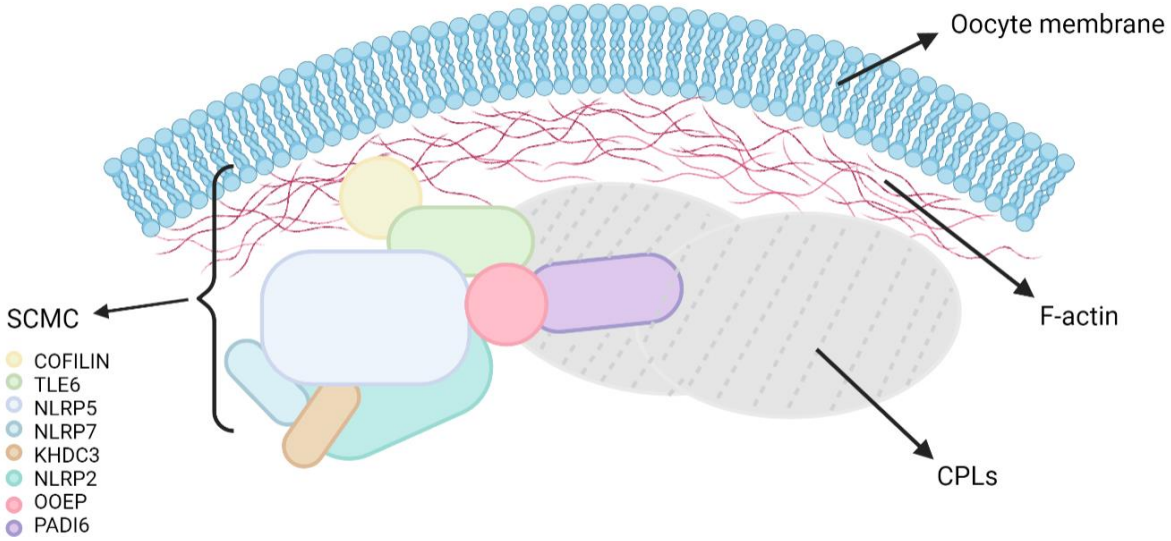

***Figure 3**: Schematic representation of the SCMC localized in the subcortical region of the oocyte. SCMS: subcortical maternal complex, CPLs: cytoplasmatic lattices, F-actin: Filamentous actin. The function of the different SCMC components: . Figure adapted from Bebbere et al (2016)*[16].

Multiple functions important for embryonic development have been linked to the SCMC [16,18]. The complex shows involvement in events taking place during the oocyte maturation, as well as in events after the fertilization. The complex does not only have a structural function, but is also involved in the redistribution of the mitochondria during maturation and after fertilization. A proper mitochondrial localization is important for the signaling events which are associated with fertilization or developmental competence. Furthermore, the SCMC participates in epigenetic reprogramming following fertilization. Accordingly, loss-of-function mutations in the genes of the SCMC result in an arrest at the two- to four-cell stage in humans and the one-cell stage in mice, at onset of the maternal-to-embryonic transition (MET)[19].

A SCMC specific gene, *TLE6*, controls the meiotic spindle formation and migration by mediating the cytoplasmic F-actin[16,18]. Furthermore, the *NLRP5* and *KHDC3L* genes mediate the epigenetic reprogramming after fertilization. A mutation in these genes will therefore be associated with imprinting disturbance. In addition, due to the fact that the *NLRP2* and *NLRP7* genes fulfill the function of reprogramming imprints in the maternal germline, mutations in these genes cause a demethylation of the maternal pronucleus leading to imprinting disorders and even biparental hydatidiform moles [20,21]. The last SCMC member, PADI6, is responsible for the post-translational modifications important for further embryo development. Therefore, *PADI6*-mutations lead to developmental arrest during the early cleavage stages. As *PADI6* is the subject of this thesis, it will be discussed further in section 3.2.2. Not only the appearance of mutations in the genes of the SCMC members, but also the other MEGs can hamper proper embryonic development in different ways. For instance, *TUBB8* is a gene encoding for a special β-tubulin isotype, which is the major structural component of the meiotic spindle and is important for the cytoskeletal function[22,23]. This function plays an important role in the completion of the meiosis after fertilization and the following first cleavages. So, loss-of-function mutation in TUBB8 lead to spindle-assembly defects during maturation and fertilization occur and arrest of the embryo follows. Furthermore, the product expressed form the *PLK4* gene controls the assembly of the daughter centriole. Problems with this product lead to alterations of its formation or even to duplication of the centriole[24].

Not only disruptions in the MEGs, and SCMC genes specifically, can lead to developmental arrest, but also problems in all other genes responsible for the pre-implantation development. Dysfunction of *NOP2*, a gene important for the first lineage specification program, causes an arrest during the transition from morula to blastocyst[25]. Furthermore, the dysfunction of *NOC4L* can also cause an arrest at this transition[26]. Expression of the gene inhibits apoptosis and promotes proliferation at the morula stage resulting in embryonic growth. In addition, problems with EGA obviously lead to a block of embryonic development, as this is a crucial step during embryogenesis. Furthermore, a lack of E-cadherin and α-catenin causes arrest at the blastocyst stage, these elements are important during the morula stage[10]. Problems occurring in other stage-specific genes **(figure 4)** can also result in arrest of the embryo. All of these are possible causes of the EDA phenomenon.

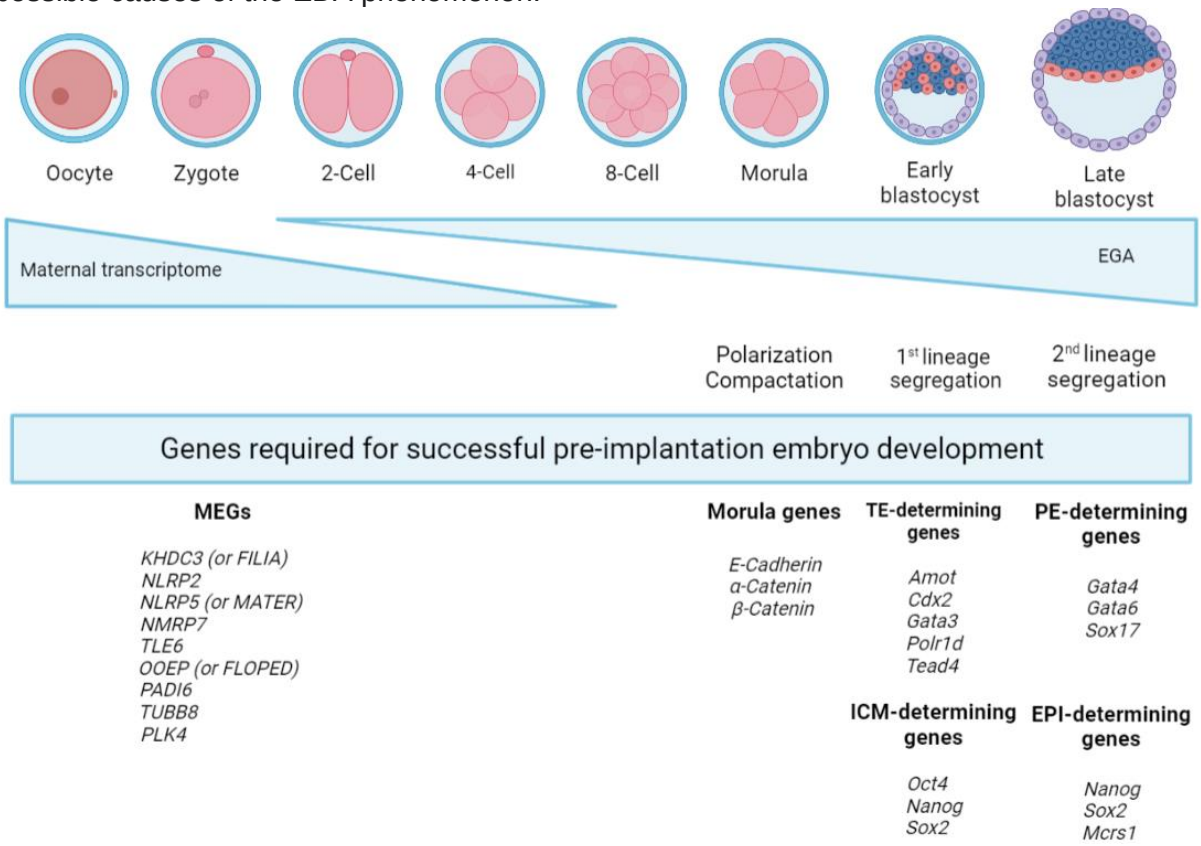

***Figure 4**: Genes required for successful pre-implantation embryo development in the mice. MEGs responsible for the first developmental stages, morula and first and second lineage specific genes are listed under the different developmental stages. Figure adapted from* [10].

3.2.2. PADI6

3.2.2.1. Expression and function

In this project the focus lies on the *PADI6* gene, a member of the SCMC. In human, this gene is located on chromosome 1:17,372,196-17,401,699 on the forward strand and is 29,50 kilobase (kb) long (Ensembl: ENSG00000276747). In mouse, *Padi6* is located on chromosome 4:140,454,666-140,469,954 on the reverse strand and is 15,29kb long (Ensembl: ENSMUSG00000040935). *PADI6,* standing for peptidyl arginine deiminase, type VI, is a member of the peptidylarginine deiminase or PAD family. These enzymes are responsible for post-translational protein modifications converting arginine (Arg) to citrulline (Cit) residues[12,27–30]. This conversion takes place in the presence of calcium ions, which makes the change of the ketene group of arginine to a ketone group possible. Citrulline has a neutral net charge, this increases the hydrophobicity of the protein and will cause changes in the protein-protein intermolecular interactions, causing changes in the folding and function. Up to now, five isoforms of mammalian PAD have been isolated; PADI1, PADI2, PADI3, PADI4 and PADI6. In general, mammalian PADs show a protein sequence similarity of 70-95%. All PAD members

are responsible for the conversion of arginine to citrulline. However, PADI6 is the only PAD for which no enzymatic activity is identified, yet. Each of the mentioned isoforms has its own substrate specificity and tissue-specific expression pattern. Strikingly, PADI6 is only expressed in the ovary and weakly in the testis, but never in other tissues. PADI6 is present in the cytoplasmatic lattices (CPLs), but is also required for its formation. CPLs are structures unique to mammalian oocytes and preimplantation embryos, but yet poorly-defined. At the cellular level, PADI6 is the first oocyte-specific protein to be localized to the CPL and plays a role in organelle positioning and redistribution[28,31–33]. Therefore it is not only an important mediator of the cell fate during the early embryonic development, but is also an important marker for oocyte quality.

Little is known about the expression regulation of the *PADI6* gene[28]. So far, for all the other PAD isoforms the transcription factors (TFs) critical for their expression have been identified **(Table 1)**. Initially, it was shown that the TF Sp1 is involved in the regulation of *PADIA, PADI2, PADI3* and *PADI4*. Although the 5'-flanking regions of the PAD genes are not conserved and the transcriptional regulation mechanisms differs between the genes, it was hypothesized that Sp1 also regulates the transcription of the *PADI6* gene, which was later experimentally confirmed[28].

Table 1: *Overview of the different transcription factors (TF) critical for the expression of the PAD genes (PADI1, PADI2, PADI3, PADI4 and PADI6).*

PAD isoform	Expression regulating TF
PADI1	MZF1 and Sp1
PADI2	Sp1/Sp3
PADI3	NF-Y and Sp1/Sp3
PADI4	AP-1, NF-Y and Sp1
PADI6	Sp1

3.2.2.2. Association of PADI6 mutations with pathologies

Since *PADI6* is crucial for embryonic development prior to and beyond the two-cell stage, mutations in this gene lead to early embryonic arrest. In patients with an EDA phenotype, homozygous and compound-heterozygous mutations have been detected[12,34–37]. Until now, five studies have analyzed the genome of ten patients suffering from EDA, from which eight different mutations have been discovered **(Table 2)**. Three types of disease-causing *PADI6* mutations have been reported: nonsense, missense and frameshift mutations (UniprotKB: Q6TGC4). Moreover, some of the found mutations are conserved in mice, such as c.1618G>A, c.970C>T, c.831_832del, c.1708C>T, c.1521dup and c.1369C>T.

Table 2*: Overview of the discovered PADI6 mutations leading to EDA. DEL = deletion, dup = duplication, * = stop codon, fs* = frameshift leading to a nonsense mediated decay, A = adenine, C = cytosine, G = guanine, T = thymine, Gln = glutamine, Gly = glycine, His = histidine, Arg = arginine, Ser = serine, Pro = proline, Ile = Isoleucine, Asn = Asparagine, Thr = Threonine, Cys = cysteine.*

Patient	Mutation	Position	Protein change	Type of mutation
1	Homozygous	c.1141C>T	p.(Gln381*)	Nonsense
2	Homozygous	c.1141C>T	p.(Gln381*)	Nonsense
3	Homozygous	c.1141C>T	p.(Gln381*)	Nonsense
4	Compound-heterozygous	c.2009_2010del / c.633T>A	p.(Glu670Glyfs*48) / p.(His211Gln)	Frameshift / Missense
5	Compound-heterozygous	c.1618G>A / c.970C>T	p.(Gly540Arg) / p.(Gln324*)	Missense / Nonsense
6	Homozygous	c.831_832del	p.(Ser278Profs*59)	Frameshift
7	Homozygous	c.1796T>A	p.(Ile599Asn)	Missense
8	Compound-heterozygous	c.1117A>C / c.1708C>T	p.(Thr373Pro) / p.(Arg570Cys)	Missense / Missense
9	Homozygous	c.1521dup	p.(Ser508Glnfs*5)	Frameshift
10	Homozygous	c.1369C>T	p.(Arg457*)	Nonsense

Interestingly, biallelic mutations in the *PADI6* gene have not only been associated with EDA but also with some other phenotypes, such as miscarriages and hydatidiform moles (HM) or molar pregnancies[31,35,38]. Hydatidiform moles are aberrant pregnancies which are identified by the absence of embryonic development or an abnormal form or by an abnormal placenta having variable trophoblastic proliferation and villous hydrops, these last one containing a high risk of developing into gestational trophoblastic neoplasia. The HM phenotype is caused by the interaction of mutant PADI6 and YAP, the downstream modulator of the Hippo signaling pathway, having a big influence on cell migration and invasion of the trophoblast. Moreover, the phenotype is also observed for other SCMC genes, namely *NLRP7* and *KHDC3L.* In addition, another pathology caused by either biallelic *PADI6* mutations or heterozygous frameshift mutations (T669Kfs*85) is the aberrant methylation of multiple imprinted loci in the genome, called multi-locus imprinting disturbance or MLID[27,39], which has been associated with the imprinting disorder Beckwith-Wiedemann syndrome (BWS). In general, this syndrome occurs sporadically, but research has shown that a significant ratio of MLID cases are familiar. About 100 loci of imprinted genes play a crucial role in fetal growth. When an imprinting disorder in one of these genes appears, some serious problems concerning development occur. Furthermore, mutations occurring in *PADI6* can lead to the occurrence of epilepsy. A study from R. J. Buono *et al.* investigated the effect of mutations located in *PADI6* and other SCMC genes, like *NLRP5 and NLRP7,* on the development of epilepsy[40]. The presence of different causal mutations in the affected patients, could be a possible cause these patients develop different phenotypes, which points to a genotype-phenotype effect.

In human patients harboring *PADI6* mutations and showing EDA, ovarian stimulation did not yield a significant difference in oocyte number and maturation rate compared to control patients. On the other hand, the fertilization rate in these patients was clearly decreased during multiple IVF/ICSI cycles[34,36]. Immunofluorescence analysis has been performed on these oocytes, to examine the expression and localization of the PADI6 protein. The signal was present in the cytoplasm of control oocytes, more specially in the subcortex, but absent in the affected oocytes containing homozygous nonsense mutations and compound-heterozygous mutations[12,37].

Interestingly, in accordance to patients with *NLRP5* and *NLRP7* mutations, patients harboring *PADI6* mutations also show a decrease in *de novo* DNA methylation and maternal methylation marks, and a diminished formation of the CPLs[35].

3.2.2.3. EDA mouse models

A number of mouse models showing relevant EDA phenotypes have already been developed: two non-*PADI6* related models, by the knock-out of two other MEGs/SCMC genes (*TLE6* and *NLRP2*) and one model containing a knock-out of the *PADI6* gene, Padi6$^{tm1.1Jgo}$/Padi6$^{tm1.1Jgo}$ [41]. All these models show a relevant phenotype associated with EDA: female infertility by failure of zygotic cell division.

The Padi6tm1.1Jgo/Padi6tm1.1Jgo mouse model contains a deletion of exon 2 and 3, resulting in a nonfunctional gene, and relies on the Cre-Lox system to obtain a gene knockout[41]. Examination of the *Padi6* knock-out (KO) mice showed no abnormalities in any of the organs and tissues. After comparison of the KO mice with the wild-type (WT) mice, it was concluded that mutant males showed normal fertility, whereas female KO mice did not produce any offspring. Furthermore, morphology and physiology comparison of ovaries from KO and WT mice did not reveal any differences concerning the number and developmental stages of follicles present in the ovaries. Furthermore, follicles were also cultured *ex vivo* to check whether KO follicles undergo normal development and maturation. Again no differences were observed between WT and KO mice. However, electron microscopy analysis in MII-arrested oocytes showed absence of the cytoplasmatic sheets in oocytes deficient for *Padi6.* Lastly, also no difference between the KO and WT mice was observed concerning endocrine function and the estrous cycle. From these results, it can be concluded that, in mouse, PADI6 is not crucial for oocyte growth, maturation and ovulation. From these elements, it became quite

certain that the PADI6 deficiency either affects the fertilization or early embryonic development. Knowing this, the research group further investigated the influence of *Padi6* mutations on zygotes and early embryonic development. During fertilization, no difference was observed in the pronuclear formation comparing KO and WT zygotes, but it was seen that none of the KO embryos developed beyond the two-cell stage. This confirms the important role of *Padi6* in early embryonic development and initiation of the EGA.

To further identify the mechanistic defects leading to EDA, the CPLs have been further studied in the *Padi6* KO mouse model[33]. Examination of MII oocytes derived from *Padi6* KO mice has shown that these structures were completely absent. So, PADI6 clearly plays a crucial role in the organization of these structures. It is yet unclear whether the organization is hampered by the absence of citrullination due to inactivation or loss of the PADI6 enzyme, or whether PADI6 has a different role in CPL development.

The major function of CPLs is the storage of different components needed for protein synthesis, such as ribosomes. Additionally, they are involved in regulation of microtubule dynamics and oocyte maturation in human and mouse. Therefore, absence of the CPLs already hints towards disturbed ribosomal distribution and hence defective EGA. Interestingly, even though lack of lattice seems to appear, it had no consequences for the general ribosomal levels in the oocyte. Moreover, the PADI6/CPL is thought to be important for the regulation of microtubule (MT) mediated organelle positioning and movement[29]. Kan *et al.* showed, in mouse WT germinal vesical (GV), MII oocytes and early embryos the specific co-localization of PADI6 with α-tubulin, further showing α-tubulin is also a component of the oocyte CPLs. These findings were found to be similar in human oocytes. Further, it is clearly seen that the spindle MTs are significantly shorter in KO oocytes compared to WT oocytes. On top of this, the diameter of the equatorial and aligned chromosomes parallel to equator is wider in KO than in WT oocytes. Next, organelle positioning is analyzed. It is seen that in the absence of PADI6, organelle distribution is more diffuse, meaning that PADI6 is important for organelle positioning in immature oocytes and redistribution during maturation. In conclusion, these findings show that an insufficient CPL formation, which is the ribosomal storage place and releases maternal factors during the embryogenesis, leads to an overall lower protein synthesis in two-cell embryos. Due to this change, an incomplete EGA takes place leading to a developmental arrest at the two-cell stage. The most interesting finding, is the fact that the origin of this two-cell arrest lies within a defect during oocyte growth[33]. Furthermore, *Padi6* mutations lead to an altered structure of the spindle MT and an altered organelle positioning[29]. All these findings shows the importance of the PADI6 and the CPLs as mediators of the cell fate during early embryonic development.

3.2.3. Treatment options for EDA

Until now, treatment options for EDA are rather limited. In practice, most of these patients have to seek oocyte donation. However, to obtain a genetically related child, some studies have shown a good outcome of the application of Assisted Oocyte Activation (AOA), which is a procedure generally used to overcome failed fertilization[42,43]. The AOA procedure aims to artificially activate the oocyte, which means the alleviation of meiotic arrest in which MII oocytes reside. There are different types of AOA methods; electrical[44], mechanical[45], or chemical activation. For the latter, with the use of Calcium ionophores (Ionomycin, A23187) the permeability of the membrane is increased. All these techniques lead to an increase of the calcium (Ca^{2+}) influx, on which oocyte activation depends. The rationale to apply AOA for EDA patients is to trigger the early post-fertilization cleavages by the induction of Ca^{2+} oscillations at fertilization.

In a study by Ebner *et al.,* patients with a history of *in vitro* developmental problems of their embryos after a previous ICSI cycle were included[43]. During ICSI, AOA using a calcium ionophore was applied. The fertilization, cleavage and clinical pregnancy rate were compared between ICSI cycle attempts with and without the performance of AOA. The results revealed no significant difference in fertilization and cleavage rate between the treated and untreated

group. Although no significant cleavage rate difference was observed, 42,9% of the treated embryos developed to the blastocyst stage compared to only 13,8% in the control group. Lastly, a significant increase of the implantation rate was seen, 44,4% compared to 12,5%. Even though these results are promising, it is unclear whether this technique truly overcomes EDA caused by specific genetic defects. However, it could be useful for a selected group of patients who experience cleavage failure due to low post-fertilization potential. Therefore, further research, involving larger sample sizes, on this approach to overcome EDA is still needed.

3.3. Genome editing

Using targeted genome editing tools, modifications at specified sites of the genome can be made. It can either be applied to analyze the function of specific genes and regulatory elements by specifically knocking them out. Alternatively, defined sequences can be knocked-in, making use of DNA templates with sequence homology[46]. This latter approach, discovered in 1989[47], was a real breakthrough, focusing on the integration of exogenous repair templates that contain sequence homology to the donor site. This study observed however that the desired targeting outcome occurred extremely infrequent (1:10^6-10^9 cells). To overcome this drawback, a series of studies was conducted by Haber and Jasin[48–53], which led to the discovery that HDR-mediated recombination events were stimulated by the introduction of DNA double-strand breaks (DSBs). Important to note is that these DSBs can be repaired by the Homologous directed repair (HDR) mediated pathway in the presence of an homology repair template, but are in fact generally repaired by the more dominant nonhomologous end-joining (NHEJ), re-ligating the broken DNA ends[54]. This pathway is however error-prone, leading to insertions (INS) and deletion (DEL) mutations into the genome at the target site.

3.3.1. Different classes of precise genome editing technologies

So far, four different classes of customizable DNA-binding proteins have been engineered to enable the introduction of a site-specific DNA DSB: meganucleases derived from mobile genetic elements, zinc finger (ZFN) nucleases based on eukaryotic transcription factors, transcription activator-like effectors (TALENs) from *Xanthomonas* bacteria and the Cas9 RNA-guided DNA endonucleases, derived from the type II bacterial adaptive immune system, CRISPR/Cas9[46,53,55–59]. The first three proteins are able to recognize DNA sequences by protein-DNA interactions. While meganucleases have integrated nuclease and DNA-binding domains, ZFNs and TALENs are made of a series of individual modules targeting respectively three or one nucleotides (nts), which are then linked to a nuclease FokI domain. ZFNs and TALENs are thus customizable, making it possible to assemble the different domains in a desired order.

Each of the techniques has however limitations. Since meganucleases only act at specific large (12-45 base pairs (bp)) DNA target sites, these are not quite often present at the locus of interest. Therefore, meganucleases are rarely used as a DNA editing technique. As for the ZFNs and TALENs, dimerization of the FokI nuclease domains is needed in order to be active, this requires the design of two monomers, each binding on one side of the targeted sequence. As for all the protein-based systems, they are all very labor-intensive to assemble, every other target is in need of a different set of DNA-binding modules making it very time-consuming to engineer. Due to the drawbacks of these protein-based techniques, the CRISPR/Cas9 technique is the most popular to use[60].

3.3.2. CRISPR/Cas9 technique

The CRISPR/Cas9 genome editing technique, acronym for Clustered Regularly Interspaced Short Palindromic Repeats/CRISPR associated proteins, is derived from an adaptive immune system of bacteria and archaea against invading viruses[46,61–63]. The technique makes use of the two-component CRISPR/Cas9 complex, which exist out of CRISPR RNAs (crRNAs) and the Cas9 RNA-endonuclease. Where the small crRNAs are able to recognize specific DNA

sequences, the Cas9 can introduce DSBs into the DNA. For an easy application, researchers introduced the 100 nt long guide RNA (gRNA), which is a chimeric RNA made up from crRNA forming a duplex with a transactivating crRNA (tracrRNA) **(Figure 5a)**. This tracrRNA:crRNA complex guides the Cas9 to the targeted sequence containing a PAM sequence or two to six nucleotides protospacer adjacent motif. Depending on the used Cas9 enzyme a different protospacer adjacent motif (PAM) sequence is required. For the *S. pyogenes* Cas9, which is used most of the time, a 5'-NGG-3' PAM needs to be present. Once this is recognized by the endonuclease, a DSB three bp upstream form the PAM is introduced.

Next, the break is repaired by either the NHEJ or the HDR pathway[64] **(Figure 5b)**. As mentioned before, NHEJ is the dominant pathway. Initiation of this pathway starts with the biding of ring-shaped Ku70/Ku80 protein heterodimers at the DSB ends, which prevents the DNA from breaking further down and it also recruits the DNA ligase.

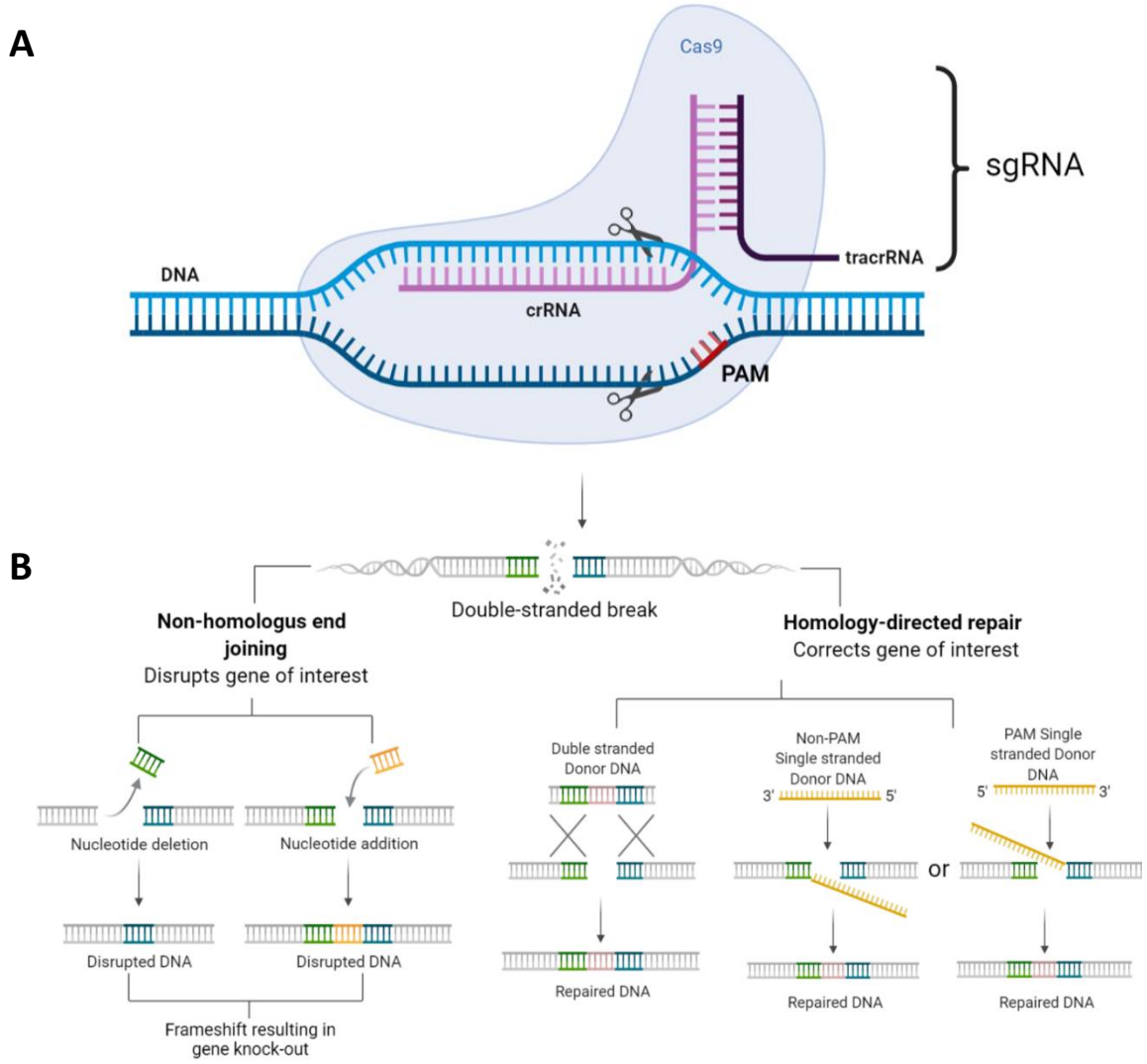

***Figure 5**: (A) Schematic overview of CRISPR/Cas9 complex and (B) endogenous repair mechanisms, Homologous direct repair (HDR) and Non-homologous end joining (NHEJ), to repair DSB introduced by CRISPR/Cas9 system.*

Re-ligation of the broken DNA ends does however not always occur correctly, leading to INS or DEL mutations, which can in turn lead to a shift in the mRNA reading frame, a premature stop codon and an impaired protein production[64,65]. Striking is that the NHEJ outcomes are not random, but they can be predicted depending on the local sequence context. Logically, the

HDR use a single-stranded (ss) or double-stranded DNA (dsDNA) template to guide the repair of the DSB.

Even though CRISPR/Cas9 had taken the edge compared to ZFNs and TALENs, it still comes with several challenges[66]. One of the major persisting limitations of targeted genome editing approaches is the potential editing at off-target sites, which are identical or similar sequences to the target DNA. When off-target editing occurs, other important genes could be knocked out resulting in misleading phenotypes. Luckily, to minimize potential off-target effects, *in silico* prediction tools can be used, so the target site containing the least potential off-targets can be selected. Next to unwanted off-target effects, unwanted on-target effects can also occur[67]. More specifically, it is possible that instead of a repair of the targeted site, partial or complete loss of the targeted chromosome takes place. Further, editing of for instance embryos using the CRISPR/Cas9 technique can be suboptimal, giving rise to mosaicism[68]. Mosaicism means that the individual contains both edited and non-edited cells. In embryos, this occurs due to the presence of at least one untargeted blastomere, meaning editing takes place after the first cleavage. A last obstacle is the PAM dependency. In theory, even with the PAM dependency, CRISPR/Cas9 can be applied to many DNA sequences, but in practice, and especially when aiming for HDR at one specific DNA locus, it can happen that the number of target sites at the locus of interest are rather limited[66].

3.3.3. CRISPR/Cas13 RNA-base editing

An alternative CRISPR/Cas system is CRISPR/Cas13, relying on the Cas13 enzyme which is able to cleave RNA[69,70]. At least four different subtypes are present in the Cas13 family: Cas13a, also known as C2c2, Cas13b, Cas13c and Cas13d. Such as Cas9, Cas13 can be isolated from bacteria where it is used in an adaptive immune system to protect against the invasion of RNA phages. Overall Cas13 proteins work similarly then Cas9. Cas13 also makes use of a gRNA, which is a crRNA forming a short hairpin structure next to a spacer sequence, approximately 64nts long. The spacer is responsible for the target specificity and therefore needs to be between 28 and 30 nucleotides long and complementary to the target sequence. As in CRISPRS/Cas9, the Cas13 protein complexes with the gRNA, which is made possible through the binding of Cas13 with a short hairpin in the crRNA. All Cas13s are able to cleave a target transcript, leading to non-specific degradation of any nearby transcript. The Cas13 activity is thought to be part of a programmed cell death pathway in bacteria.

Cas13s have already been successfully applied in mammalian cells to obtain transcript knockdown [71–73]. Subtype Cas13a and certain orthologs of Cas13b show good activity for RNA knockdown or editing, but remarkable is that the Cas13b orthologs are more stable and robust in mammalian cells. More recent, in 2018, Cas13d has proven to be very efficient and robust for knockdown experiment across endogenous transcripts and can also be used for the modulation of splicing of these transcripts.

Further engineering of the Cas13 enzyme has enabled more precise RNA editing approaches, such as RNA base editing, which enables the introduction or restoration of a mutation in the transcript. This first developed system, called RNA Editing for Programmable A to I Replacement (REPAIR), was developed by the Zhang Lab. In this approach, dead Cas13 (dCas13) is paired to an 'adenosine deaminases acting on RNA' or short $ADAR_2$ (adenosine deaminase acting on RNA) molecule. By using this fusion protein together with a target-specific crRNA, the $ADAR_2$ enzyme can deaminate adenosines (A) mispaired with cytidine (C) based on RNA duplexes (cRNA:target RNA)[69]. The deaminated A is later changed to an inosine (I), a nucleobase functionally equivalent to guanosine (G) in translation and splicing. The deaminase activity of ADAR depends on the duplex length and also the position of A within the duplex. Research showed that a gRNA length of 50nts and the target base on 34th nucleotide position provides the most robust efficiency. Depending on the deaminase protein linked to Cas13, not only A can be modified to G, but also C can be modified to U using this technique. In this way the targeted RNAs can lead to a temporary base pair change, which can either lead to a halt (introduction of mutation) or restoration (correction of mutation) of protein production.

This leads to the idea that the RNA-editing system can be used to develop treatments for genetic diseases.

Further engineering of the REPAIR system has led to two subtypes: $REPAIR_{V1}$ (version 1) and $REPAIR_{V2}$ (version 2)[69,74]. $REPAIR_{V1}$ showed to many off-targets due to a high activity and overexpression of ADAR. These high off-target rates can be reduced by using the $REPAIR_{V2}$, where the catalytic site of $ADAR_{2DD}$ ($ADAR_2$ deaminase domain) is mutated (E488Q). A drawback of the last system is the presence of a lower editing efficiency. Depending on the application, either one of the systems can be used, however, further modifications combining the best qualities of each system, would be preferred. In this sense, in 2020, a new REPAIR system was created: $REPAIR_x$ (version X), this version is as specific as version 2 and as active as version 1.

4. Research objectives

Most of the patients diagnosed with EDA must rely on oocyte donation to fulfill their child wish. Using this technique, good quality oocytes from a healthy donor are collected followed by performing IVF or ICSI cycles using the sperm of the father. However, due to a strong desire for a genetically related child, we aim to assess three potential treatment options to overcome EDA, making use of a *Padi6* mouse model:

1) Complementary RNA (cRNA) injection. With this technique the defective mRNA will be complemented and fulfill its function.

2) Repairing the defective *Padi6* mRNA by using CRISPR/Cas13 base editing, in a temporary fashion, aiming to reinitiate functional protein production.

3) Nuclear transfer, meant to replace the defective *Padi6* mRNA present in the oocyte by transferring the nucleus of the diseased oocyte to a healthy donor oocyte.

4.1. Short-term objectives

The embryos of a *Padi6* KO mouse model will be used to evaluate the different treatment options. For cRNA injection and nuclear transfer, any *Padi6* KO mouse model can be used. However, for repair of the nonfunctional *Padi6* mRNA, a specific model needs to be produced. As this technique only allows modifications in the RNA C>U or A>G, this model needs to contain a missense mutation in the *Padi6* gene. More specifically, a model containing a substitution of G>A on position 1582 in the cDNA will be made, which is conserved in humans **(Table 2. patient 5)**. By the use of the CRISPR/Cas9 genome editing technique and a repair template, manipulation of WT mice zygotes to incorporate the specific mutation can take place **(Figure 6)**.

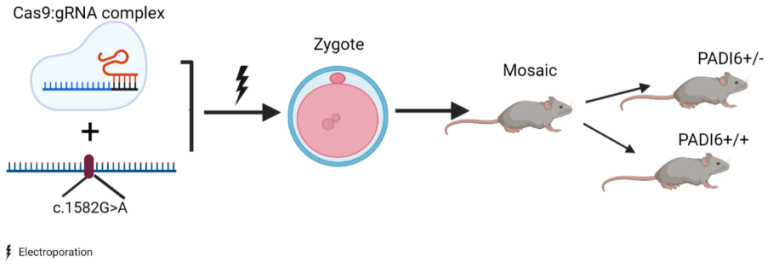

***Figure 6**: Schematic overview of procedure for specific mouse model production using the CRISPR/Cas9 gene editing technique, the CRISPR components were introduced into the zygote by electroporation.*

Further, the *Padi6* cRNA used to complement the defective mRNA will be produced. WT mRNA is produced by *in vitro* transcription (IVT) form WT cDNA which is incorporated in an expression

vector, a plasmid containing an enhancer and promoter region leading to an efficient transcription of the gene.

Lastly, because the CRISPR/Cas13 RNA-base editing technique is not yet often used, it still needs to be optimized before the efficiency of the technique can be examined. No software to identify the optimal target is yet designed, so different gRNAs need to be tested. Optimization of this technique will be performed in WT mice zygotes.

4.2. Long-term objectives

In the future, these two treatment options will be further investigated. Both techniques will be tested using *Padi6* KO mouse zygotes to test their efficiency. Experiments concerning delivery efficiency, *in vivo* expression and the functionality will be performed. Furthermore, a third possible treatment method will be examined, nuclear transfer. Nuclear transfer will be performed by transferring the nucleus of the defected oocyte to an enucleated healthy, WT oocytes.

Once these methods are optimized, all three treatments will be evaluated using the produced specific mouse model and compared to each other to see if one or more of them are efficient and safe to use. Eventually one or more will be used in subfertile human couples diagnosed with EDA.

5. Materials & Methods

5.1. Production of the mouse model

5.1.1. Zygote manipulation

5.1.1.1. Design crRNA and repair template

For the development of a disease-relevant mouse model, the c.1618G>A mutation was chosen, since it has been detected in patients experiencing EDA, and is conserved in mouse (c.1582G>A). With the use of the Benchling algorithm, a crRNA targeting *Padi6* was selected. All possible crRNAs were evaluated in the region of interest, which is g.11686 – g.11759, or exon 13 **(Figure 7)**. The guide parameters were set to 20 for guide length, GRCm38 (mm10, *Mus Musculus*) for genome and NGG (SpCas9, 3' side) as PAM sequence. Based on the position, specificity and efficiency score the best predicted crRNA was chosen. Because it is meant to produce a mouse model containing a point mutation, G>A, on position g.11732 exon 13, the crRNA design with sequence 5'-GCGCAGAACAGCTCCTTTCTA-3' has preference, since repair will demolish PAM site from TGG>TAG.

***Figure 7**: Benchling algorithm outcome for the design of crRNA targeting exon 13 of the Padi6 gene. Underlined in blue is the PAM sequence (TGG), indicated in green is the target sequence and indicated in red is the base needed to be changed.*

As for the repair template design the HDR IDT tool was used[75]. By choosing the desired template length, position and type of base pair alteration, the tool proposes HDR template sequences in accordance to the forward strand or reverse strand, which are reported to have a similar potency[76]. **(Table 3)**.

***Table 3**: Overview of the possible forward and reversed repair templates with their sequence. Mutation to be incorporated is indicated in red.*

Strand	Template Sequence
Forward (+)	TGAGGTGGGGAAGGAGGGCACTAGGCGGGAGTCACCTTACTATTAGAAAGGA GCTGTTCTGCTCCAATGTCTTCAAACAGGGTCA
Reverse (-)	TGACCCTGTTTGAAGACATTGGAGCAGAACAGCTCCTTTCTAATAGTAAGGTGA CTCCCGCCTAGTGCCCTCCTTCCCCACCTCA

5.1.1.2. Assemblage CRISPR/Cas9 RNP complex

Assemblage of the CRISPR/Cas9 ribonucleoprotein (RNP) complex consist of three steps. First, the resuspension of the lyophilized crRNA (5'-GCAGAACAGCTCCTTTCTAA-3', Integrated DNA Technologies (IDT)) and tracrRNA (#1073190, IDT) oligos was performed in Tris-EDTA buffer solution (TE buffer) (#93283-100ML, Sigma-Aldrich) to a final concentration of 100µM, aliquoted and stored at -20°C. Next, these two oligos were mixed in equimolar concentration in a sterile microcentrifuge tube **(Table 4)**.

***Table 4**: Used oligos, crRNA and tracrRNA, with their final concentration.*

Component	Final Concentration (µM)
CRISPR/Cas9 crRNA	100
CRISPR/Cas9 tracrRNA	100

This mixture was heated at 95°C for 5 minutes and afterwards cooled down to 15-25°C, mixed with Alt-R *S.p.* Cas9 Nuclease (#1081059, IDT) and incubated for 5 minutes. Subsequently, the repair template and OptiMEM™ (#31985-062, Thermo Fisher Scientific) solution were added, the solution was distributed in aliquots of 5µL stored at -80°C until use **(Table 5)**.

***Table 5**: Different components mixed for the RNP production, crRNA:tracrRNA duplex, Cas9, Template and OptiMEM™, with their final concentration.*

Component	Amount
crRNA:tracrRNA duplex (50µM)	0,1 µg/µL
Cas9 enzyme (10µg/µL stock)	0,2 µg/µL
Template (3,70191 µg/µL)	0,1 µg/µL
OptiMEM™	To 25,43µL

5.1.1.3. Zygote collection

Eight to twelve-week old B6D2F1 female mice (Janvier laboratories) underwent an intraperitoneal injection with 0.10mL 5 IU or pregnant mare's serum gonadotrophin (PMSG, Folligon®) (Invert, Boxmeer, the Netherlands) and 48 hours later with 0.10mL 10 IU, human Chorionic Gonadotrophin (hCG, Chorulon®) (Invert, Boxmeer, the Netherlands), after which they were mated overnight with male B6D2F1 mice, younger than six months. Nineteen to twenty-one hours after the hCG injection, these females were sacrificed, ovaries were dissected out and collected in 2mL KSOM-HEPES medium (in house, 10mL KSOM-HEPES containing 0,04g bovine serum albumin (BSA, #12657, Sigma-Aldrich)) and cumulus oocyte complexes (COCs) were isolated from the oviduct's ampullae. Afterwards, COCs were shortly incubated in hyaluronidase (in house, 200 IU/mL hyaluronidase in KSOM-HEPES) for maximum 5 minutes, causing the detachment of the cumulus cells surrounding the zygote. The cleared zygotes were washed in KSOM-HEPES and transferred to KSOM (in house, 10mL KSOM-low glucose containing 0,04g BSA) for incubation at 37°C (5% O_2 and 6% CO_2). Embryos were transferred to Syndey IVF blastocyst medium (50mL) (#G20929, Cook Medical) 68-72 hours after Chorulon® injection. Embryonic development to the two-cell and blastocyst stage was assessed respectively 48 and 120 hours post Chorulon® administration.

5.1.1.4. Electroporation of the zygotes

For the electroporation, zygote collection was performed until the KSOM-HEPES wash steps, followed by pooling of the zygotes in KSOM-HEPES, after which a group of +/- 15 zygotes was washed in OptiMEM™ medium. Subsequently, 5µL of the RNP complex was pipetted in between the lanes of the glass microslide (#45-0104, BTX), which was connected with the electroporator (ECM 830, BTX), after which the zygotes were added to the drop of RNP. Electroporation was carried out with the following setting: 2 pulses at 30V, 2ms pulse duration with a 100ms interval. Electroporated zygotes were recollected and transferred to the KSOM-HEPES dish for washing steps and were finally collected in the KSOM dish for further incubation. Two types of controls were included: medium controls, collected by conventional zygote collection and negative controls were obtained by the electroporation with a RNP containing a nonfunctional RNP complex, with the Alt-R® CRISPR/Cas9 Negative control crRNA #2 (IDT) **(Figure 8)**.

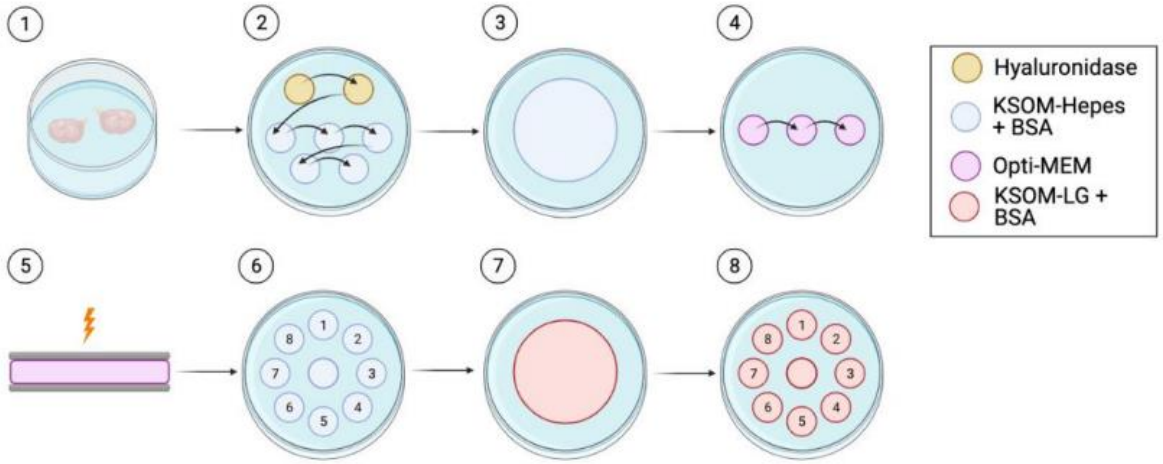

Figure 8: *Schematic overview of the set-up for mouse zygote electroporation. Ovaries are collected in 2mL KSOM-HEPES and COCs are isolated from the oviduct's ampullae (1). The collected COCs are briefly incubated in hyaluronidase to get rid of the surrounding cumulus cells, followed by a wash in KSOM-HEPES (2). All the zygotes are pooled in KSOM-HEPES (3). A group of 15 zygotes is washed in OptiMEM (4) and put in RNP complex between the two electrodes of the microslide (5). The electroporated zygotes are again collected and transferred to a KSOM-HEPES culture dish (6), transferred and washed in KSOM (7) and lastly, transferred to the KSOM culture dish wish is placed in the incubator (8)*[77].

5.1.1.5. DNA editing analysis

To check the editing efficiency after performing electroporation, the embryos were collected and DNA extraction was performed using the PicoPure™ DNA extraction kit (#KIT0103, Thermo Fisher Scientific). Using this kit, per each 10µL of extraction solution, which is a mixture of 155µL reconstitution buffer with 20mg/mL proteinase K, one embryo was collected. Hereafter, the tubes were incubated for 3 hours at 65°C and proteinase K was inactivated for 10 minutes at 95°C. Following DNA extraction, a polymerase chain reaction (PCR) was performed after which PCR samples were analyzed by next-generation sequencing (NGS) at the Center for Medical Genetics, Ghent[78]. The raw NGS data were evaluated using BATCH-GE bioinformatics, developed in house[79], and visually screened using the Integrative Genomics Viewer (IGV).

5.1.1.5.1. Polymerase chain reaction

The PCR mastermix was made by mixing Kapa2G Robust MM (#KK5701, Sigma-Aldrich), a forward (5'-AAC AAC GAC CAG AAG GTT GG-3') and reversed primer (5'- GGT CGC AAC CAA AAG ACA TT-3') (IDT) both with a concentration of 2µM **(Table 7)**.

Table 7*: Different components mixed to produce the PCR mastermix and the amount needed per PCR reaction.*

Product	Amount (µL per PCR reaction)
Kapa2G Robust MM	5
Forward Primer (2µM)	1,25
Reversed Primer (2µM)	1,25
DNA	2,5
Total volume	**To 10µL**

To a volume of 7,5µL mastermix, 2,5µL of the extracted DNA was added. A touchdown PCR reaction was performed on a Proflex machine (#4484073, Thermo Fisher Scientific) **(Table 8)**, after which PCR samples were analyzed by next-generation sequencing (NGS) at the Center for Medical Genetics Ghent[78]. The raw NGS data were evaluated using the in-house developed BATCH-GE bioinformatics tool[79], and visually screened using Integrative Genomics Viewer (IGV).

***Table 8**: Overview of the different steps in the touchdown PCR reaction process*

	Time	Temperature (°C)	
1.Activation	3 min	95	
2.Denaturation	15 sec	95	**12X**
3.Annealing	10 sec	X (-1 every cycle)	
4.Elongation	15 sec	72	
2.Denaturation	15 sec	95	**12X**
3.Annealing	10 sec	X - 12	
4.Elongation	15 sec	72	
5.Final	10 min	72	
Hold	infinite	15	

5.1.1.6. Embryo transfer to pseudo-pregnant mice

For embryo transfer experiments, female and vasectomized male mice of the CD1 strain were used. Three days before mating, female mice were placed on dirty male bedding material, in order to stimulate the Whitten effect. Hereafter, on the day of zygote collection and electroporation, breeding of female CD1 mice in proestrus or estrus with a vasectomized male was set up. The next morning, a check of the plug was being performed and the mice were separated again until embryo transfer, which took place three days later. Good quality E3.5 embryos were transferred to pseudopregnant female mice using the Non-Surgical Embryo Transfer device for mice (mNEST, #60010, ParaTech). First the embryos were transferred to KSOM medium. A group of 12-20 embryos were then slowly pulled into the tip of the mNSET device put onto a P-2 pipetman set to 1.8µL. After the pipetman is set to 2.0µL, aimed to create an air bubble at the catheter tip, the mNSET tip was inserted into the speculum used to spread and hold open the vaginal walls. While holding the mice by the tail and in an angle of 45-70°, undisturbed insertion of the mNSET tip could take place. The embryos were then released by pushing the plunger until the second pipet stop and without releasing the plunger the mNSET device was released from the speculum. Delivery was expected eighteen days following embryo transfer.

5.1.1.7. Offspring analysis

5.1.1.7.1. Toe clipping

Toe clipping was performed on 1 week old pups, using small, sharp scissors. In this way not only the genotype of these mice could be analyzed, but it also marked the different pups. Toes are always clipped form the hind legs, from left to right starting at the right hind leg and all separately collected in 0,2 mL PCR tubes.

5.1.1.7.2. DNA extraction from the clipped toes

Toe clipping was followed by DNA extraction[80]. Fifty µL of Alkaline Lysis Reagent (in-house made mixture of NaOH, EDTA and ddH_2O (distilled water), pH 12) was added to the obtained tissue, followed by 30 minutes heating at 95°C and afterwards cooled down to 4°C **(Table 6 A)**. Next, 50µL neutralization Buffer (in-house made mixture of Tris-HCL and ddH_2O, pH 5) was added **(Table 6 B)**.

Table 6: Components mixed for the production of (A) the alkaline lyse reagent and (B) the neutralization buffer, with their final concentration.

A

Alkaline Lysis Reagent

Reagent	*Final concentration (mM)*
NaOH	25
EDTA	0.2
ddH_2O	/

B

Neutralization Buffer

Reagent	*Final concentration (mM)*
Tris-HCL	40
ddH_2O	/

5.1.2. Immunostaining of the embryos

Embryos were fixated by incubating them into paraformaldehyde 4% (PFA) (in house) for 30 minutes at room temperature (RT), after which they were washed one time in PBS 1X at RT and once in ice-cold PBS1X, each time for 10 minutes. If not immediately stained, the dish containing the embryos was closed with parafilm and stored at 4°C.

When staining oocytes coming from the fridge, they are first washed in PBS 1X for 5 minutes at RT. Following, is the permeabilization step where the embryos were brought into PBT 0.5% and put on the shaker for 20 minutes at RT. Thereafter, all the embryos were transferred to the blocking solution and put on the shaker for 1 hour of incubation. A 1:250 dilution of the primary antibody (Ab), anti-PADI6 (#orb312631, Biorbyt), in blocking solution was made. The embryos were incubated overnight on the shaker at RT. A part of the embryos were incubated in the primary Ab solution and a couple of embryos were used as negative control, these were incubated in blocking solution.

The next day, all the embryos were stained with the secondary Ab, starting with washing the embryos three times in PBT 0.1% for 10 minutes. Following the wash steps the embryos are incubated for 1 hour with the secondary Ab solution, which is a mixture of 1:500 diluted secondary Ab (#A21206, Thermo Fisher Scientific), DAPI (#62248, Thermo Fisher Scientific) 1:100 dilution and blocking solution. From this step onwards, it is important to keep the secondary Ab solution and the stained embryos in the dark to prevent bleaching. Following incubation with the secondary Ab, the embryos were washed in blocking solution and each embryo was placed in a <5µL drop of PBS 1X. These drops were placed on the imaging dish, WillCo® glass bottom dish (#GWST-5040, WillCo Wells BV) covered with oil. Once all the embryos were transferred to a drop, the staining could be visualized by confocal imaging.

5.1.3. Ovary staining

Following zygote collection, the remaining ovarian tissue was fixated by incubation in PFA overnight. The next day, the ovaries were transferred to 70% ethanol and stored at 4°C until the tissue was embedded in paraffin using standard procedures. Every 50µm in the ovary tissue two 5µm coupes were collected an a glass slide, which were later stained by hematoxylin and eosin, using standard procedures and visualized using a stereomicroscope.

5.2. Production of the *Padi6* cRNA

5.2.1. Preparation bacterial work

To 9,6g Lysogeny Broth (LB) agar (#22700041, Thermo Fisher Scientific) or 6g LB broth (#12780052, Thermo Fisher Scientific), 300mL distilled water was added, shaken until everything was dissolved and put into the autoclave. After cooling the media down, the produced LB agar medium was used to prepare the agar plates, taking place in a laminar air flow. Either ampicillin (AMP, 1:1000) (#11593027, Thermo Fisher Scientific) or Kanamycin (KAN, 1:1000) (#11815024, Thermo Fisher Scientific) was added to the medium, before

pouring the Petri dishes. As for the LB broth medium, it was stored at 4°C until the liquid cultures for upscaling of the bacteria, needed to be prepared.

5.2.2. Production of the expression vector containing the *Padi6* cDNA

5.2.2.1. Transformation into E.coli bacteria

At the day of transformation, 1pg-100ng plasmid DNA (*Padi6* (NM_153106) mouse untagged clone plasmid (#MC201892, Clini Sciences/Origen)) was added to 50µL 5-alpha competent *E.coli* mixture (#C2987H, New England Biolabs® (NEB®)). After an incubation of 30 minutes on ice, the bacteria underwent a heat shock by placing them in a heat bath of 45°C for 30 seconds and set back on ice. Following the incubation on ice for 5 minutes, 950µL of Super Optimal broth with Catabolite repression (SOC) outgrowth medium (#B9020S, NEB®) was added and the mixture was incubated at 37°C for 1 hour on the shaker, whereafter the bacteria were spread onto the antibiotic-containing agar plates.

5.2.2.2. Upscaling of bacterial colonies

When colonies were formed on the plate, liquid upscaling was performed. First, the colonies were enlarged on a new plate by drawing a line with an inoculation swab used to pick up a part of the colony. Secondly, the other part of the colony was also picked up and placed in a tube containing antibiotic-containing LB broth. The liquid culture and the plate were incubated overnight at 37°C (not longer than 16 hours), the morning after the plate was closed with parafilm and stored at 4°C. The liquid culture was used to both prepare a bacterial glycerol stock, as well as extract large amounts of plasmid DNA.

5.2.2.3. DNA extraction and DNA concentration measuring

Before the DNA is extracted, a 1mL glycerol stock that can be stored at -80°C was made **(Table 9)**.

***Table 9**: Components and their amounts need to make a glycerol stock of the bacterial colonies.*

Component	Amount (µL)
Glycerol (#G5516-100ML, Sigma-Aldrich)	¼ total volume
Sterile H_2O	¼ total volume
Liquid culture	½ total volume

The Spin Miniprep Kit (#27104, QIAgen) is designed to extract plasmid DNA from bacterial cultures. After the liquid cultures were centrifuged, the formed pellet was resuspended in resuspension buffer (P1). 250µL was transferred to a microcentrifuge and mixed with the same amount of lyse buffer (P2). After 5 minutes of incubation, neutralization buffer (N3) was added and centrifugation was performed, whereafter the supernatant was centrifuged again using a QIAprep 2.0 Spin Column. Further, two wash steps were performed, the first one using washing buffer (PB) and the second one using a purification buffer (PE). Lastly, the DNA was eluted from the spin column by adding elution buffer (EB) and centrifuging.

Once all the DNA was eluted, the concentration was measured using the Qubit® 2.0 fluorometer and Qubit™ dsDNA HS Assay Kit (#Q32851, Thermo Fisher Scientific). A working solution, which is Qubit™ reagent 1:200 diluted in Qubit™ buffer, for the amount of samples and two standards was made. Further, the assay tubes were prepared, two of them containing 190µL working solution and 10µL of standard 1 or 2 and the other tubes containing 199µL working solution and 1µL sample. Right before the concentration measuring the tubes were vortexed.

5.2.2.4. Ligation of Padi6 cDNA into expression vector of Plcz1

5.2.2.4.1. LR- PCR, purification and concentration measuring of *Padi6* plasmid DNA

To amplify the Padi6 cDNA from the *Padi6* (NM_153106) mouse untagged clone plasmid (#MC201892, Clini Sciences/Origen), a long-range PCR was performed. From a 100µM stock of primers containing a restriction site for the NotI-HF® (#R3189S, NEB) and HindIII-HF®

(#R3104S, NEB) restriction enzymes, a 10µM working solution was made. Further, a mixture using the components present in the TaKaRa La Taq® kit (#RR002M, Cionech) and with a total volume of 50µL per PCR reaction was prepared **(Table 10)**. The Long-Range (LR) PCR was performed on the Proflex machine **(Table 11)**. The amplified DNA region was further purified by making use of the QIAquick® PCR & Gel Cleanup kit (#28506, QIAgen). When the color of the PCR product PB mixture changes sodium acetate (pH 5.0) was added and the solution was centrifuged using a QIAquick column. After the DNA was washed using PE buffer, the DNA could be diluted by adding EB buffer. Once the DNA was collected the concentration was measured using Qubit® 2.0 fluorometer.

***Table 10**: (A) Overview of the different components with their final concentration mixed for the LR-PCR reaction and (B) an overview of the sequence of the primers used to perform LR-PCR to make ligation possible. Indicated in red is a random added sequence and the underlined region indicates the restriction site.*

A

Component	Final concentration
Takara LA Taq	5U/µL
10X LA PCR Buffer II	1ml
$MgCl_2$	25mM
dNTP Mixture	2,5 mM
Template	<1µg (optimal: 0,5µg)
Forward primer	0,2 – 1µM
Reversed primer	0,2 – 1µM
H_2O	To 50µL

B

Primer	Sequence
Forward	GGAGCTAAGCTTATGTCTTTTCAGAACTCACTCAGC
Reversed	AGATCCGCGGCCGCTTATGGGGTCATCTTCCACCAC

***Table 11**: Overview of the different steps in the LR-PCR reaction process.*

	Time	Temperature (°C)	
1.Activation	1 min	94	
2.Denaturation	10 sec	98	**30X**
3.Annealing & elongation	2 min	68 (0,5-1 min/kb)	
4.Final	10 min	72	

5.2.2.4.2. Restriction digest of PCR product and expression vector

The amplified PCR fragment will be cloned into an expression vector. In order to do so, both the PCR product and the expression vector were digested by restriction enzymes, NotI-HF® and HindIII-HF® (mixture composition, see **Table 12**). The mixture was then incubated for 10 minutes at 37°C.

***Table 12**: Overview of the different components with their final concentration for the preparation of the restriction digest mixture.*

Components	Final concentration
DNA	1µg
10X rCutSmart™ Buffer (#B6004S, NEB)	1X
NotI-HF	20 U
HindIII-HF	20 U
Nuclease-Free water (#B1500L, NEB)	To 50µL

Where the restricted PCR product was again purified using the QIAquick® PCR & Gel Cleanup kit and the DNA concentration was measured using Qubit® 2.0 fluorometer, the restricted expression vector was loaded on a agarose gel.

5.2.2.4.3. Gel electrophoresis and gel extraction of vector

Agarose gel was made according standard procedure. The agarose gel was placed in an electrophoresis tank with the same type of buffer as used in the gel, TAE, slots closest to the cathode. Once the combs were removed the slots were filled with either a DNA ladder, or the sample, mixed with loading **(Table 13)**.

***Table 13**: Preparation of loading mixtures, all components with their amount needed for the (A) ladder mixture and (B) the sample mixture.*

A

Component	Amount (µL)
ddH_2O	4µL
Gel loading dye 6X (#B7021S, NEB)	1µL
DNA ladder (#N3200S, NEB)	1µL

B

Component	Amount
Gel loading dye 6X	1 volume
DNA (Vector)	5 volume

Following sufficient size separation the DNA band matching the size of the vector backbone, around 3kb, was cut out of the gel aided by UV visualization. The DNA was purified again using the QIAquick® PCR & Gel Cleanup kit and measured using the Qubit® 2.0 fluorometer.

5.2.2.4.4. Ligation process

A reaction containing: T4 DNA ligase reaction buffer (#B0202S, NEB), vector DNA, insert DNA, nuclease-free water and Hi-T4™ DNA ligase ((#M2622S, NEB), which was added at last, was set up on ice and incubated for 10 minutes at RT **(Table 14)**. Following the 10 minutes incubation, the mixture underwent heat inactivation for 10 minutes at 65°C. Once the reaction is then chilled on ice, 5µL is transformed into 50µL competent cells.

***Table 14**: All components with their final concentration needed for the production of the reaction to perform ligation.*

Components	Final concentration
T4 DNA ligase reaction buffer	10X
Vector DNA (3kb)	50 ng (0.020 pmol)
Insert DNA (*Padi6* cDNA) (2kb)	37.5 ng (0.060 pmol)
Nuclease-free water	To 20µL
Hi-T4™ DNA ligase	

5.2.2.4.5. Colony PCR after ligation

To check if the ligation process was successful, a colony PCR was conducted. Two primer pairs, binding near the ligation regions, were mixed together with Kapa2G Robust and nuclease-free water **(Table 15)**. To this mixture a part of the bacterial colonies was added and a standard PCR reaction was performed on a Proflex machine **(Table 16)**. The remaining part of the colonies was used to set up colony growth on a new agar plate and for the liquid culture upscaling, in the presence of ampicillin. After colony PCR, the samples were assessed on the fragment analyzer, which analyzes PCR by capillary electrophoresis.

***Table 15**: (A) Overview of the different components with their used amount mixed for the colony-PCR reaction and (B) an overview of the sequence of the primers used to perform colony-PCR to control the incorporation of the insert, Padi6 cDNA.*

A

Components	Amount (µL)
Kapa	5
Forward primer	1,25
Reversed Primer	1,25
Nuclease-free H_2O	To 2,5

B

Primer pair 1

Primer	Sequence
Forward	TGTGTGGAATTGTGAGCGGA
Reversed	TTCACAAGCAGGATGGCTCC

Primer pair 2

Primer	Sequence
Forward	GGGAACGTGACCCTGTTTGA
Reversed	TTGGGTAACGCCAGGGTTTT

***Table 16**: Overview of the different steps in the FORD PCR reaction process.*

	Time	Temperature °C	
1.Activation	3 min	95	
2.Denaturation	15 sec	95	**35X**
3.Annealing	10 sec	75	
4.Elongation	15 sec	72	
5.Final	1 min	72	
Hold	Infinite	15	

5.2.2.4.6. Sanger sequencing

Bacterial DNA was prepared from liquid cultures for which the corresponding colony PCRs showed PCR bands of expected sizes. From these bacterial DNA samples, the full sequence was assessed by Sanger sequencing. In order to do so, first, several PCR reactions, amplifying regions of approximately 500 bp, were performed **(Table 17)**. Next using an enzyme solution consisting of Antarctic Phosphatase (5000U/mL) (#M0289L, NEB) and Exonuclease I (2000U/mL) (#M0568S, NEB) mixed with nuclease-free water, the PCR products were purified. To 1 volume of the enzyme solution, 5 volumes of the PCR product were added and incubated for 15 minutes at 37°C followed by a heat inactivation at 80°C for 20 minutes.

***Table 17**: Overview of the used flanking primers (flanking the whole Padi6 gene) and internal primers (primers to amplify internal parts of the Padi6 gene) of the Padi6 region to perform Sanger sequencing.*

Primer	Sequence
Flanking *Padi6*	
Forward	TGTGTGGAATTGTGAGCGGA
Reversed	TTGGGTAACGCCAGGGTTTT
Internal primers	
1 Forward	CAAGCGCGCAATTAACCCTC
1 Reversed	TTCACAAGCAGGATGGCTCC
2 Forward	ATCTCCCTGGAGGCAGACAT
2 Reversed	TCTAGAGGCATCTGGGTGCT
3 Forward	GGGCCTGATCTCCTTGTCAC
3 Reversed	AAAGCTGCCACCAATGAGGA
4 Forward	TAGCCTGGATTCCATCGGGA
4 Reversed	GTTTGGTGCTCTGCTGGTTG
5 Forward	GGGAACGTGACCCTGTTTGA
5 Reversed	GGGTGTTCTTGAGGCTGGTT

A 1µM solution of the same primers used for PCR, was used to perform cycle sequencing. Therefore, 9µL of a master mix **(Table 18)** was added to 1µL of the purified PCR product and the cycle sequencing reaction was continued **(Table 19)**. This mixture contains the DNA template, sequencing primer, a thermostable polymerase, deoxyribonucleotide triphosphate (dNTPs), dideoxynucleotide triphosphates (ddNTPs) and a buffer.

***Table 18**: Components of the Sanger master mix.*

Component	Amount (µL)
Ready Reaction	(n+1) x 0.5
ABI-buffer 5X	(n+1) x 2
Primer (forward/reversed, 1µM)	(n+1) x 2
Nuclease-free H_2O	(n+1) x 4,5

***Table 19**: Overview of the different steps of the cycle sequencing reaction.*

	Time	Temperature °C	
1.Activation	5 min	95	
2.Denaturation	10 sec	95	**25X**
3.Annealing	5 sec	55	
4.Elongation	2 min	60	
5.Final	10 min	15	
Hold	Infinite	15	

The resulting sequencing reaction was purified with the use of magnetic beads (GC Biotech). DNA binds to these beads, after washing them three times with a 85% ethanol solution and placing them on the magnet, the DNA was eluted by adding water. These reactions were then analyzed using the sequencer (#ABI3730XL, Applied Biosystems) and using Finch TV (Geospiza).

5.2.2.4.7. Side-directed mutagenesis

To correct incorporated single nucleotide polymorphisms in the *Padi6* cDNA incorporated in the expression plasmid, site directed mutagenesis was performed using the Q5® Site-Directed Mutagenesis Kit (#E0554S, NEB). Therefore, two primer pairs containing the desired sequence were designed using the NEB primer design software, NEBaseChanger™ **(Table 19)**. Due to the presence of two undesired single nucleotide polymorphisms, this mutagenesis procedure needed to be performed sequentially two times.

***Table 19**: Overview of the primers designed to perform mutagenesis. Incorporated mutation is indicated in red.*

Primer	Sequence
Primer pair 1	
2577-C-T-F	GAGGCAGACAtCTATCGAGATG
2577-C-T-R	CAGGGAGATCTCGATGCC
Primer pair 2	
2399-G-A-F	CAAAGAGGACaCTGTGGTCTGGAG
2399-G-A-R	CCAGCGATGACGGAGCTA

The whole mutagenesis process consist of three steps, starting with the exponential amplification. During this step a mixture **(Table 20 A)** underwent exponential amplification by conducting a PCR reaction on the Proflex machine **(Table 20 B)**. Amplification of the plasmid occurs by back to back annealing of the designed primers containing the wanted mutation, after denaturation of the DNA took place. This amplification results in a linearized PCR product of the plasmid.

***Table 20:** (A) Overview of the different components with their used amount mixed for the mutagenesis process and (B) an overview of the different steps of the PCR reaction.*

A

Component	Final concentration
Q5 Hot Start High-Fidelity 2X Master Mix	1X
Forward primer (10µM)	0,5 µM
Reversed primer (10µM)	0,5 µM
Template DNA	1-25ng
Nuclease-free water	To 25µL

B

	Time	Temperature °C	
1.Initial Denaturation	30 sec	98	
2.Denaturation	10 sec	98	**25X**
3.Annealing	10-30 sec	50-72	
4.Elongation	20-30 sec/kb	72	
5.Final Extension	2 min	72	
Hold	Infinite	5-10	

Following the amplification, a Kinase-Ligase-DpnI (KLD) reaction was performed. This reaction causes circulation of the PCR product and removal of the template. A mixture consisting of 4 components **(Table 21)** was made and incubated for 5 minutes at RT, whereafter transformation to competent cells was conducted.

***Table 20:** Overview of the different components with their used amount mixed for the Kinase-ligase-DpnI reaction during mutagenesis process (A)*

Component	Amount
PCR product	1µL
2X KLD Reaction Buffer	Final concentration: 1X
10X KLD Enzyme Mix	Final concentration 1X
Nuclease-free water	To 10µL

5.2.2.4.8. *In vitro* transcription

To produce ready-to-deliver *Padi6* cRNA, *in vitro* transcription (IVT) of the produced expression plasmid was performed. Before IVT can be conducted, a fresh LR-PCR reaction of the plasmid needed to be performed. In the used reaction mixture, a forward primer located upstream of the start codon, and a reverse primer located downstream of the poly A signal incorporated in the plasmid sequence, were used **(Table 22)**.

Table 22: *Overview of the used primers (forward and reversed), designed for the PlcZ plasmid, needed to perform LR-PCR possible.*

Primer	Sequence
Forward	TGTGTGGAATTGTGAGCGGA
Reversed	TTGGGTAACGCCAGGGTTTT

For the IVT mMESSAGE mMACHINE™ T3 transcription kit (#AM1348, Thermo Fisher Scientific) was used. The procedure starts with a capped transcription reaction assembly where the transcription reaction is assembled at RT **(Table 23)**, mixed and incubated at 37°C for 1 hour, whereafter 1µL TURBO DNase was added and incubated for another 15 minutes at 37°C.

Table 23: *Overview of the different components with their used amount, mixed to make a capped transcription reaction possible.*

Component	Amount
Nuclease-free water	To 20µL
2X NTP/CAP	10µL
10X Reaction Buffer	2µL
Linear Template DNA	0,1-1µg
T3 enzyme Mix	2µL

Following the transcription reaction, recovery of RNA was performed using the MEGAclear™ kit (#AM1908, Thermo Fisher Scientific). The resulting RNA sample was mixed with Elution Solution, Binding Solution and 100% ethanol, whereafter the mixture was applied to a filter cartridge and centrifuged. Next, the RNA attached to the filter was washed two times using Wash Solution and by applying Elution Solution, the RNA could be collected.

The obtained RNA was assessed for its concentration using Qubit® 2.0 fluorometer and Qubit™ RNA HS Assay Kit (#Q32852, Thermo Fisher Scientific) and quality by analyzation on the fragment analyzer using the Fragment Analyzer Systems RNA Kit (#DNF-471-0500, Aligent)

5.3. CRISPR/Cas13 base editing

5.3.1. Production of the gRNA

Until now, programs for designing a suitable gRNA do not yet exist. Therefore a suitable design was made by searching the literature. The Zhang lab showed that the optimal length of the gRNA would be 50 nts consisting from only a crRNA. The optimal position of the incorporated mutation is at position 32, 34 or 36, but further there are no strict design rules yet. Based on these rules and the cDNA sequence of *Padi6* containing the G>A point mutation, possible gRNAs were designed **(Table 24)**. Because the mouse model containing this point mutation does not yet exist, the CRISPR/Cas13 base editing is first tested in WT mice zygotes, therefore other gRNAs were designed **(Table 24)**. These gRNAs contain a mismatch with an adenosine, present in the WT sequence, two nucleotides upstream from the point mutation.

Table 24: *Overview of the CRISPR/Cas13 gRNA designs, to make gene editing possible of the point mutation present in Padi6 mutated genome and WT genome. In red the position of the U, which needs to be mismatched with the A needed to be edited.*

Position of mismatching U in gRNA	Sequence (3'- -5')
Mutated genome (G>A, position g.11732)	
36	UCGAGGAAAGAUUAUCAUUCCACUGAGGGCGGAUCACGGGAGGAAGGGGU
34	UGUCGAGGAAAGAUUAUCAUUCCACUGAGGGCGGAUCACGGGAGGAAGGG
32	CUUGUCGAGGAAAGAUUAUCAUUCCACUGAGGGCGGAUCACGGGAGGAAG
WT genome	
36	CUUGUCGAGGAAAGAUUACCAUUCCACUGAGGGCGGAUCACGGGAGGAAG
34	GUCUUGUCGAGGAAAGAUUACCAUUCCACUGAGGGCGGAUCACGGGAGGA
32	UCGUCUUGUCGAGGAAAGAUUACCAUUCCACUGAGGGCGGAUCACGGGAG

5.3.2. Production Cas13 base editor

A plasmid containing the cDNA for dca s13-ADARdd, TC1316 (#164883, Addgene) is made available by the Zhang lab. IVT was conducted on this plasmid, in order to produce the Cas13 cRNA.

Again the IVT starts with the LR-PCR reaction of the plasmid. Primers used to perform this reaction were designed using the Primer3Plus program **(Table 25)**. These primers needed to be between 22 and 30 nts long, having <50% GC content, a low capacity of secondary structure formation and the annealing temperature needed to be between 58°C and 68°C.

Table 25: *Overview of the primers (two forward and one reversed primer) designed to perform IVT.*

Primer	Sequence
Forward 1	GTCGGATCCATCGAGAAGAA
Forward 2	GAAAGTCGGATCCATCGAGA
Reversed	CTTGTACAGCTCGTCCATGC

For the IVT mMESSAGE mMACHINE™ T7 ULTRA transcription kit (#AM1345, Thermo Fisher Scientific) was used. Using this kit the procedure starts also with a capped transcription reaction assembly where the transcription reaction is assembled at RT **(Table 26)**, mixed and incubated at 37°C for 1 hour, whereafter 1µL TURBO DNase was added and incubated for another 15 minutes at 37°C.

Table 26: *Overview of the different components with their used amount, mixed to make a capped transcription reaction possible.*

Component	Amount
Nuclease-free water	To 20µL
T7 2X NTP/ARCA	10µL
10X T7 Reaction Buffer	2µL
Linear Template DNA	0,1-1µg
T7 enzyme Mix	2µL

Before recovery of the RNA can take place, a poly(A) tailing procedure needed to be performed. To the RNA solution tailing reagents was added **(Table 26)**, after setting 2,5µL aside, 4µL *E*-PAP enzyme was added and incubated for 30 minutes at 37°C. Lastly, the RNA is recovered, again using the MEGAclear™ kit and quality was assessed by capillary electrophoresis (fragment analyzer, Agilent).

5.4. Statistics

By the use of SPSS® Statistics software (IBM) statistical analysis was performed. First, the normality and homogeneity of variance were evaluated using Shapiro-wilk and Levene's test. When the assumptions were met, one-way ANOVA analysis was performed to compare the means between different groups. If ANOVA showed significant statistical difference, a Tukey post-hoc test was conducted. If one or both assumptions were not met, the non-parametric Kruskal-Wallis test was performed. For each test the significance level was set at 0.05.

6. Results

6.1. Production of the mouse model

6.1.1. Optimalisation gene editing

WT mouse zygotes were electroporated with the CRISPR/Cas9 RNP complex targeting *Padi6* and a DNA template molecule containing the desired base pair substitution G>A. For the optimization of the procedure, a total of seven electroporation experiment was conducted.

In total n= 392 zygotes were collected from n=17 mice and divided into seven groups to compare embryonic development until blastocyst stage between the different electroporation conditions **(Table 27)**. First, the embryonic development was just compared between embryos electroporated with the forward template at 30V, negative control groups and medium control groups. Later, four extra conditions were added: electroporation with the forward template at 20V, the forward template together with an electroporation enhancer at 30V and lastly two groups of zygotes electroporated with the reversed template with and without enhancer at 30V. Because these last three conditions were not conducted in triplicate, no statistical analysis could be performed. All electroporation conditions were compared to each other and two different control groups, the medium and negative control. The medium control group contain embryos which did not undergo electroporation. The negative control groups includes embryos which did undergo electroporation, however with a nonfunctional CRISPR/Cas9 complex.

Table 27: *Overview of the electroporation optimization experiments, listing the surviving embryo numbers together with their percentage of survival and standard deviation per electroporation condition every day after the electroporation until the blastocyst stage. F/RRT = forward/reversed repair template, +E/-E= with/without enhancer. Morula and blastocyst percentages were calculated relative to the amount of two-cell embryos.*

Electroporation	**E0 (Fertilization)**	**E1 (Two-cell)**	**E2 (Morula)**	**E3,5 (Blastocyst)**
Padi6 KO (20V; FRT; -E)	39	33 (84,62% ±9,19)	20 (60,61%)	20 (60,61%)
Padi6 KO (30V; FRT; -E)	108	105 (97,22% ±14,73)	89 (84,76% ±14,52)	37 (35,24% ±6,01)
Padi6 KO (30V; FRT; +E)	28	28 (100%)	28 (100%)	8 (28,57%)
Padi6 KO (30V; RRT; -E)	55	55 (100%)	55 (100%)	27 (49,09%)
Padi6 KO (30V; RRT; +E)	43	43 (100%)	43 (100%)	15 (34,88%)
Negative control	19	13 (68,42% ±2,31)	10 (76,92% ±0,58)	9 (69,23% ±1)
Medium control	101	88 (87,13% ±10,39)	70 (79,55% ±6,11)	40 (45,45% ±4,72)

Figure 9 provides an overview of the mean developmental rate each day per experimental condition. From the curves, no big differences in blastocyst formation rate between the different electroporation groups, at least performed two times, could be observed. Statistical analysis confirmed no significant difference existed (p=0,583). Even though no statical analysis from the last three electroporation conditions could be done, the figure shows no big difference concerning the blastocyst formation rate between these last electroporation conditions and control groups.

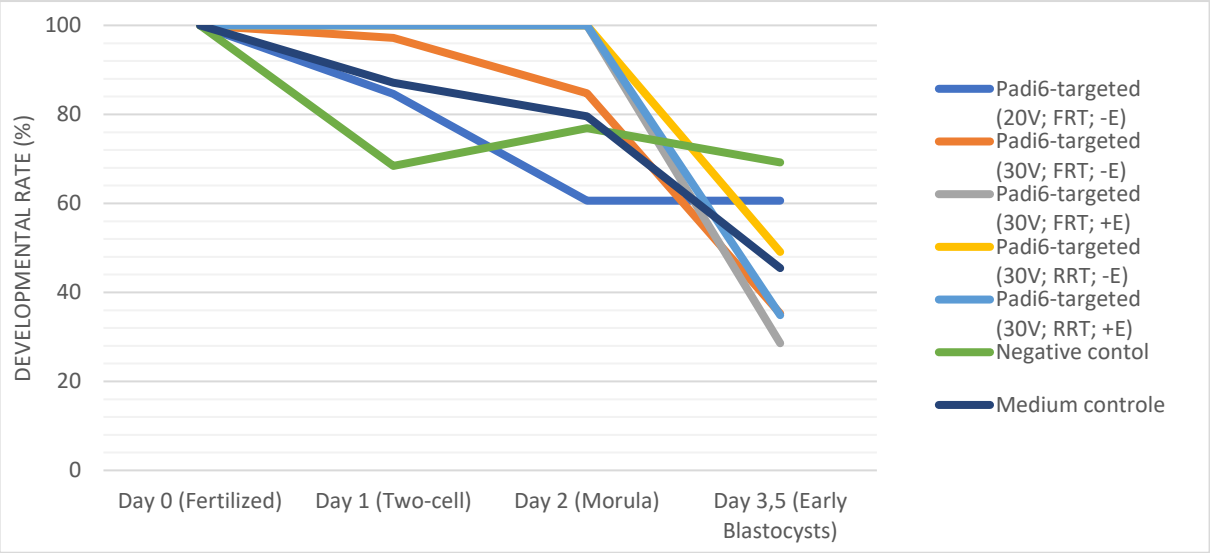

Figure 9: *Developmental rate percentages until E3,5 of embryos electroporated with different conditions, negative and medium control. Two-cell percentages were calculated relative to the amount of fertilized zygotes, whereas morula and blastocyst percentages were calculated relative to the amount of two-cell embryos. The exact embryo numbers are listed in* ***Table 27*** *.*

A sequence analysis of *Padi6*-targeted embryos electroporated with the forward repair template, with or without enhancer and at 20V or 30V was performed. **Figure 10** shows the mean mutagenesis efficiency (indels) per experimental group (left). Since repair occurred in several embryos, however, always mosaic, calculating the mean repair efficiency would not be so informative. Therefore, in **Figure 10** (right), the percentage of embryos having a repair efficiency >5% (right) is depicted for the different conditions.

The embryos electroporated at 20V show a significantly lower mean mutagenesis efficiency compared to the other two conditions (p<0,001). Although the mean mutagenesis efficiency of the embryos electroporated at 30V without and with enhancer differs (98,30% > 71,68%), the statistical analysis showed no significant difference between these groups (p=0,121). As for the repair efficiency it is seen that in only one out of nineteen (5,26%) embryos electroporated at 20V, repair took place in a mosaic fashion since 38,49% of the NGS reads harbored the base repair substitution of interest. Also in only one out of seven (14,29%) embryos electroporated at 30V with an enhancer repair was present, this time only in 8,13% of the cells and lastly in 10 out of 73 (13,70%) embryos electroporated at 30V without enhancer, repair took place with mosaicism varying between 0,13 and 64,18%. These results turned out to be not statistically different from each other (p=0.598). The exact mutagenesis and repair efficiencies per analyzed embryo per condition are shown in **Table S1**.

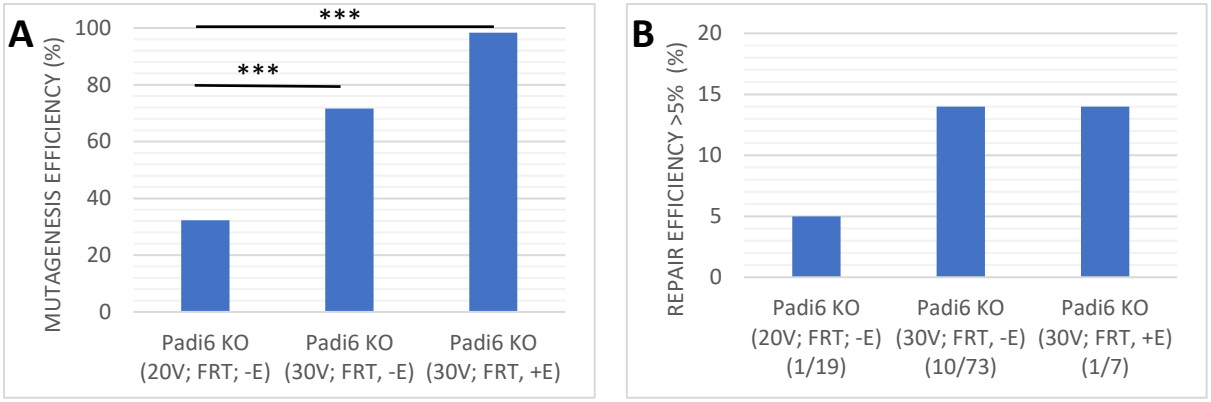

Figure 10: *(A) Mean mutagenesis efficiencies of embryos per electroporation condition (20V, 30V without enhancer (-E) and 30V with enhancer (+E), all with forward repair template (FRT)), with significancy (p<0,001, ***). (B) Percentage of electroporated embryos with a repair efficiency >5% per electroporation condition.*

Due to unavailability of NGS sequencing, embryos electroporated with the reversed repair template at 30V with and without enhancer were preliminary analyzed by Sanger sequencing **(Table S2)**. Appearance of the repair was evaluated based on the presence of the g.12426G>A substitution. However, this method is not sensitive enough to discriminate multiple low frequent alleles within one sample, therefore NGS analysis will be performed as well.

6.1.2. Electroporation experiments followed by ET

From the optimization experiments, all conditions applying 30V during electroporation were highly efficient, which was applied during further experiments. Furthermore, inclusion of a negative control in the exploratory experiments showed that electroporation did not have any influence on the survival of the embryos. Therefore, during the following electroporation experiments, only a medium control was incorporated. A total of six electroporation experiments to obtain genetically adapted embryos to conduct ET were performed **(Table 28)**.

Table 28: *Overview of the electroporation experiments followed by ET, listing the surviving embryo numbers together with their percentage of survival and standard deviation per electroporation condition every day after the electroporation until the blastocyst stage. F/RRT = forward/reversed repair template, +E/-E= with/without enhancer.*

Electroporation	Day 0 (Fertilization)	Day 1 (Two-cell)	Day 2 (Morula)	Day 3,5 (Blastocyst)
Padi6 KO (20V; FRT; -E)	14	10 (71,43%)	9 (90%)	9 (90%)
Padi6 KO (30V; FRT; -E)	239	230 (96,23% ±36,15)	203 (88,26% ±32,71)	168 (73,04% ±23,54)
Padi6 KO (30V; FRT; -E; Template conc. X2)	83	73 (87,95% ±9,19)	72 (98,63% ±8,49)	35 (47,95% ±14,85)
Padi6 KO (30V; FRT; +E)	16	15 (93,75%)	14 (93,33%)	14 (93,33%)
Padi6 KO (30V; RRT; -E)	57	52 (91,23% ±21,21)	50 (96,15% ±22,63)	30 (57,69% ±9,90)
Padi6 KO (30V; RRT; +E)	58	42 (72,41% ±11,31)	29 (69,05% ±20,51)	10 (23,81% ±7,07)
Medium controls	119	100 (84,03% ±8,12)	91 (91% ±8,15)	80 (80% ±8,82)

Electroporated embryos that reached the early blastocyst stage were used for fresh embryo transfer if, after mating of CD1 female mice with vasectomized males, a plug was observed the following morning. When none of the mice showed a plug, the embryos were vitrified for later use or cultured till E4,5 to perform a PADI6 immunostaining (thirteen KO and nine

controls, see 6.1.5 Immunostaining WT and KO embryos). N=65 of the embryos electroporated with the FRT were vitrified form which 24 were already used to perform three ETs, resulting in one mouse giving birth to two pups. Moreover, 40 embryos electroporated with the RRT with and without an enhancer were also vitrified, but not yet used for ET.

A total of n=13 mice underwent ET, of which n=6 mice gave birth, even though, according to weight measurements of the female mice during the days following embryo transfer, we expected more mice to give birth. The average combined litter size was n=3 pups. However, when the litter obtained from WT embryos was excluded, the average litter size dropped to n=2 pups, suggesting an effect of CRISPR/Cas9 targeting and/or the corresponding experimental procedures. Because the ET procedure was never conducted before in our lab, the first mouse was transferred with twelve WT blastocysts. This transfer resulted in an offspring of six pups born seventeen days after ET. Nine ET were conducted with fresh *Padi6* KO embryos. All these embryos were electroporated at 30V with the FRT form which ±15 without the use of an enhancer, ±15 with enhancer and 58 with a 2 times higher concentration of the repair template. From the ET using the electroporated embryos without enhancer, n=2 mice successfully gave birth to seven pups. The ETs (n=4) with embryos electroporated with a 2x higher concentration of the repair template, resulted in one mouse having three pups. Lastly, only one mouse was transferred using the embryos electroporated with an enhancer, which turned out not successful. As an attempt to achieve more mice having a plug, the female CD1 mice were put on the dirty male bedding three days before mating, and when they were five months of age, they were replaced by younger mice (ET 10/03/2022) **(Table 29)**.

Analysis on toe tissue of the resulting (potential mosaic) offspring revealed a high editing efficiency, although we have not yet identified offspring with the incorporation of the desired G>A point mutation **(Table 29)**.

Table 29: *Overview of the performed ET experiments; date of transfer, the number of vitrified or non-vitrified embryos that were transferred. DOB = date of birth, Vit = vitrified INS = insertion, DEL = deletion, WT = wild type.*

Date ET	DOB mother	# transferred embryos	Electroporation conditions	Fresh/ Vit	DOB	Litter size	Sex	Mutation	Editing efficiency (%)	Note
6/11/2021	15/09/2021	12	Medium controls	Fresh	25/11/2021	6	/	WT		
18/11/2021	15/09/2021	13	30V; FRT; -E	Fresh	06/12/2021	3	M	INS1	100	Kept for breeding
							F	INS1+DEL14	99,83	Kept for breeding
							M	INS1	100	
22/11/2021	15/09/2021	17	30V; FRT; -E	Fresh	/	/	/	/		Deceased during procedure
22/11/2021	15/09/2021	13	30V; FRT; -E	Vit	11/12/2021	2	M	INS1+DEL4	93,07	
							F	DEL7+INS4	69,78	
25/11/2021	15/09/2021	15	30V; FRT; -E	Fresh	13/12/2021	5	M	WT		
							M	WT		
							M	INS1	37,70	Kept for breeding
							F	INS1+bp substitution	34,25	
							F	INS1+DEL8	100	Kept for breeding
17/12/2021	15/09/2021	14	30V; FRT; -E	Vit	/	/	/	/		
17/12/2021	15/09/2021	14	30V; FRT; -E	Vit	/	/	/	/		
25/01/2022	15/09/2021	14	30V; 2x FRT; -E	Fresh	11/02/2021	3	M	INS2	99,88	
							F	DEL2	99,91	Kept for experiment
							F	INS1	99,65	Kept for experiment
25/01/2022	15/09/2021	14	30V; 2x FRT; -E	Fresh	/	/	/	/		
1/02/2022	15/09/2021	15	30V; 2x FRT; -E	Fresh	/	/	/	/		
1/02/2022	15/09/2021	15	30V; 2x FRT; -E	Fresh	/	/	/	/		
10/03/2022	26/01/2022	±15	30V; FRT; -E	Fresh	28/03/2021	1	/	/		Pre-weaning death
10/03/2022	26/01/2022	±15	30V; FRT; +E	Fresh	/	/	/	/		/

6.1.3. Zygote collection from *Padi6* KO mice

In order to evaluate the development of embryos originating from PADI6-deficient oocytes, three female *Padi6* KO mice obtained following the embryo transfer experiments described above, underwent ovarian stimulation, overnight mating with a B6D2F1 male, and were then sacrificed to collect their zygotes. As a control, a B6D2F1 female was sacrificed as well, to enable comparison of the development between *Padi6* KO and WT embryos possible. During the first experiment, some of the oocytes/embryos were fixated and later stained for PADI6 (6.1.5 Immunostaining WT and KO embryos).

By comparing the survival of the collected WT and KO embryos, it was seen that some oocytes obtained from *Padi6* KO females failed to fertilize, and when they did fertilize, embryos arrested between the one-cell and two-cell stage, whereas the WT embryos did not arrest **(Table 30 and Figure S1, S2, S3, S4)**. N=20 embryos from the first collection were stained for PADI6 (see 6.1.5 Immunostaining WT and KO embryos), eight embryos (four KO and four WT) were fixated at E1, while four controls and eight KO embryos were fixated the following day. Moreover, after collections, ovaries of both WT and KO mice were fixated to later make and stain tissue coupes.

Table 30: *Overview of zygote collections of Padi6-targeted F0 mice, listing the surviving embryo numbers per condition every day after collection. During the first collection, both zygotes, unfertilized oocytes and two-cell stage embryos were removed from the developmental follow up to perform immunostaining and genome analysis. Numbers indicated in red are the amount of embryos fixated at day 0 and indicated in blue are the amount of embryos fixated at day 1.*

Collection	Type	Day 0 (Zygote)		Day 1 (Two-cell)	Day 2 (Morula)	Day 3.5 (Early Blasto)
		2 PN or 2 PB	Unfertilized			
1	WT	14 (-4)	1	10/10 (-5)	5/5	5/5
	Padi6 KO	7 (-2) (-4)	13 (-2) (-4)	0/5	0/5	0/5
2	WT	11	9	2/11	0/11	0/11
	Padi6 KO	22	22	9/22	0/22	0/22
3	WT	5	0	1/5	0/5	0/5
	Padi6 KO	4	7	4/4	4/4	4/4

6.1.4. Breeding with KO male and female mice

Two male and two female founder mice were mated with WT C57BL/6 mice to establish a stable mutant line. This mating was executed to validate whether the KO mutation was present in their germ cells – thus hereditary – and whether these mice were fertile. Three trios were set up, containing two female and one male mice. Over two months of time, the two trios containing a KO male mouse produced eight litters **(Table 31)**. The trio with the KO female mice on the other hand did not give birth during these two months. The resulting offspring was genotyped through Sanger sequencing, to confirm whether the expected *Padi6* mutation was present in heterozygosity. Only the mice showing heterozygosity were kept for further research. Interestingly, male 2 developed epilepsy, which is a phenotype also recurring in human.

Table 31: *Overview of all the litters resulting from the breedings set up between a Padi6 KO male and two WT female. Next to the set up trio, date of birth (DOB) of the pups, litter size, mutated/WT and sex is presented.*

KO male mouse in trio	DOB	Litter size	Genotype
Male 1	04/03/2022	8	WT
	28/03/2022	8	/
	13/04/2022	11	WT
	29/04/2022	6	WT
Male 2	06/03/2022	7	4 KO 3 WT
	07/03/2022	5	1 KO 4 WT
	30/03/2022	3	/
	09/05/2022	9	4 KO 5 WT

6.1.5. Immunostaining WT and KO embryos

Three immunostaining experiments were performed. The first two immunostainings were conducted on WT and *Padi6*-targeted embryos, for which we expected close to 100% editing efficiency, taking our previous experiments into account. The third staining was performed on both embryos and fertilized oocytes originating from *Padi6*-targeted F0 mice.

During the first immunostaining experiment, n=18 embryos were stained, divided into three groups. The control group and electroporated at 30V with the forward repair template or KO group both contained eight WT or electroporated embryos and from each group one embryo was not incubated with the primary Ab serving as the negative control **(Figure S5)**. For the following staining, n=27 embryos electroporated at 30V with the forward repair template, from which thirteen with enhancer and fourteen without enhancer, ten negative and medium controls were stained **(Figure S6)**. In the third experiment, n=20 WT embryos and unfertilized oocytes or embryos originating from *Padi6*-targeted F0 mice, were fixated over two days (day 0 and day 1) to stain the different stages until development arrest occurred **(Figure 11)**.

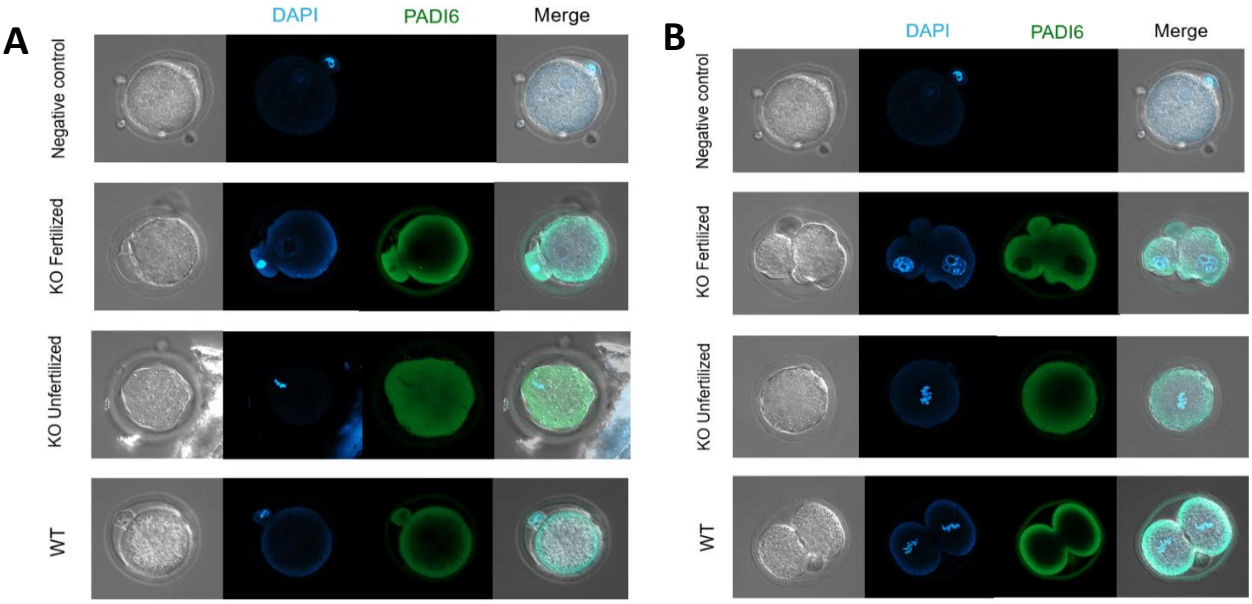

Figure 11: *IF image of* PADI6 *(green) expression in wild-type (WT), KO embryos and unfertilized oocytes and negative control embryos fixated on (A) E0 or (B) E1.*

In the first two stainings, a signal was observed in both the control and electroporated groups. Unexpectedly, in the third experiment, a fluorescent signal was also observed in oocytes and embryos obtained from *Padi6*-targeted F0 mice. In all stained oocytes and embryos, the fluorescent signal was located cytoplasmatic, more specifically in the subcortex.

6.1.6. Hematoxylin and eosin ovarian staining

A hematoxylin and eosin (H&E) staining on the collected stimulated WT and KO mouse ovaries was performed. Hematoxylin stains the cell nuclei purplish blue, whereas eosin provides a pink color to the cytoplasm and extracellular matrix structures. The presence of the different follicle maturation stages was verified and compared **(Figure 12)**. Presence of the different oocyte maturation stages in both WT and *Padi6* KO ovaries indicates that loss of *Padi6* has no influence on the follicle maturation process.

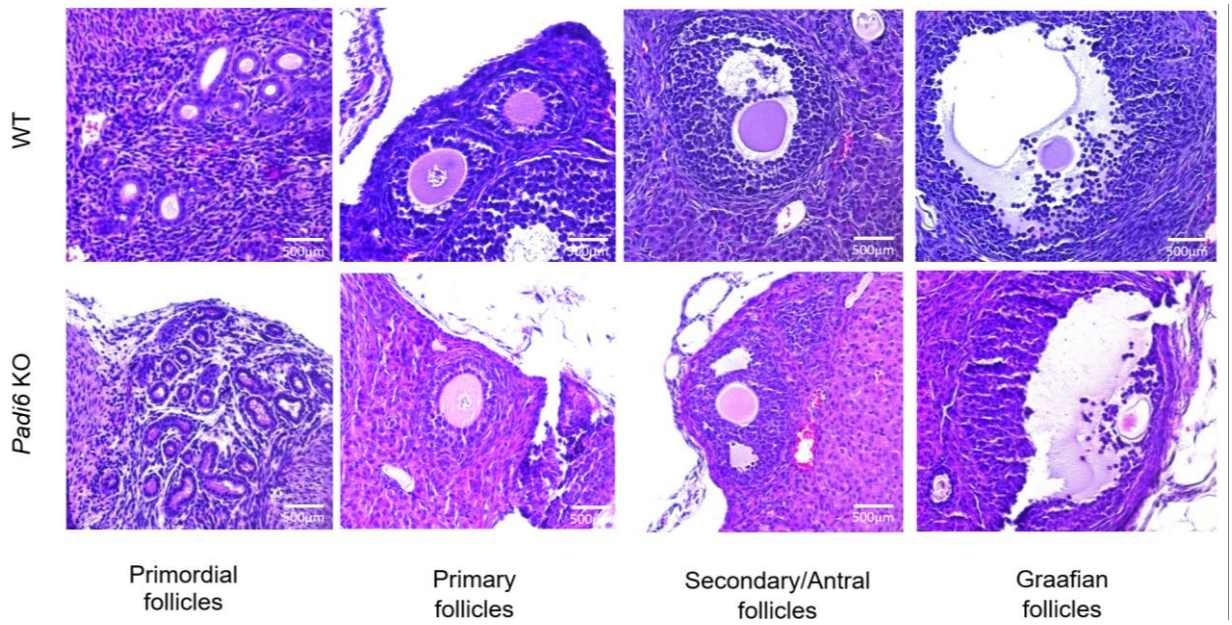

Figure 12: *H&E staining of the fixated WT and Padi6 KO mouse ovaries indicating the presence of the different oocyte maturation stages. Scale bar = 500µm*

6.2. Production of *Padi6* cRNA

To produce *Padi6* cRNA, a LR-PCR of the cDNA clone (NM_153106) containing the *Padi6* cDNA was performed, followed by restriction digest and ligation of the cDNA into an expression vector. These plasmids were transfected to *E.Coli* bacteria. Once the bacteria were grown on the agar plate **(Figure S7)**, colony PCR to asses correct ligation was performed **(Figure S8)**. These results revealed which colonies incorporated the plasmid containing *Padi6* cDNA, only colony five and fourteen did not contain the insert. Sanger sequencing of the positive colonies revealed the incorporation of two unexpected mutations into the *Padi6* cDNA **(Table 32 and Figure S9)**. Therefore, sequential mutagenesis using adapted primers containing the base pair change was performed in order to restore the wild type genetic sequence.

Table 32: *Overview of the unexpected incorporated mutations in the Padi6 cDNA after ligation of the insert and expression vector.*

Position (refseq)	Base	Old codon	New codon	Old AA	New AA
c.238	A>G	ACT	GCT	Thr	Ala
c.416	T>C	ATC	ACC	Ile	Thr

Once the first mutagenesis, meant to restore the c.238A>G mutation, was performed, Sanger sequencing was used to select successfully mutagenized colonies. The outcome showed that

in only three out of 24 (12,5%) plasmids the mutagenesis was successful. In two of these plasmids not only the restore took place, but also an insertion of 106bp and deletion of 1bp were found **(Figure S10)**. Therefore, only the DNA of one plasmid could be further used. With this plasmid, the same approach was followed to restore the c.416T>C mutation. Mutagenesis was successful in two of the twelve (16,67%) colonies that were analyzed by Sanger sequencing. Again in only one plasmid the mutation was restored without the appearance of other mutations **(Figure S11)**. This plasmid was stored until IVT was being performed. After a successful first IVT of the *Padi6* cDNA, the concentration of the recovered RNA was measured, showing a stock concentration of 196ng/µL and analyzed by capillary electrophoresis for quality assessment **(Figure 13)**.

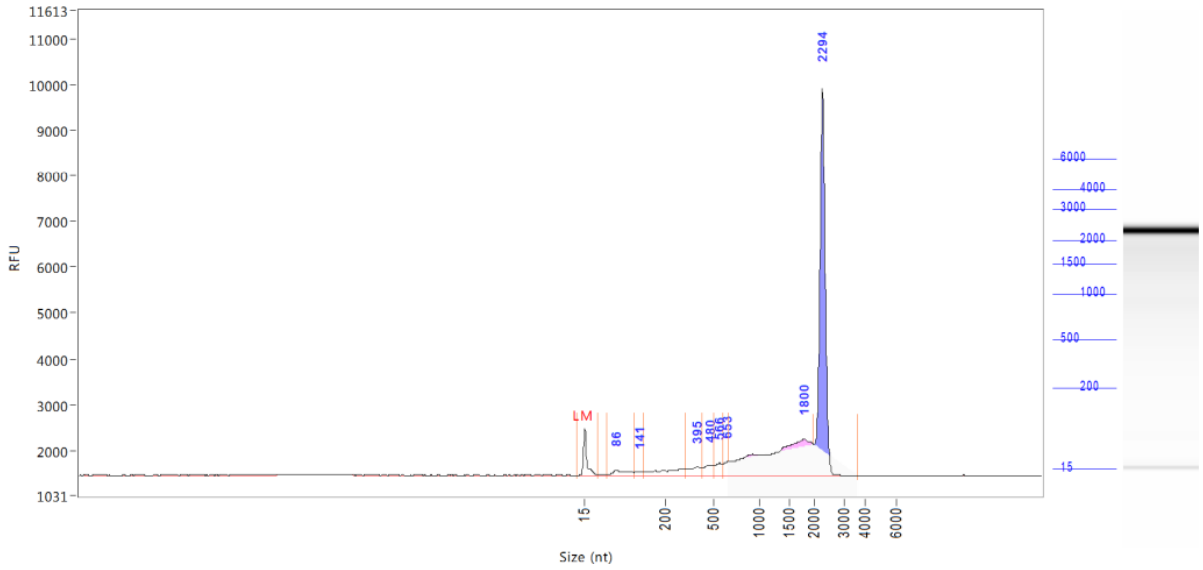

Peak	Size (nt)	Conc. (ng/uL)	From (nt)	To (nt)	RFU
1	15 (LM)	0.0296	0	45	1015
2	86	0.1286	66	128	111
3	141	0.0517	128	151	76
4	395	0.1589	326	428	175
5	480	0.1470	428	501	219
6	566	0.1410	501	601	258
7	653	0.0934	601	657	299
8	1800	2.5301	657	2001	790
9	2294	2.8540	2001	3653	8450

TIC:	6.1048	ng/uL
TIM:	18.5634	nmole/L
Total Conc.:	6.3463	ng/uL
28S/18S:	11.8	
RQN	10.0	

Figure 13: *Fragment analyzation results of the by IVT produced Padi6 mRNA.*

6.3. CRISPR/Cas13 base editing

6.3.1. Optimization LR-PCR

First a LR-PCR of the TC1316 plasmid was performed using two sets of designed LR primers. Analysis of the resulting product on the fragment analyzer revealed a concentration of 1,8ng/µL, which was too low to conduct IVT.

By adapting the amount of the primers and template and annealing temperature, a second LR-PCR was conducted, resulting in an increased amount of the product: 84,4 ng/µL and 103,8 ng/µL **(Figure 14)**. Where the added amount of the primers was 0,4µM in the first LR-PCR, the added primer amount was now 1µM. As for the template, instead of adding 1µL or 0,193µg,

0,5µg was added in the second attempt. Furthermore, the annealing temperature was set to 60°C instead of 68°C.

A

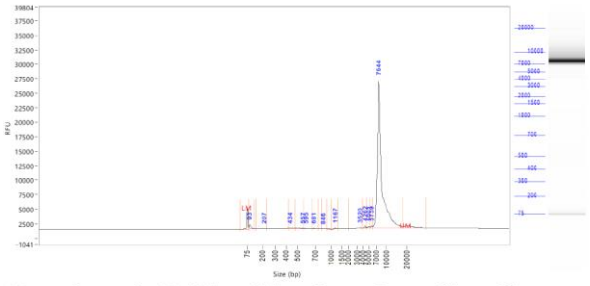

Peak	Size (bp)	Concentration (ng/uL)	Relative concentration Percent	Molarity (nmole/L)	From (bp)	To (bp)	CV%	RFU
1	75 (LM)	0,5000		11,2364	20	84	6,85	3818
2	93	2,2965	2,1	39,2784	84	133	8,39	835
3	207	0,3268	0,3	2,8281	148	226	11,04	53
4	434	0,4017	0,4	1,4686	421	480	3,79	68
5	557	0,5568	0,5	1,7451	480	574	5,34	64
6	595	0,3242	0,3	0,8864	574	668	3,39	67
7	681	0,1367	0,1	0,3304	668	746	1,02	115
8	846	0,1385	0,1	0,2669	819	914	2,13	69
9	1167	0,2720	0,2	0,3876	1012	1334	2,60	234
10	3520	0,2583	0,2	0,1329	2030	3840	12,03	96
11	4262	0,4875	0,4	0,1875	3840	4566	2,93	369
12	5001	0,5932	0,5	0,1978	4566	5277	3,73	286
13	5759	0,5251	0,5	0,1533	5277	5966	3,67	289
14	7644	103,8391	94,3	19,8827	5966	18334	21,03	25224
15	20000 (UM)	0,2062		0,0158	18334	29676	10,56	393
	TIC:	110,1564	ng/uL					
	TIM:	67,7456	nmole/L					
	Total concentration:	110,8770	ng/uL					

B

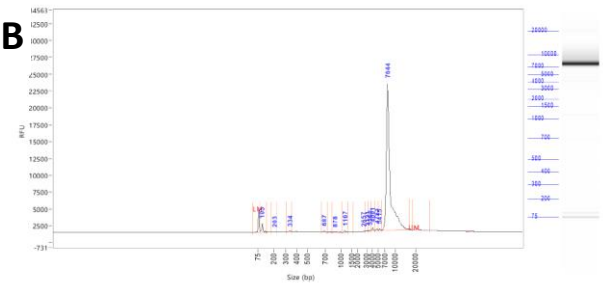

Peak	Size (bp)	Concentration (ng/uL)	Relative concentration Percent	Molarity (nmole/L)	From (bp)	To (bp)	CV%	RFU
1	75 (LM)	0,5000		11,2364	31	86	6,11	3561
2	105	3,0858	3,4	49,2003	86	139	8,33	1314
3	203	0,2134	0,2	1,7807	179	222	4,63	58
4	334	0,2059	0,2	1,0203	305	354	3,14	56
5	667	0,2994	0,3	0,7215	660	733	1,12	212
6	678	0,2029	0,2	0,3778	823	1023	4,40	65
7	1167	0,3217	0,4	0,4572	1023	1311	2,25	257
8	2657	0,1005	0,1	0,0665	1641	2800	10,38	63
9	3121	0,1316	0,1	0,0716	2800	3321	3,23	70
10	3560	0,1126	0,1	0,0522	3321	3840	2,94	97
11	4001	0,6895	0,8	0,2806	3840	4435	2,85	522
12	4783	0,4843	0,5	0,1678	4435	5000	2,74	313
13	5415	0,5003	0,6	0,1531	5000	5897	4,54	266
14	7644	84,3552	93,0	16,5347	5897	17143	16,76	21711
15	20000 (UM)	0,0888		0,0070	18572	27316	6,56	383
	TIC:	90,7032	ng/uL					
	TIM:	70,8844	nmole/L					
	Total concentration:	92,1116	ng/uL					

Figure 14: *The fragment analyzation results of TC1316 plasmid LR-PCR optimizations using (A) first primer pair and (B) second primer pair.*

6.3.2. IVT of the TC1316 plasmid

The LR-PCR with the first primer set was used as input for IVT. The first conducted IVT resulted in the recovery of RNA with a concentration of 130ng/µL, whereas the concentration of the produced product form the second IVT, where the second primer set was used, was only 18,5µg/µL. Again the product was analyzed by capillary electrophoresis for quality assessment **(Figure 15)**.

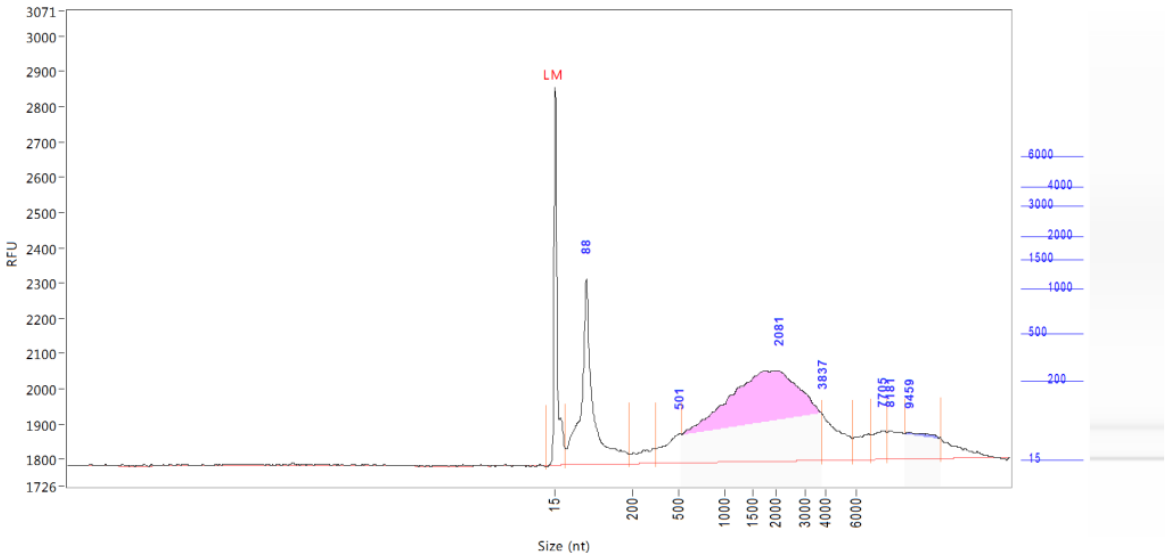

Peak	Size (nt)	Conc. (ng/uL)	From (nt)	To (nt)	RFU
1	15 (LM)	0.0296	0	40	1068
2	88	0.4973	40	190	525
3	501	0.0959	344	527	81
4	2081	1.4097	527	3837	255
5	3837	0.1345	3837	5798	134
6	7705	0.0580	6953	8030	79
7	8181	0.0629	8030	9184	78
8	9459	0.1083	9184	11515	75

TIC:	2.3665	ng/uL
TIM:	19.4214	nmole/L
Total Conc.:	2.5155	ng/uL
28S/18S:	0.0	
RQN	9.8	

Figure 15: *Fragment analyzation results of the by IVT produced TC1316 plasmid insert Cas13 base editor, s13d-ADARdd.*

7. Discussion

7.1. Production of the mouse model

The first goal of this project was to produce a mouse model containing a substitution of G>A on position 1582. For this, we opted to electroporate mouse embryos at the zygote stage, a process which has previously been optimized in our lab to obtain efficient gene knock-out (optimal settings 30V pulses, 2 pulses of 2ms and 100ms between each pulls)[77]. This optimized protocol was implemented in our experimental set-up, however, we still investigated how slight adaptations influenced the homology-directed repair pathway, while maintaining a good embryos development rate as well.

The performed electroporation optimization experiments showed no significant difference in blastocyst formation rate between the groups electroporated with *Padi6*-targeting CRISPR/Cas9 components, the negative control group, and the medium control group. Therefore, we concluded that the electroporation process itself, the voltage parameter (20V vs 30V), and the presence of the CRISPR/Cas9 components do not have and influence on blastocyst formation ability. Moreover, we tested some additional conditions, such as the addition of an electroporation enhancer. However, not in multiple replicates, so from these experiments, no conclusions on influence on blastocyst formation rate can be drawn yet. It must be noted that, in general, blastocyst formation rates were rather low, compared to earlier

findings[77]. We suspect that this is probably due to the experimental set-up and a practical learning curve. More specially, a crucial factor is speed, and we believe a long incubation time into KSOM-HEPES medium, outside of the incubator during the procedure, might have influenced the developmental rates as previous research also investigated[81,82]. To avoid this problem, the mice could be for instance sacrificed one by one, instead of at the same time, and experiments could be performed with two operators instead of one.

Next-generation sequencing analysis allowed for the calculation of the mutagenesis (indel) and repair (base pair substitution) efficiency per electroporated embryo. The revealed significant lower mutagenesis efficiency of the embryos electroporated at 20V compared to 30V conditions shows that the 30V conditions are preferred in order to obtain genetically adapted mice. Considering the HDR pathway, in which we were mostly interested, in general a low number of embryos were observed containing the precise base pair substitution of interest. If precise editing was observed, it was also always in a mosaic fashion, meaning there is still room to improve the efficiency. It is known that that the NHEJ pathway is dominant over the HDR pathway, which explains these low percentages[54,64,83,84]. Previous studies showed that adding a electroporation enhancer has the ability to increase the HDR rate[85–87]. Therefore, an electroporation enhancer was added to the RNP complex and electroporation using the reverse repair template, possibly in the combination of the enhancer were conducted. Still the experiment needs to be repeated and NGS needs to be performed in order to conclude the success of these interventions. The use of an electroporation enhancer seems to influence general mutagenesis efficiency, but did not influence the HDR rate. Whether the use of different repair templates (such as the revers template tested here once), has an influence, needs to be determined in additional experiments. Up until now it is not yet clear which condition is best to obtain a good repair efficiency in a high amount of embryos. If possible it would be advised to not use the electroporation enhancer. The used enhancer is dissolved in dimethyl sulfoxide (DMSO)[88] and as research has determined, DMSO has a cytotoxic effect on the mouse preimplantation embryos[89]. From our developmental curves **(Figure 9)**, this cytotoxic effect could potentially already be noticed, looking at the blastocyst formation rates of the performed experiments, but, since include embryo numbers are low, the experiments must be further repeated. Moreover, the repair efficiency could be enhanced in other ways[90,91]. Instead of trying to increase the HDR efficiency, the NHEJ pathway could be inhibited. Different chemical elements or small interfering RNA (siRNA) can be used to inhibit key regulators of this pathway. The downside of these methods is the presence of many safety issues. The use of chemicals are able to increase the toxicity and lead to apoptosis. Moreover, the low repair efficiency could occur due to a low repair potency of the gene itself. Even though the low repair efficiencies, the numbers concerning repair efficiency show that at least one in seven electroporated embryos carries the desired point mutation. Injection at the oocyte stage instead of at the zygote stage could have a positive influence, but is practically more challenging[92].

In general, the higher the editing percentage, the higher the amount of cells containing the mutation and, if we would proceed to embryo transfer, the higher the chance that the mutation of interest would be present in the germ cells of the obtained pups. From the numbers we have shown here, it could be estimated that one out of seven pups would carry the specific point mutation. However, these pups are mosaic, so there is no guarantee that the germ cells would contain the mutation of interest, which would be necessary to obtain a constitutive mutant mouse line. Furthermore, indications from our, and previous research we expect that only the male mice are fertile and can transfer the mutation their offspring [29,33]. In conclusion, there is a one in fourteen chance that a pup would contain the desired mutation, albeit in a mosaic fashion.

Although for each ET experiment three or four CD1 mice were mated with a vasectomized male, none, one or two mice showed a plug the next day, not being abnormal but which complicated fresh ET attempts[93,94]. Therefore, we have also conducted ET experiments with vitrified-thawed embryos, however, inexperience with the technique might have compromised pregnancies with these pups. Alternatively, to boost the number of fresh ET experiments, from

the fifth ET experiment onwards, the female mice were put on the dirty bedding of the male mice, three days before the mating, in order to provoke the Whitten effect. Due to the presence of male pheromones, the estrus stage of the estrous cycle can be induced, which makes the females receptive to mating[95,96]. We have obtained mixed effects with this approach, however only conclusions can be drawn from this approach when performed for an increased number of experiments. Looking at the different ET experiments itself, it stands out the ET efficiency was rather acceptable during the first attempts, but was decreasing by time. AT the moment the female CD1 mice were five months of age, new mice were bought to check if age has an influence on the ET efficiency. The first experiments with the new CD1 mice were not successful to date, so it is still unsure what the reasons behind the latest failures are. Interestingly, weight measurements of the mice after embryo transfer often indicated that these mice could be pregnant. However, only some provided offspring. Either the pregnancy was lost during the last stages, or the pups were still born and removed by either the mothers or the caretakers before we had the chance to notice. Lastly, it is also possible that the mother showed a phantom pregnancy. Other research showed the use of the mNSET device leads to an pregnancy rate around 80% and in 35% of the cases to live born mice[97,98].

Failed attempts of ET could be attributed to a number of factors. Firstly, due to inexperience with the technique. Previous research has shown that in the first year of using the mNSET device to perform ET, a decrease of the pregnancy rate and pups born alive was observed compared to when the surgical technique was used[97]. Due to more experience, they observed an increase in efficiency, which even surpassed the one obtained using the surgical method. Next, the application of genome editing itself and potential toxicity of the products could also influence the success rate, which is also seen in previous research[97]. In order to rule out one of these problems as possible cause, each time ET with KO embryos is carried out ,a control ET with negative or medium control embryos should be carried out in parallel. As an alternative, ET could also be conducted in surgical manner, but literature stated the non-surgical would be better[99–101]. Not only the success rate is low, the technique is more complex, slower, more expensive, more likely to get contaminated and there is a need of specialized apparatus.

Nonetheless, the obtained offspring from this project showed high editing efficiency, but the desired mutation was not yet incorporated. Because repair appeared in a small amount of electroporated embryos, there is a lower chance the right embryo implanted in the uterus and gave rise to a live offspring. One way to make sure the right embryos are transferred and implanted is by performing a pre-implantation genetic test on the electroporated embryos[102]. During this procedure a few cells are taken from the trophectoderm of the formed electroporated blastocyst to analyze the genome. On top of the higher price, the technique is rather complex, because several risky steps such as electroporation, biopsy at E3.5, vitrification and thawing, need to be performed. Therefore, in order to obtain the mouse model containing the desired point mutation, ET experiments should continue to be performed regularly.

Six mice form the ET's resulting offspring were kept for further breeding. Most interest went to the male pups because these mice are able to transfer the mutation to their offspring in order to produce a constitutive *Padi6* KO mouse line. But also four female mice were kept to check if they were indeed infertile, which was confirmed by two experiments: firstly, the female KO mice were not able to produce any offspring over a breeding of two months. Secondly, collection and follow up experiments of the embryos obtained form *Padi6*-targeted F0 mice, showed decreased fertilization rates, embryos arrested between E1 and E2, while more fertilization and less arrest was present in the WT group, which corresponds to the literature (mouse and human) [34,36,37,41].

The breeding set-up with male KO mice resulted in different litters with an average litter size of seven. Furthermore, we checked heterozygosity of the resulting offspring, which indicated that in fact only one of the two kept KO males carried indicated *Padi6* mutation in the germ cells, because all litters from male 1 were always WT. This is an excellent example of

mosaicism, since analysis of toe tissue from this mouse showed a *Padi6* mutation, while his germ cells apparently did not contain any mutation. Heterozygous offspring will be further bred to obtain both *Padi6* $^{+/+}$ and *Padi6* $^{-/-}$ mice, to use in further experiments.

7.1.1. Immunostaining experiments

Immunostaining of *Padi6* KO embryos collected from *Padi6*-deficient mice, electroporated and WT embryos were conducted in order to evaluate the PADI Ab purchased form Biorbyt.

Visualization of the stained embryos showed the presence of a fluorescent signal in the WT embryos as well as in the electroporated and KO embryos. Because no signal was present in the embryos from the negative control, no non-specific staining of the secondary antibody was present. As the *Padi6* gene was mutated on zygote level by electroporation, PADI6 protein should no longer be produced. Furthermore, the EGA phenomenon, taking place at E1, causes degradation of the present maternal products, such as PADI6, and no further PADI6 production in later developmental stages[103]. Due to these reasons PADI6 should not be detectible after staining was performed on the blastocyst stages of the KO embryos.

Appearance of the PADI6 signal in the electroporated embryos could be attributed to different reasons. First of all, it could be possible PADI6 was still present from the zygote stage and the protein degraded slow or not at all. Therefore some PADI6 was still present in the embryos at the moment of fixation. But because the embryos were fixated and stained at the blastocyst stage, no degradation of PADI6 is peculiar. Further, the genome of the stained embryos will be analyzed by NGS to make sure the genome of these embryos was indeed edited and editing failure can be ruled out as possible cause of a clear PADI6 signal. Lastly, the fact that the used Ab did not work specific enough is another reason for the presence of PADI6 staining. Because staining of the KO embryos also showed a clear PADI6 signal, it is most likely the used PADI6 Ab did not bind specifically on PADI6, but would also bind on other PADI proteins found in the subcortex, such as PADI2, PADI3 and PADI4[104].

To confirm PADI6 protein absence in KO embryos, additional antibodies should be assessed or their specificity, but not many are available. Coonrod's research group produced their own PADI6 Ab, which was successfully used[33]. If possible, a collaboration could be set up. Investigating PADI6 production at mRNA level instead of protein level is another method to examine successful *Padi6* targeting. The amount of *Padi6* mRNA production is measured by performing real-time quantitative PCR (qPCR), which makes use of a reversed transcription reaction[105].

7.1.2. Hematoxylin-eosin staining experiments

H&E staining of the WT and KO mouse ovary tissues was conducted in order to evaluate the follicle formation ability in *Padi6* KO mice compared to WT mice. These stainings revealed all the different follicle developmental stages were present in both ovaries. Therefore it could be concluded the *Padi6* mutation did not have any influence on the maturation of the oocytes, which is corresponding with previous findings in the already existing EDA mouse models, other SCMC mouse models and humans[17,41,106–108]. These investigations showed the knock-out of these genes had no influence on the folliculogenesis, all follicle developmental stages were found in WT as well as mutated individuals.

Furthermore, the ultrastructure of the collected WT and KO oocytes can be visualized and analyzed using transmission electron microscopy (TEM)[109,110]. As PADI6 is required for the CPLs formation, we mainly expect to see defects in these structures.

7.2. Production of *Padi6* cRNA

In order to evaluate the *Padi6* cRNA injection method, *Padi6* cRNA was produced by transferring the *Padi6* cDNA of a clonal vector to an expression vector followed by IVT. As mentioned, unexpected substitutions were incorporated into the *Padi6* cDNA. These mutations were solved by performing two consecutive mutagenesis. Despite the mutagenesis efficiency of the used kit is around 90%, a success rate amounted only 12,5% and 16,67% for the first

and second performed mutagenesis[111,112]. The low efficiency could be linked to the sequence of the targeted DNA sequence. These can acquire secondary structures, such as stem-loops. It is possible that these structures interfere with the annealing of the used primers, which needs to occur simultaneously in order to provide a successful mutagenesis. PCR-fragmented directed DNA synthesis could be performed if the mutagenesis efficiency wanted to be increased[113]. With this technique a region of the DNA lying between the annealed selection and mutagenic primers is being amplified, in order to generate the desired mutant DNA sequence. Later on, by using this fragment as a primer, heteroduplex DNA is produced. The high efficiency of this site-directed mutagenesis method is possible due to presence of both, the desired and selection mutation, into the formed fragment. To avoid the limitations of this method, a cDNA library could also be made ourselves, but is time consuming and more expensive[114]. A cDNA library is made by *Padi6* mRNA isolation followed by reversed transcription to the gene's cDNA and ending with ligation in to an expression vector, which is then transfected to *E. Coli* bacteria. Because the mRNA is mostly present in the oocyte, a large number of oocytes is needed in order to obtain a usable *Padi6* mRNA amount to perform these different steps.

Even though a low mutagenesis efficiency rate was observed, one of the formed plasmids was further used to perform a successful IVT. Measuring of the formed mRNA concentration and evaluation of the fragment analyzer results, showed the success of the conduct experiment. A good quality (RQN = 10) and concentration (2,85ng/µL) of the *in vitro* transcribed mRNA was obtained. In the future the produced mRNA will be delivered into WT mouse zygotes in order to investigate the different delivery efficiency using different methods, by electroporation or by injection, and the *in vivo* expression of the mRNA[115]. When these are optimized, the mRNA will be delivered into *Padi6* KO mouse zygotes and the functionality will be examined.

7.3. CRISPR/Cas13 base editing

Such as the CRISPR/Cas9 technique, two components are needed in order to apply the CRISPR/Cas13 technique: gRNA, which can be bought, and the Cas13 base editor, which is not yet commercially available as a protein, but as plasmid containing the Cas13 base editor's cDNA[69].

In order to conduct a successful IVT experiment, the concentration of the LR-PCR product needs to be at least 0,2µg/µL[116]. Meaning the obtained TC1316 LR-PCR product concentration was too low to be able to conduct IVT. In order to obtain a higher concentration a LR-PCR optimization experiment was set up. In the first place, minimal recommended amount of primer and template was used. By increasing the amount of primers and template and decreasing the temperature of the primer annealing step, a concentration >0,2µg/µL was obtained. To perform LR-PCR, primers with a predicted melting temperature of 60-65°C need to be produced[117]. Furthermore, the used of a lower annealing temperature would be beneficial for the PCR reaction due to the enhance of the PCR-suppression effect[118].

These optimized LR-PCR conditions were further used to produce the *in vitro* transcribed mRNA of Cas13-ADAR$_{dd}$. Even though the obtained concentrations were quite low, the mRNA was of good quality (RQN=9,8). Further, this mRNA will be delivered by electroporation into WT zygotes together with a pre-formed fluorophore[119]. When the mRNA is translated a fluorescence signal will be present revealing *in vivo* transcription of the produced mRNA is possible. Due to a low obtained mRNA concentration, it is to be expected no signal will be seen and so no transcription will take place. In order to solve this problem, the cDNA insert of the TC1316 plasmid can be transferred to the same expression vector used to express *Padi6* cDNA. As seen in experiment performing IVT of the *Padi6* cDNA, a high concentration of good quality mRNA was achieved. If the *in vivo* transcription is successful, WT mouse zygotes will be used to optimize the CRISPR/Cas13 technique. Eventually, the CRISPR/Cas13 technique will be applied on the zygotes of the produced mouse model.

Other than the achievement of a high concentration of good quality, the approach provides more challenges[120,121]. Next to the arising batch-to-batch variabilities during the preparation of Cas mRNA, the introduction of the Cas enzyme's mRNA leads to a later functionality of the enzyme, due to the fact *in vivo* translation to the proteins still needs to take place. In addition, by co-delivering the gRNA and Cas mRNA, it is possible that once the Cas mRNA is fully translated, the gRNA starts to degrade. By delaying gRNA delivery or chemically modify the gRNA molecule, its stability can be enhanced. In addition, Cas mRNA is less stable and susceptible to degradation by present RNAses, making fast degradation possible. Next, some other elements occurring during this procedure makes the base editing method challenging[122]. Firstly, limitation in the targeted site can occur, making base editing difficult. Further, there is always a chance for the appearance unexpected off-targets. Due to the fact PADI6 is normally expressed during the oocyte and zygote stages and important for the first cleavage stages, timing of the CRISPR/Cas13 administration is important to make sure a functional editing can take place. Further research should reveal at which stage the CRISPR/Cas13 administration is the most functional.

8. Conclusion

This thesis forms the basis for further research on possible strategies to overcome EDA in a mouse model. Starting the project, it was aimed to produce a mouse model containing a specific mutation in the *Padi6* gene, which was shown to induce EDA in one patient. By performing electroporation with *Padi6*-targeting CRISPR/Cas components of mouse zygotes followed by ET of the resulting blastocyst, genetically edited mouse were obtained. More specifically, *Padi6* KO mice were obtained, mainly containing a 1bp insertion, yet no model displayed the desired mutation, c.1582G>A was obtained. In order to incorporate the specific mutation, HDR needs to take place in the electroporated embryos in an efficient manner. However, NGS analysis of these embryos revealed that a low number of embryos underwent HDR, and if they did, it was in a mosaic fashion. In order to increase the HDR efficiency to obtain the specific mutation into the genome, further modifications of the protocol should be evaluated.

As a *Padi6* KO mouse model is already obtained and *Padi6* cRNA is produced in this thesis, both nuclear transfer and cRNA administration can already be assessed for their potency as a good treatment strategy.

If the treatment strategies prove to be efficient in mice, still some hurdles will have to be overcome to bring this research from bench to bedside. Firstly, *Padi6* cRNA administration is only possible in patients with *PADI6* mutations. For patients diagnosed with EDA caused by mutations present in other MEGs, such as *NLRP2, NLRP5, NLRP7, TLE6, KHDC3 and OOEP,* administration of this cRNA would not be helpful, so cRNA of their mutated genes should be first administered and evaluated in mice. Secondly, although NT represents a more general and practical treatment strategy, this technique entails various ethical and safety concerns. Lastly, even though CRISPR/Cas13 base editing is the newest technique and carries the same disadvantage as the *Padi6* cRNA method, it is a good model to investigate the potential of this method to solve infertility and could be promising towards other techniques.

9. Reference list

1. Wang, H. *et al.* Physiological and molecular determinants of embryo implantation. *Molecular Aspects of Medicine* vol. 34 (2013).

2. Shi, L. & Wu, J. Epigenetic regulation in mammalian preimplantation embryo development. *Reproductive Biology and Endocrinology* vol. 7 (2009).

3. Bhakta, H. H., Refai, F. H. & Avella, M. A. The molecular mechanisms mediating mammalian fertilization. *Development (Cambridge)* vol. 146 (2019).

4. Talbot, P., Shur, B. D. & Myles, D. G. Cell adhesion and fertilization: Steps in oocyte transport, sperm-zona pellucida interactions, and sperm-egg fusion. *Biology of Reproduction* vol. 68 (2003).

5. Simons, J. & Fauci, L. A Model for the Acrosome Reaction in Mammalian Sperm. *Bulletin of Mathematical Biology* **80**, (2018).

6. Lefièvre, L. *et al.* Four zona pellucida glycoproteins are expressed in the human. *Human Reproduction* **19**, (2004).

7. Yonezawa, N., Kanai-Kitayama, S., Kitayama, T., Hamano, A. & Nakano, M. Porcine zona pellucida glycoprotein ZP4 is responsible for the sperm-binding activity of the ZP3/ZP4 complex. *Zygote* **20**, (2012).

8. Boja, E. S., Hoodbhoy, T., Fales, H. M. & Deanll, J. Structural Characterization of Native Mouse Zona Pellucida Proteins Using Mass Spectrometry. *Journal of Biological Chemistry* **278**, (2003).

9. Yeste, M., Jones, C., Amdani, S. N. & Coward, K. Oocyte activation and fertilisation: Crucial contributors from the sperm and oocyte. in *Results and Problems in Cell Differentiation* vol. 59 (2017).

10. Paonessa, M., Borini, A. & Coticchio, G. Genetic causes of preimplantation embryo developmental failure. *Molecular Reproduction and Development* vol. 88 (2021).

11. Hemberger, M., Hanna, C. W. & Dean, W. Mechanisms of early placental development in mouse and humans. *Nature Reviews Genetics* vol. 21 (2020).

12. Xu, Y. *et al.* Mutations in PADI6 Cause Female Infertility Characterized by Early Embryonic Arrest. *American Journal of Human Genetics* **99**, (2016).

13. Palermo, G., Joris, H., Devroey, P. & van Steirteghem, A. C. Pregnancies after intracytoplasmic injection of single spermatozoon into an oocyte. *The Lancet* **340**, (1992).

14. Betts, D. H. & Madan, P. Permanent embryo arrest: Molecular and cellular concepts. *Molecular Human Reproduction* **14**, (2008).

15. Hanna, C. W., Demond, H. & Kelsey, G. Epigenetic regulation in development: Is the mouse a good model for the human? *Human Reproduction Update* **24**, (2018).

16. Bebbere, D., Masala, L., Albertini, D. F. & Ledda, S. The subcortical maternal complex: multiple functions for one biological structure? *Journal of Assisted Reproduction and Genetics* vol. 33 (2016).

17. Bebbere, D. *et al.* Expression of maternally derived KHDC3, NLRP5, OOEP and TLE6 is associated with oocyte developmental competence in the ovine species. *BMC Developmental Biology* **14**, (2014).

18. Bebbere, D., Albertini, D. F., Coticchio, G., Borini, A. & Ledda, S. The subcortical maternal complex: Emerging roles and novel perspectives. *Molecular Human Reproduction* vol. 27 (2021).

19. Mitchell, L. E. Maternal effect genes: Update and review of evidence for a link with birth defects. *Human Genetics and Genomics Advances* vol. 3 (2022).

20. Aghajanova, L. *et al.* No evidence for mutations in NLRP7, NLRP2 or KHDC3L in women with unexplained recurrent pregnancy loss or infertility. *Human Reproduction* **30**, (2015).

21. Duéñez-Guzmán, E. A. & Haig, D. The evolution of reproduction-related NLRP genes. *Journal of Molecular Evolution* vol. 78 (2014).

22. Chen, B. *et al.* Novel mutations and structural deletions in TUBB8: Expanding mutational and phenotypic spectrum of patients with arrest in oocyte maturation, fertilization or early embryonic development. *Human Reproduction* **32**, (2017).

23. Feng, R. *et al.* Mutations in TUBB8 and Human Oocyte Meiotic Arrest . *New England Journal of Medicine* **374**, (2016).

24. McCoy, R. C. *et al.* Tripolar chromosome segregation drives the association between maternal genotype at variants spanning PLK4 and aneuploidy in human preimplantation embryos. *Human Molecular Genetics* **27**, (2018).

25. Wang, H. *et al.* The nucleolar protein NOP2 is required for nucleolar maturation and ribosome biogenesis during preimplantation development in mammals. *FASEB Journal* **34**, (2020).

26. Qin, Y. *et al.* Targeted disruption of Noc4l leads to preimplantation embryonic lethality in mice. *Protein and Cell* vol. 8 (2017).

27. Cubellis, M. V. *et al.* Loss-of-function maternal-effect mutations of PADI6 are associated with familial and sporadic Beckwith-Wiedemann syndrome with multi-locus imprinting disturbance. *Clinical Epigenetics* **12**, (2020).

28. Xia, X. *et al.* Characterization of the porcine peptidylarginine deiminase type VI gene (PADI6) promoter: Sp1 regulates basal transcription of the porcine PADI6. *Gene* **575**, (2016).

29. Kan, R. *et al.* Regulation of mouse oocyte microtubule and organelle dynamics by PADI6 and the cytoplasmic lattices. *Developmental Biology* **350**, (2011).

30. Snow, A. J. *et al.* Phosphorylation-dependent interaction of tyrosine 3-monooxygenase/ tryptophan 5-monooxygenase activation protein (YWHA) with PADI6 following oocyte maturation in mice. *Biology of Reproduction* **79**, (2008).

31. Huang, B. *et al.* Padi6 regulates trophoblast cell migration-invasion through the hippo/yap1 pathway in hydatidiform moles. *Journal of Inflammation Research* **14**, (2021).

32. Liu, X. *et al.* Role for PADI6 in securing the mRNA-MSY2 complex to the oocyte cytoplasmic lattices. *Cell Cycle* **16**, (2017).

33. Yurttas, P. *et al.* Role for PADI6 and the cytoplasmic lattices in ribosomal storage in oocytes and translational control in the early mouse embryo. *Development* **135**, (2008).

34. Liu, J. *et al.* Two novel mutations in PADI6 and TLE6 genes cause female infertility due to arrest in embryonic development. *Journal of Assisted Reproduction and Genetics* **38**, (2021).

35. Rezaei, M. *et al.* Novel pathogenic variants in NLRP7, NLRP5, and PADI6 in patients with recurrent hydatidiform moles and reproductive failure. *Clinical Genetics* **99**, (2021).

36. Zheng, W. *et al.* New biallelic mutations in PADI6 cause recurrent preimplantation embryonic arrest characterized by direct cleavage. *Journal of Assisted Reproduction and Genetics* **37**, (2020).

37. Wang, X. *et al.* Novel mutations in genes encoding subcortical maternal complex proteins may cause human embryonic developmental arrest. *Reproductive BioMedicine Online* **36**, (2018).

38. Qian, J. *et al.* Biallelic PADI6 variants linking infertility, miscarriages, and hydatidiform moles. *European Journal of Human Genetics* **26**, (2018).

39. Eggermann, T., Kadgien, G., Begemann, M. & Elbracht, M. Biallelic PADI6 variants cause multilocus imprinting disturbances and miscarriages in the same family. *European Journal of Human Genetics* **29**, (2021).

40. Buono, R. J. *et al.* Genetic variation in PADI6-PADI4 on 1p36.13 is associated with common forms of human generalized epilepsy. *Genes (Basel)* **12**, (2021).

41. Esposito, G. *et al.* Peptidylarginine deiminase (PAD) 6 is essential for oocyte cytoskeletal sheet formation and female fertility. *Molecular and Cellular Endocrinology* **273**, (2007).

42. Darwish, E. & Magdi, Y. A preliminary report of successful cleavage after calcium ionophore activation at ICSI in cases with previous arrest at the pronuclear stage. *Reproductive BioMedicine Online* **31**, (2015).

43. Ebner, T. *et al.* Treatment with Ca2+ ionophore improves embryo development and outcome in cases with previous developmental problems: A prospective multicenter study. *Human Reproduction* **30**, (2015).

44. Baltaci, V. *et al.* The effectiveness of intracytoplasmic sperm injection combined with piezoelectric stimulation in infertile couples with total fertilization failure. *Fertility and Sterility* **94**, (2010).

45. Tesarik, J., Rienzi, L., Ubaldi, F., Mendoza, C. & Greco, E. Use of a modified intracytoplasmic sperm injection technique to overcome sperm-borne and oocyte-borne oocyte activation failures. *Fertility and Sterility* **78**, (2002).

46. Hsu, P. D., Lander, E. S. & Zhang, F. Development and applications of CRISPR-Cas9 for genome engineering. *Cell* vol. 157 (2014).

47. Capecchi, M. R. Altering the genome by homologous recombination. *Science (1979)* **244**, (1989).

48. Rudin, N., Sugarman, E. & Haber, J. E. Genetic and physical analysis of double-strand break repair and recombination in Saccharomyces cerevisiae. *Genetics* **122**, (1989).

49. Plessis, A., Perrin, A., Haber, J. E. & Dujon, B. Site-specific recombination determined by I-SceI, a mitochondrial group I intron-encoded endonuclease expressed in the yeast nucleus. *Genetics* **130**, (1992).

50. Rouet, P., Smih, F. & Jasin, M. Introduction of double-strand breaks into the genome of mouse cells by expression of a rare-cutting endonuclease. *Molecular and Cellular Biology* **14**, (1994).

51. Choulika, A., Perrin, A., Dujon, B. & Nicolas, J. F. Induction of homologous recombination in mammalian chromosomes by using the I-SceI system of Saccharomyces cerevisiae. *Molecular and Cellular Biology* **15**, (1995).

52. Bibikova, M. *et al.* Stimulation of Homologous Recombination through Targeted Cleavage by Chimeric Nucleases. *Molecular and Cellular Biology* **21**, (2001).

53. Bibikova, M., Beumer, K., Trautman, J. K. & Carroll, D. Enhancing gene targeting with designed zinc finger nucleases. *Science* vol. 300 (2003).

54. Schubert, M., Thommandru, B. & Wang, B. Want to achieve higher rates of homology-directed repair in your CRISPR HDR experiment? *https://eu.idtdna.com/pages/education/decoded/article/want-to-achieve-higher-rates-of-homology-directed-repair-(hdr)-in-your-crispr-experiment* (2018).

55. Smith, J. *et al.* A combinatorial approach to create artificial homing endonucleases cleaving chosen sequences. *Nucleic Acids Research* **34**, (2006).

56. Urnov, F. D. *et al.* Highly efficient endogenous human gene correction using designed zinc-finger nucleases. *Nature* **435**, (2005).

57. Miller, J. C. *et al.* An improved zinc-finger nuclease architecture for highly specific genome editing. *Nature Biotechnology* **25**, (2007).

58. Miller, J. C. *et al.* A TALE nuclease architecture for efficient genome editing. *Nature Biotechnology* **29**, (2011).

59. Cong, L. *et al.* Multiplex genome engineering using CRISPR/Cas systems. *Science (1979)* **339**, (2013).

60. Jinek, M. *et al.* A programmable dual-RNA-guided DNA endonuclease in adaptive bacterial immunity. *Science (1979)* **337**, (2012).

61. Adli, M. The CRISPR tool kit for genome editing and beyond. *Nature Communications* vol. 9 (2018).

62. Liang, P. *et al.* CRISPR/Cas9-mediated gene editing in human tripronuclear zygotes. *Protein and Cell* **6**, (2015).

63. Reardon, S. Step aside CRISPR, RNA editing is taking off. *Nature* vol. 578 (2020).

64. Xue, C. & Greene, E. C. DNA Repair Pathway Choices in CRISPR-Cas9-Mediated Genome Editing. *Trends in Genetics* vol. 37 (2021).

65. Liang, X., Potter, J., Kumar, S., Ravinder, N. & Chesnut, J. D. Enhanced CRISPR/Cas9-mediated precise genome editing by improved design and delivery of gRNA, Cas9 nuclease, and donor DNA. *Journal of Biotechnology* **241**, (2017).

66. Zhang, F., Wen, Y. & Guo, X. CRISPR/Cas9 for genome editing: Progress, implications and challenges. *Human Molecular Genetics* **23**, (2014).

67. Zuccaro, M. v. *et al.* Allele-Specific Chromosome Removal after Cas9 Cleavage in Human Embryos. *Cell* **183**, (2020).

68. Ma, H. *et al.* Correction of a pathogenic gene mutation in human embryos. *Nature* **548**, (2017).

69. Cox, D. B. T. *et al.* RNA editing with CRISPR-Cas13. *Science (1979)* **358**, (2017).

70. Huynh, N., Depner, N., Larson, R. & King-Jones, K. A versatile toolkit for CRISPR-Cas13-based RNA manipulation in Drosophila. *Genome Biology* **21**, (2020).

71. Abudayyeh, O. & Gootenberg, J. Tips and Tricks for Cas13. *https://zlab.bio/cas13*.

72. Zhang, C. *et al.* Structural Basis for the RNA-Guided Ribonuclease Activity of CRISPR-Cas13d. *Cell* **175**, (2018).

73. Abudayyeh, O. O. *et al.* RNA targeting with CRISPR-Cas13. *Nature* **550**, (2017).

74. Liu, Y. *et al.* REPAIR x, a specific yet highly efficient programmable A > I RNA base editor . *The EMBO Journal* **39**, (2020).

75. Alt-R™ HDR Design Tool. *https://eu.idtdna.com/site/order/designtool/index/HDRDESIGN*.

76. Platt, R. J. *et al.* CRISPR-Cas9 knockin mice for genome editing and cancer modeling. *Cell* **159**, (2014).

77. Pascal, E. Using CRISPR/Cas9 to study the first cell fate decision during early embryonic development. *https://lib.ugent.be/en/catalog/rug01:003008387?i=1&q=eva+pascal* (2021).

78. de Leeneer, K. *et al.* Flexible, scalable, and efficient targeted resequencing on a benchtop sequencer for variant detection in clinical practice. *Human Mutation* **36**, (2015).

79. Boel, A. *et al.* BATCH-GE: Batch analysis of Next-Generation Sequencing data for genome editing assessment. *Scientific Reports* **6**, (2016).

80. Truett, G. E. *et al.* Preparation of PCR-quality mouse genomic dna with hot sodium hydroxide and tris (HotSHOT). *Biotechniques* **29**, (2000).

81. Walters, E. A., Brown, J. L., Krisher, R., Voelkel, S. & Swain, J. E. Impact of a controlled culture temperature gradient on mouse embryo development and morphokinetics. *Reproductive BioMedicine Online* **40**, (2020).

82. Nguyen, Q. *et al.* Effects of opening the incubator on morphokinetics in mouse embryos. *European Journal of Obstetrics and Gynecology and Reproductive Biology* **229**, (2018).

83. Pinder, J., Salsman, J. & Dellaire, G. Nuclear domain “knock-in” screen for the evaluation and identification of small molecule enhancers of CRISPR-based genome editing. *Nucleic Acids Research* **43**, (2015).

84. Spencer, N. Y. Improved methods for CRISPR homology-directed repair (HDR) using Alt-R HDR Enhancer and ssDNA donors with optimized design. *https://eu.idtdna.com/pages/education/decoded/article/improved-methods-for-crispr-homology-directed-repair-(hdr)-using-alt-r-hdr-enhancer-and-ssdna-donors-with-optimized-design* (2019).

85. Li, X. *et al.* A high-efficiency and versatile CRISPR/Cas9-mediated HDR-based biallelic editing system. *Journal of Zhejiang University: Science B* **23**, (2022).

86. Schubert, M. S. *et al.* Optimized design parameters for CRISPR Cas9 and Cas12a homology-directed repair. *Scientific Reports* **11**, (2021).

87. Yu, C. *et al.* Small molecules enhance crispr genome editing in pluripotent stem cells. *Cell Stem Cell* **16**, (2015).

88. Genome editing with CRISPR-Cas9, IDT. *https://eu.idtdna.com/pages/products/crispr-genome-editing/alt-r-crispr-cas9-system?gclid=CjwKCAjwj42UBhAAEiwACIhADtO4uY9GK1Ztb_T2HgqPvNFcthzHE3NE8KlFMZm5cLATa5QmK64g5RoCnUkQAvD_BwE*.

89. Kang, M. H. *et al.* The cytotoxic effects of dimethyl sulfoxide in mouse preimplantation embryos: A mechanistic study. *Theranostics* **7**, (2017).

90. Liu, M. *et al.* Methodologies for improving HDR efficiency. *Frontiers in Genetics* vol. 10 (2019).

91. Yang, H. *et al.* Methods favoring homology-directed repair choice in response to crispr/cas9 induced-double strand breaks. *International Journal of Molecular Sciences* vol. 21 (2020).

92. Ma, H. *et al.* Ma et al. reply. *Nature* **560**, (2018).

93. Ma, W., Miao, Z. & Novotny, M. v. Induction of estrus in grouped female mice (Mus domesticus) by synthetic analogues of preputial gland constituents. *Chemical Senses* **24**, (1999).

94. Behringer, R., Gertsenstein, M., Nagy, K. V. & Nagy, A. Selecting female mice in estrus and checking plugs. *Cold Spring Harbor Protocols* **2016**, (2016).

95. Byers, S. L., Wiles, M. v., Dunn, S. L. & Taft, R. A. Mouse estrous cycle identification tool and images. *PLoS ONE* **7**, (2012).

96. Gangrade, B. K. & Dominic, C. J. Studies of the male-originating pheromones involved in the Whitten effect and Bruce effect in mice. *Biology of Reproduction* **31**, (1984).

97. bin Ali, R. *et al.* Improved pregnancy and birth rates with routine application of nonsurgical embryo transfer. *Transgenic Research* **23**, (2014).

98. van der Hoeven, F. A., Schouten, M. & de Boer, P. Embryo survival in pseudopregnant and in pregnant but genetically semi-sterile recipients after nonsurgical embryo transfer in the mouse. *Theriogenology* **36**, (1991).

99. Larson, M. A. Embryo Transfer Surgery. in *Methods in Molecular Biology* vol. 2066 (2020).

100. Steele, K. H. *et al.* Nonsurgical embryo transfer device compared with surgery for embryo transfer in mice. in *Journal of the American Association for Laboratory Animal Science* vol. 52 (2013).

101. Cui, L. *et al.* Transcervical embryo transfer in mice. *Journal of the American Association for Laboratory Animal Science* **53**, (2014).

102. Takeuchi, K. Pre-implantation genetic testing: Past, present, future. *Reproductive Medicine and Biology* vol. 20 (2021).

103. Blakeley, P. *et al.* Defining the three cell lineages of the human blastocyst by single-cell RNA-seq. *Development (Cambridge)* **142**, (2015).

104. Zhang, X. *et al.* Peptidylarginine deiminase 1-catalyzed histone citrullination is essential for early embryo development. *Scientific Reports* **6**, (2016).

105. Nolan, T., Hands, R. E. & Bustin, S. A. Quantification of mRNA using real-time RT-PCR. *Nature Protocols* **1**, (2006).

106. Yu, X. J. *et al.* The subcortical maternal complex controls symmetric division of mouse zygotes by regulating F-actin dynamics. *Nat Commun* **5**, (2014).

107. Begemann, M. *et al.* Maternal variants in NLRP and other maternal effect proteins are associated with multilocus imprinting disturbance in offspring. *Journal of Medical Genetics* **55**, (2018).

108. Monk, D., Sanchez-Delgado, M. & Fisher, R. NLRPS, the subcortical maternal complex and genomic imprinting. *Reproduction* vol. 154 (2017).

109. Nottola, S. A. *et al.* Ultrastructure of isolated mouse ovarian follicles cultured in vitro. *Reproductive Biology and Endocrinology* **9**, (2011).

110. Qin, D. *et al.* The subcortical maternal complex protein Nlrp4f is involved in cytoplasmic lattice formation and organelle distribution. *Development (Cambridge)* **146**, (2019).

111. Kalnins, A., Otto, K., Rüther, U. & Müller-Hill, B. Sequence of the lacZ gene of Escherichia coli. *EMBO J* **2**, (1983).

112. Dickinson, D. J., Ward, J. D., Reiner, D. J. & Goldstein, B. Engineering the Caenorhabditis elegans genome using Cas9-triggered homologous recombination. *Nature Methods* **10**, (2013).

113. Chen, X., Liu, W., Quinto, I. & Scala, G. High efficiency of site-directed mutagenesis mediated by a single PCR product. *Nucleic Acids Research* **25**, (1997).

114. Zhao, Y. X. *et al.* Construction of a cDNA library from the ephemeral plant olimarabidopsis pumila and preliminary analysis of expressed sequence tags. *Zeitschrift fur Naturforschung - Section C Journal of Biosciences* **68 C**, (2013).

115. Hashimoto, M. & Takemoto, T. Electroporation enables the efficient mRNA delivery into the mouse zygotes and facilitates CRISPR/Cas9-based genome editing. *Scientific Reports* **5**, (2015).

116. Beckert, B. & Masquida, B. Synthesis of RNA by in vitro transcription. *Methods Mol Biol* **703**, (2011).

117. Karunanathie, H., Kee, P. S., Ng, S. F., Kennedy, M. A. & Chua, E. W. PCR enhancers: Types, mechanisms, and applications in long-range PCR. *Biochimie* vol. 197 (2022).

118. Dai, Z. M., Zhu, X. J., Chen, Q. & Yang, W. J. PCR-suppression effect: Kinetic analysis and application to representative or long-molecule biased PCR-based amplification of complex samples. *Journal of Biotechnology* **128**, (2007).

119. Wang, C., Han, B., Zhou, R. & Zhuang, X. Real-Time Imaging of Translation on Single mRNA Transcripts in Live Cells. *Cell* **165**, (2016).

120. Glass, Z., Lee, M., Li, Y. & Xu, Q. Engineering the Delivery System for CRISPR-Based Genome Editing. *Trends in Biotechnology* vol. 36 (2018).

121. Cebrian-Serrano, A. *et al.* Maternal supply of cas9 to zygotes facilitates the efficient generation of site-specific mutant mouse models. *PLoS ONE* **12**, (2017).

122. Jeong, Y. K., Song, B. & Bae, S. Current Status and Challenges of DNA Base Editing Tools. *Molecular Therapy* vol. 28 (2020).

10. Poster

Investigation of novel treatment methods to overcome early embryonic developmental arrest due to *PADI6* mutations

Silke De Norre; Annekatrien Boel and Björn Heindryckx

Gent Fertility and Stem Cell Team (G-FaST) Department for Reproductive Medicine, Ghent University Hospital, Belgium

UNIVERSITEIT GENT — FACULTY OF MEDICINE AND HEALTH SCIENCES

UZ GENT — G-FaST Ghent Fertility and Stem cell Team

Introduction

Embryo Developmental Arrest (EDA) is a rare infertility phenotype, characterized by arrest of the embryo during the first cleavage stages, which is mainly attributed to inferior oocyte quality. One of the maternal genes already associated with EDA is *PADI6*. *PADI6 is* a maternal effect gene, whose mRNA transcripts are expressed exclusively in oocytes and early embryos, making them responsible for the first stages of embryonic development. As treatment options for EDA are limited, the majority of EDA patients has to rely on oocyte donation to obtain children. Therefore, research is set up to investigate new possible treatment options to overcome EDA using a mouse model.

Objectives

1. **Production of a *Padi6* mutant mouse model by CRISPR/Cas9-mediated DNA editing (c.1582G>A)** (Focus)
2. Use of the *Padi6* mutant mouse model to compare new possible EDA treatment options:
   - I. Nuclear transfer to replace the defective ooplasm
   - II. CRISPR/Cas13 mRNA base editing to correct the defective *Padi6* mRNA molecules
   - III. ***Padi6* complementary RNA (cRNA) injection, to complement the defective *Padi6* mRNA molecules** (Focus)

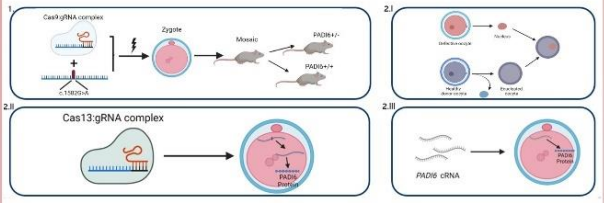

Figure 1: Schematic overview of the different objectives.
1.Shows the workflow of the *Padi6* mutant mouse model production, using the CRISPR/Cas9 DNA editing technique. The Cas9:gRNA complex, together with the template is being electroporated in a (wild-type) WT zygote. These electroporated embryos are then transferred to a pseudopregnant mouse. 2.I Shows the workflow of a nuclear transfer procedure, where the nucleus of the deceased oocyte (*PADI6* mutant) is isolated and transferred to a WT enucleated oocyte, containing functional *Padi6* mRNA molecules. 2.II CRISPR/Cas13 is used to edit the defective mRNA by the electroporation of a Cas13:gRNA complex into the defective zygote. Once the defective mRNA is repaired, transcription to the WT PADI6 protein can take place. 2.III Once WT cRNA is produced, this can be injected into the zygote. In this way the defective mRNA is complemented and WT Padi6 proteins can be produced.

Materials & Methods

1. Mouse model:

Employing the ECM 830 electroporator (BTX), electroporation was carried out at the zygote stage with the following settings: 30V, 2pulses, 100ms. At day 3,5 of *in vitro* culture, good quality embryos were transferred to pseudo-pregnant female mice using the Non-Surgical Embryo Transfer device for mice (mNSET™, #60010, ParaTech), according to the manufacturer's instructions. Either at the blastocyst stage (during optimization experiments) or using toe-tissue of 7-day old pups, DNA was extracted, PCR-amplified and assessed by NGS.

2.III *Padi6* cRNA Production:

By means of long-range PCR, restriction digest and ligation steps, *Padi6* cDNA was transferred from a commercial cloning vector (Origen) to an expression vector to produce *Padi6* cRNA. The incorporation and sequence of the cDNA insert was evaluated through colony PCR and Sanger Sequencing. To remove unexpected mutations, mutagenesis was performed using the Q5 Site directed mutagenesis kit from NEB.

Results

1. Production of mouse model

Wild-type (WT) mouse zygotes were electroporated with a CRISPR/Cas9 RNP complex targeting *Padi6* and a DNA template molecule containing the desired base pair substitution G>A. Comparison of electroporation set-ups revealed a drastic increase in editing efficiency in embryos electroporated at 30V (86%) compared to 20V (12%). Next, electroporation was conducted by applying optimized conditions (30V, 2 pulses, 100ms interval). Once the electroporated embryos reached the early blastocyst stage, they were used for embryo transfer (ET). N=10 mice underwent ET, of which n=3 mice got pregnant, resulting in an average litter size of n=3 pups. Analysis of the resulting (potential mosaic) offspring revealed a high editing efficiency, although we have not yet identified offspring with the incorporation of the desired G>A point mutation (**Table 1**).

Table 1: Overview of the successful ET experiments; date of transfer, the number of vitrified or non-vitrified embryos that were transferred. DOB = date of birth, INS = insertion, DEL = deletion, WT = wild type

ET	Date	# Transferred embryos	Vitrified embryos	DOB	Litter Size	Sex	Identified Mutations
1	18/11 2021	13	NO	6/12 2021	4	M	INS1
						F	INS1 + DEL14
						F	INS1
2	22/11 2021	13	YES	11/12 2021	2	M	INS1 + DEL3
						F	DEL7 + INS4
3	25/11 2021	15	NO	14/12 2021	5	M	WT
						M	WT
						M	INS1
						F	INS1 + base pair substitution
						F	INS1 +DEL8

2. Treatment options (focus cRNA)

To produce *Padi6* cRNA, *Padi6* cDNA has been incorporated into an active expression vector using *E. Coli* bacteria (**Figure 2**).

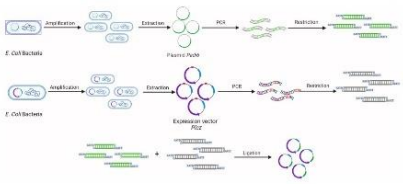

Figure 2: Schematic overview showing incorporation of the cDNA in the expression vector.

The newly formed plasmid contains unexpected mutations, which need to be restored (**Figure 3**). Therefore, mutagenesis using adapted primers is currently being performed (**Figure 4**).

```
col11.1F    GCTGTGGTCTGGAGGTCAATGAACCATCCCACAGTGGCATTGGTGAGGATGGTGGCGCCC  123
refseq      ACTGTGGTCTGGAGGTCAATGAACCATCCCACAGTGGCATTGGTGAGGATGGTGGCGCCC  297
col11.1R    GCTGTGGTCTGGAGGTCAATGAACCATCCCACAGTGGCATTGGTGAGGATGGTGGCGCCC  360
            ************************************************************

col11.1F    AGCCCCACTGTGGATGAAGACAAGGTGCTGGTCTCCTACTTCTGTCCTGACCAAGAAGTC  183
refseq      AGCCCCACTGTGGATGAAGACAAGGTGCTGGTCTCCTACTTCTGTCCTGACCAAGAAGTC  357
col11.1R    AGCCCCACTGTGGATGAAGACAAGGTGCTGGTCTCCTACTTCTGTCCTGACCAAGAAGTC  360
            ************************************************************

col11.1F    CCCACGGCCACAGCTGTGCTGTTTCTCACCGGCATCGAGATCTCCCTGGAGGCAGACATC  243
refseq      CCCACGGCCACAGCTGTGCTGTTTCTCACCGGCATCGAGATCTCCCTGGAGGCAGACATC  417
col11.1R    CCCACGGCCACAGCTGTGCTGTTTCTCACCGGCATCGAGATCTCCCTGGAGGCAGACATC  420
            ************************************************************
```

Figure 3: Print sanger sequence of the incorporated plasmid cDNA. Here a part of the plasmid cDNA (col11.1F and col11.1R) is compared to the WT DNA (refseq), the found mutations are marked in yellow.

A.

Primer pair 1: Padi6-2399 G-A
F: 5'-CAAAGAGGACACTGTGGTCTGGAG-3'
R: 5'-CCAGCGATGACGGAGCTA-3'

Primer pair 2: Padi6-2577 C-T
F: 5'-GAGGCAGACATCTATCGAGATG-3'
R: 5'-CAGGGAGATCTCGATGCC-3'

B.

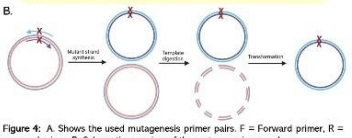

Figure 4: A. Shows the used mutagenesis primer pairs. F = Forward primer, R = reversed primer B. Schematic overview of the mutagenesis procedure

Conclusions/Future Perspectives

1. Production of mouse model

No HDR edited embryos were observed among the 10 mouse pups obtained by embryo transfer. Future perspectives include continuing ET and increase the repair efficiency.

2. Treatment options

Mutations were found in the *Padi6* cDNA incorporated in the plasmid in comparison with the WT sequence. No successful mutagenesis is performed yet. Once mutagenesis is successful, production and functional testing of cRNA will follow.

Next to cRNA injections, additional focus will be applied on the CRISPR/Cas13 treatment option, by optimizing the technology in WT mice.

Contact Details: silke.denorre@ugent.be - Phone: +32 479 68 24 11 - Connect with me on social media

11. Addendum

11.1. Supplementary Tables

Table S1: *Overview of NGS analyzes (mutagenesis and repair efficiencies) of each electroporated embryo per electroporation condition, used to optimize the zygote electroporation. All the embryos were electroporated with the forward repair template (FRT) at 20V or 30V and with or without enhancer (+E or -E).*

Electroporated Embryo	Mutagenesis efficiency (readpairs with indels / readpairs without indels)	Repair efficiency (readpairs with repair / total readpairs)
Padi6 KO 1 (20V; FRT; -E)	99,88% (870/1)	00,00%
Padi6 KO 2 (20V; FRT; -E)	0,63% (15/2350)	0,29% (7/2365)
Padi6 KO 3 (20V; FRT; -E)	56,58% (1139/874)	38,49% (775/2013)
Padi6 KO 4 (20V; FRT; -E)	99,72% (1836/5)	00,00%
Padi6 KO 5 (20V; FRT; -E)	99,41% (678/4)	00,00%
Padi6 KO 6 (20V; FRT; -E)	99,74% (391/1)	00,00%
Padi6 KO 7 (20V; FRT; -E)	0,66% (2/299)	0,33% (1/301)
Padi6 KO 8 (20V; FRT; -E)	0,79% (2/250)	0,39% (1/252)
Padi6 KO 9 (20V; FRT; -E)	1,07% (2/184)	00,00%
Padi6 KO 10 (20V; FRT; -E)	22,72% (220/748)	0,10% (1/968)
Padi6 KO 11 (20V; FRT; -E)	1,09% (11/992)	0,29% (3/1003)
Padi6 KO 12 (20V; FRT; -E)	1,76% (23/1278)	0,00%
Padi6 KO 13 (20V; FRT; -E)	1,10%(16/1429)	0,13% (2/1445)
Padi6 KO 14 (20V; FRT; -E)	19,16% (244/1029)	0,00%
Padi6 KO 15 (20V; FRT; -E)	0,82% (6/723)	0,27% (2/729)
Padi6 KO 16 (20V; FRT; -E)	65,42% (282/149)	0,00%
Padi6 KO 17 (20V; FRT; -E)	14,90% (97/554)	0,00%
Padi6 KO 18 (20V; FRT; -E)	1,40% (9/632)	0,00%
Padi6 KO 19 (20V; FRT; -E)	27,24% (188/502)	0,00%
Padi6 KO 1 (30V; FRT, -E)	100% (2/0)	00,00%
Padi6 KO 2 (30V; FRT, -E)	42,66% (64/86)	52,66% (79/150)
Padi6 KO 3 (30V; FRT, -E)	53,23% (263/231)	00,00%
Padi6 KO 4 (30V; FRT, -E)	55,90% (317/250)	36,15% (205/567)
Padi6 KO 5 (30V; FRT, -E)	95,09% (288/20)	3,67% (15/408)
Padi6 KO 6 (30V; FRT, -E)	98,50% (132/2)	00,00%
Padi6 KO 7 (30V; FRT, -E)	100% (1/0)	00,00%
Padi6 KO 8 (30V; FRT, -E)	35,42% (130/237)	56,13% (206/367)
Padi6 KO 9 (30V; FRT, -E)	88,16% (693/93)	8,65% (68/786)
Padi6 KO 10 (30V; FRT, -E)	95,45 % (42/2)	2,27% (1/44)
Padi6 KO 11 (30V; FRT, -E)	62,31% (169/103)	00,00%
Padi6 KO 12 (30V; FRT, -E)	84,24% (353/66)	11,45% (48/419)
Padi6 KO 13 (30V; FRT, -E)	99,75% (408/1)	00,00%
Padi6 KO 14 (30V; FRT, -E)	36,17% (17/30)	51,06% (24/47)
Padi6 KO 15 (30V; FRT, -E)	97,20% (521/15)	00,00%
Padi6 KO 16 (30V; FRT, -E)	98,11% (52/1)	00,00%
Padi6 KO 17 (30V; FRT, -E)	77,04% (1383/412)	00,00%
Padi6 KO 18 (30V; FRT, -E)	67,02% (252/124)	00,00%
Padi6 KO 19 (30V; FRT, -E) (Arrested)	98,96% (191/2)	00,00%
Padi6 KO 20 (30V; FRT, -E)	61,41% (444/279)	00,00%
Padi6 KO 21 (30V; FRT, -E) (Arrested)	10,71% (6/50	00,00%
Padi6 KO 22 (30V; FRT, -E) (Arrested)	28,57% (4/10)	00,00%
Padi6 KO 23 (30V; FRT, -E) (Arrested)	26,78% (30/82)	00,00%

Padi6 KO 24 (30V; FRT, -E) (Arrested)	72,82% (134/50)	00,00%
Padi6 KO 25 (30V; FRT, -E) (Arrested)	23,73% (244/784)	0,29% (3/1028)
Padi6 KO 26 (30V; FRT, -E)	0,83% (3/256)	00,00%
Padi6 KO 27 (30V; FRT, -E)	34,00% (521/1011)	0,13% (2/1532)
Padi6 KO 28 (30V; FRT, -E)	1,08% (9/820)	0,24% (2/829)
Padi6 KO 29 (30V; FRT, -E)	28,01% (297/763)	0,18% (2/1060)
Padi6 KO 30 (30V; FRT, -E)	95,87% (1466/63)	00,00%
Padi6 KO 31 (30V; FRT, -E)	99,82% (1726/3)	00,00%
Padi6 KO 32 (30V; FRT, -E)	99,86% (1485/2)	00,00%
Padi6 KO 33 (30V; FRT, -E)	1,76% (23/1278)	0,29% (3/1003)
Padi6 KO 34 (30V; FRT, -E)	1,10% (16/1429)	00,00%
Padi6 KO 35 (30V; FRT, -E)	19,16% (244/1029)	0,13% (2/1445)
Padi6 KO 36 (30V; FRT, -E)	0,82% (6/723)	00,00%
Padi6 KO 37 (30V; FRT, -E)	65,42% (282/149)	0,27% (2/729)
Padi6 KO 38 (30V; FRT, -E)	14,90% (97/554)	00,00%
Padi6 KO 39 (30V; FRT, -E)	1,40% (9/632)	00,00%
Padi6 KO 40 (30V; FRT, -E)	27,24% (188/502)	00,00%
Padi6 KO 41 (30V; FRT, -E)	94, 35 (853/51)	00,00%
Padi6 KO 42 (30V; FRT, -E) (Arrested)	99,78% (1831/4)	00,00%
Padi6 KO 43 (30V; FRT, -E) *(Arrested)*	100% (1/0)	00,00%
Padi6 KO 44 (30V; FRT, -E) (Arrested)	97,43% (683/18)	00,00%
Padi6 KO 45 (30V; FRT, -E) *(Arrested)*	99,93% (1495/1)	00,00%
Padi6 KO 46 (30V; FRT, -E)	96,76% (1912/64)	00,00%
Padi6 KO 47 (30V; FRT, -E)	100% (199/0)	00,00%
Padi6 KO 48 (30V; FRT, -E)	99,68% (1272/4)	00,00%
Padi6 KO 49 (30V; FRT, -E)	27,52% (259/682)	64,18% (604/941)
Padi6 KO 50 (30V; FRT, -E)	100% (105/0)	00,00%
Padi6 KO 51 (30V; FRT, -E)	99,83% (1200/2)	00,00%
Padi6 KO 52 (30V; FRT, -E)	96,91% (849/27)	00,00%
Padi6 KO 53 (30V; FRT, -E)	100% (808/0)	00,00%
Padi6 KO 54 (30V; FRT, -E)	99,95% (2142/1)	00,00%
Padi6 KO 55 (30V; FRT, -E)	95,81% (848/37)	00,00%
Padi6 KO 56 (30V; FRT, -E)	99,93% (1527/1)	00,00%
Padi6 KO 57 (30V; FRT, -E)	85,20% (432/75)	13,41% (68/507)
Padi6 KO 58 (30V; FRT, -E)	99,86% (734/1)	00,00%
Padi6 KO 59 (30V; FRT, -E)	100% (350/0)	00,00%
Padi6 KO 60 (30V; FRT, -E)	99,89% (918/1)	00,00%
Padi6 KO 61 (30V; FRT, -E)	100% (435/0)	00,00%
Padi6 KO 62 (30V; FRT, -E)	96,32% (708/27)	00,00%
Padi6 KO 63 (30V; FRT, -E)	100% (600/0)	00,00%
Padi6 KO 64 (30V; FRT, -E)	95,81% (458/20)	00,00%
Padi6 KO 65 (30V; FRT, -E)	41,59% (47/66)	00,00%
Padi6 KO 66 (30V; FRT, -E)	98,68% (678/9)	00,00%
Padi6 KO 67 (30V; FRT, -E)	24,32% (99/308)	62,40% (254/407)
Padi6 KO 68 (30V; FRT, -E)	99,17% (239/2)	00,00%
Padi6 KO 69 (30V; FRT, -E)	99,35%(460/3)	00,00%
Padi6 KO 70 (30V; FRT, -E)	99,85% (1374/2)	00,00%
Padi6 KO 71 (30V; FRT, -E)	87,35% (311/45)	10,67% (38/356)
Padi6 KO 72 (30V; FRT, -E)	98,22% (388/7)	00,00%
Padi6 KO 73 (30V; FRT, -E)	98,41% (310/5)	00,00%
Padi6 KO 1 (30V; FRT, +E)	98,93% (93/1)	00,00%
Padi6 KO 2 (30V; FRT, +E)	99,88% (897/1)	00,00%

Padi6 KO 3 (30V; FRT, +E)	100% (147/0)	00,00%
Padi6 KO 4 (30V; FRT, +E)	98,63% (290/4)	00,00%
Padi6 KO 5 (30V; FRT, +E)	98,97% (388/4)	00,00%
Padi6 KO 6 (30V; FRT, +E)	91,56% (304/28)	8,13% (27/332)
Padi6 KO 7 (30V; FRT, +E)	99,15% (468/4)	00,00%

Table S2: *Sanger sequencing results from embryos electroporated using the reversed repair template (RRT). The first twelve embryos were electroporated without enhancer (-E), the last thirteen with enhancer (+E). The Sanger results of the region around the wanted mutation (g.12426G>A) per embryo are compared with the reference sequence (Refseq.).*

Electroporated embryos	Sanger analysis
Padi6 KO 1 (30V; RRT; -E) (Blastocyst)	Refseq. -CCTTTCTAATGGTAAGGTGAC- Padi6 KO -CCTTTCTAWTGSYAAGGTGAC-
Padi6 KO 2 (30V; RRT; -E) (Blastocyst)	Refseq. -CCTTTCTAATGGTAAGGTGAC- Padi6 KO -CCTTTCTAATGGTAAGGTGAC-
Padi6 KO 3 (30V; RRT; -E) (Blastocyst)	Refseq. -CCTTTCTAATGGTAAGGTGAC- Padi6 KO -CCTTTCTAATGGTAAGGTGAC-
Padi6 KO 4 (30V; RRT; -E) (Blastocyst)	Refseq. -CCTTTCTAATGGTAAGGTGAC- Padi6 KO -CCTTTCTAATGGTAAGGTGAC-
Padi6 KO 5 (30V; RRT; -E) (Blastocyst)	Refseq. -CCTTTCTAATGGTAAGGTGAC- Padi6 KO -CCTTTCTAATGGTAAGGTGAC-
Padi6 KO 6 (30V; RRT; -E) (Morula)	Refseq. -CCTTTCTAATGGTAAGGTGAC- Padi6 KO -CCTTTCTAATGGTAAGGKGAC-
Padi6 KO 7 (30V; RRT; -E) (Morula)	Refseq. -CCTTTCTAATGGTAAGGTGAC- Padi6 KO -CCTTTCTAATGGTAAGGTGAC-
Padi6 KO 8 (30V; RRT; -E) (Morula)	Refseq. -CCTTTCTAATGGTAAGGTGAC- Padi6 KO -CCTTTCTAATGGTAAGGGGAC-
Padi6 KO 9 (30V; RRT; -E) (Morula)	Refseq. -CCTTTCTAATGGTAAGGTGAC- Padi6 KO -CCTTTCTAATGGTAAGGTGAC-
Padi6 KO 10 (30V; RRT; -E) (Morula)	Refseq. -CCTTTCTAATGGTAAGGTGAC- Padi6 KO -CCTTTYTAAKGGTAAGGKGAY-
Padi6 KO 11 (30V; RRT; -E) (Morula)	Refseq. -CCTTTCTAATGGTAAGGTGAC- Padi6 KO -CCTTTCTAATGGTAAGGTGAC-
Padi6 KO 12 (30V; RRT; -E) (Morula)	Refseq. -CCTTTCTAATGGTAAGGTGAC- Padi6 KO -CCTTTCTAATGGTAAGGTGAC-
Padi6 KO 1 (30V; RRT; +E) (Blastocyst)	Refseq. -CCTTTCTAATGGTAAGGTGAC- Padi6 KO -CCTTTCTAATGGTAAGGTGAC-
Padi6 KO 2 (30V; RRT; +E) (Blastocyst)	Refseq. -CCTTTCTAATGGTAAGGTGAC- Padi6 KO -CCTTTCTAATGGTAAGGTGAC-
Padi6 KO 3 (30V; RRT; +E) (Blastocyst)	Refseq. -CCTTTCTAATGGTAAGGTGAC- Padi6 KO -CCTTTCTAATGGTAAGGTGAC-
Padi6 KO 4 (30V; RRT; +E) (Blastocyst)	Refseq. -CCTTTCTAATGGTAAGGTGAC- Padi6 KO -CCTTTCTAATGGTAAGGTGAC-
Padi6 KO 5 (30V; RRT; +E) (Blastocyst)	Refseq. -CCTTTCTAATGGTAAGGTGAC- Padi6 KO -CCTTTYTAATGGTAAGGKGAC-
Padi6 KO 6 (30V; RRT; +E) (Morula)	Refseq. -CCTTTCTAATGGTAAGGTGAC- Padi6 KO -CCTTTCTAATGGTAAGGTGAC-
Padi6 KO 7 (30V; RRT; +E) (Morula)	Refseq. -CCTTTCTAATGGTAAGGTGAC- Padi6 KO -CCTTTCTAATGTTKGGAACTC-
Padi6 KO 8 (30V; RRT; +E) (Morula)	Refseq. -CCTTTCTAATGGTAAGGTGAC- Padi6 KO -CCTTTCTAATGGTAAGGKGAC-
Padi6 KO 9 (30V; RRT; +E) (Morula)	Refseq. -CCTTTCTAATGGTAAGGTGAC- Padi6 KO -CCTTTCTAATGGKAAGGKGAC-
Padi6 KO 10 (30V; RRT; +E) (Morula)	Refseq. -CCTTTCTAATGGTAAGGTGAC- Padi6 KO -CCTTTCTAATGGTAAGGTGAC-
Padi6 KO 11 (30V; RRT; +E) (Morula)	Refseq. -CCTTTCTAATGGTAAGGTGAC- Padi6 KO -CCTTTCTAATGGTAAGGTGAC-
Padi6 KO 12 (30V; RRT; +E) (Morula)	Refseq. -CCTTTCTAATGGTAAGGTGAC- Padi6 KO -CCTTTCTAATGGTAAGGTGAC-
Padi6 KO 13 (30V; RRT; +E) (Morula)	Refseq. -CCTTTCTAATGGTAAGGTGAC- Padi6 KO -CCTTTCTAWTGGWAAGGKGAY-

11.2. Supplementary Figures

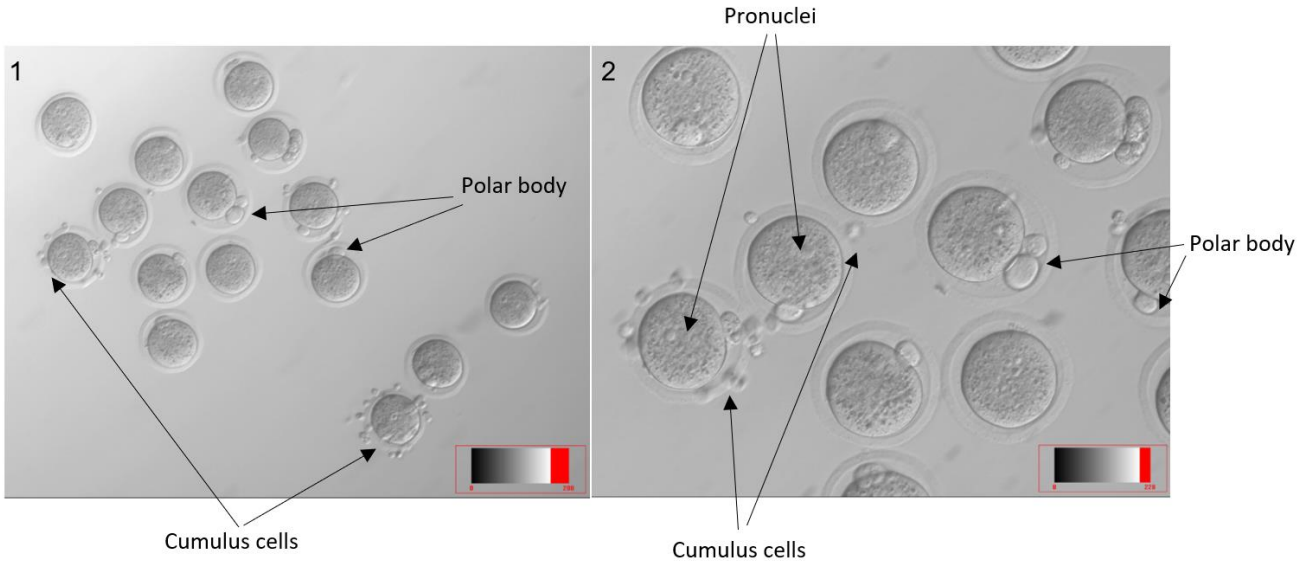

Figure S1: *Stereo microscopy pictures of WT embryos at E0 (one -cell) at an enlargement of (1) 10x (2) 20x. The presence of pronuclei and the disappearance of the conus distinguish the fertilized eggs from the unfertilized once.*

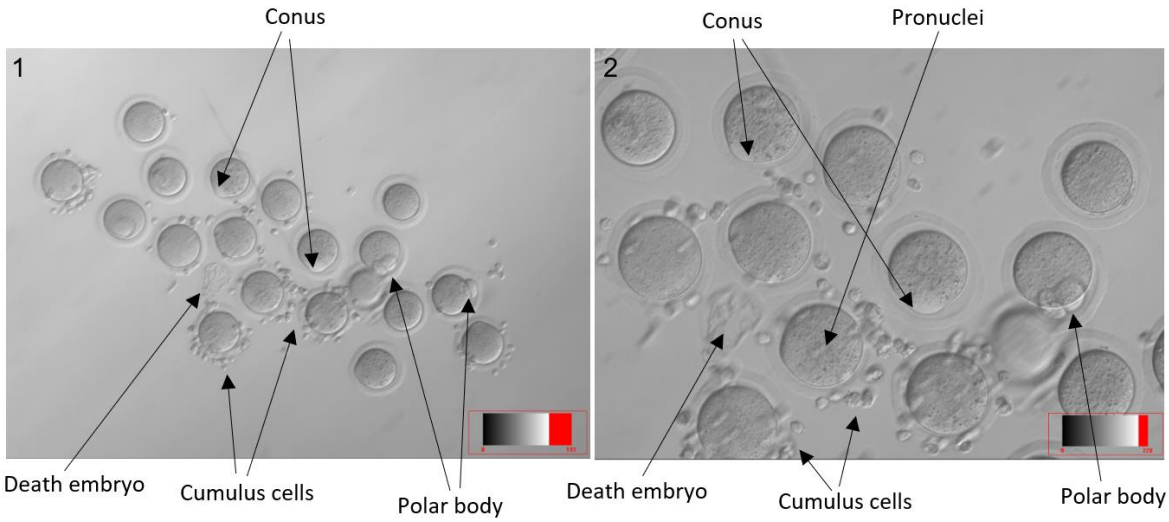

Figure S2: *Stereo microscopy pictures of Padi6 KO embryos at E0 (one -cell) at an enlargement of (1) 10x (2) 20x. The presence and of pronuclei and the disappearance of the conus distinguish the fertilized eggs from the unfertilized once.*

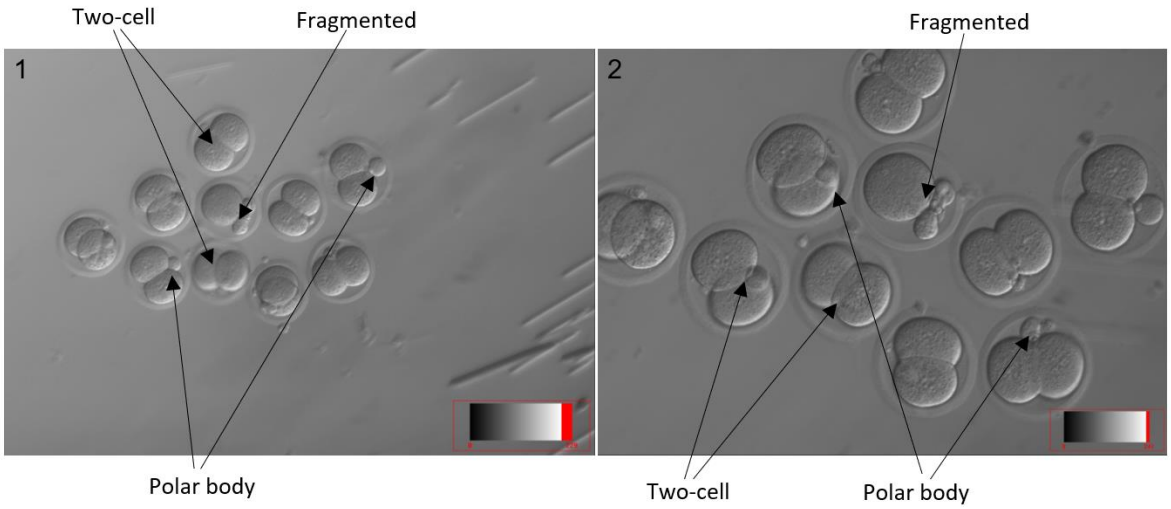

Figure S3: *Stereo microscopy pictures of WT embryos at E1 (two-cell) at an enlargement of (1) 10x (2) 20x.*

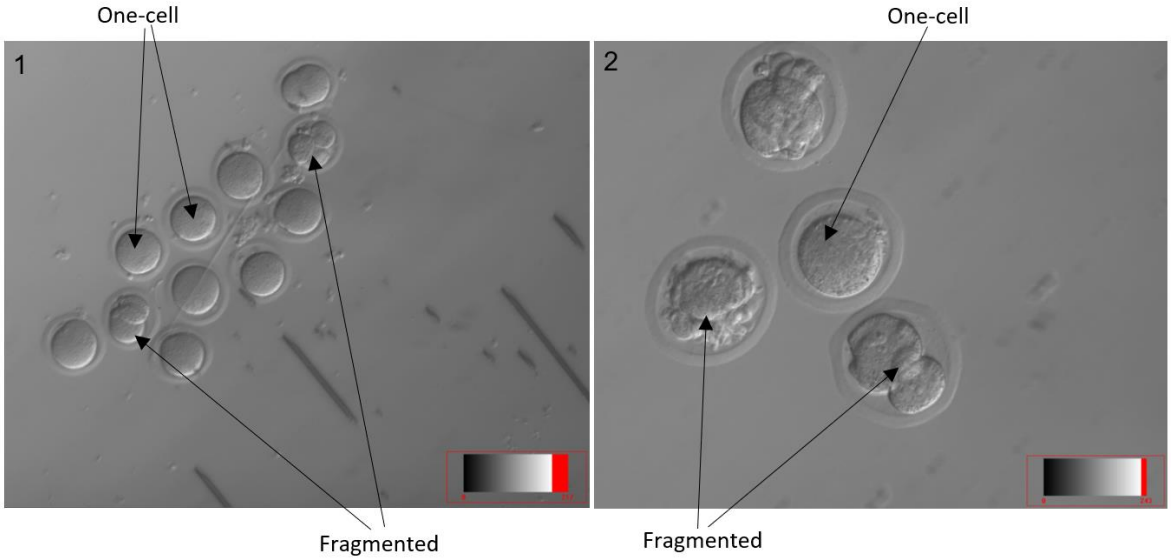

Figure S4: *Stereo microscopy pictures of Padi6 KO embryos at E1 (two-cell) at an enlargement of (1) 10x (2) 20x.*

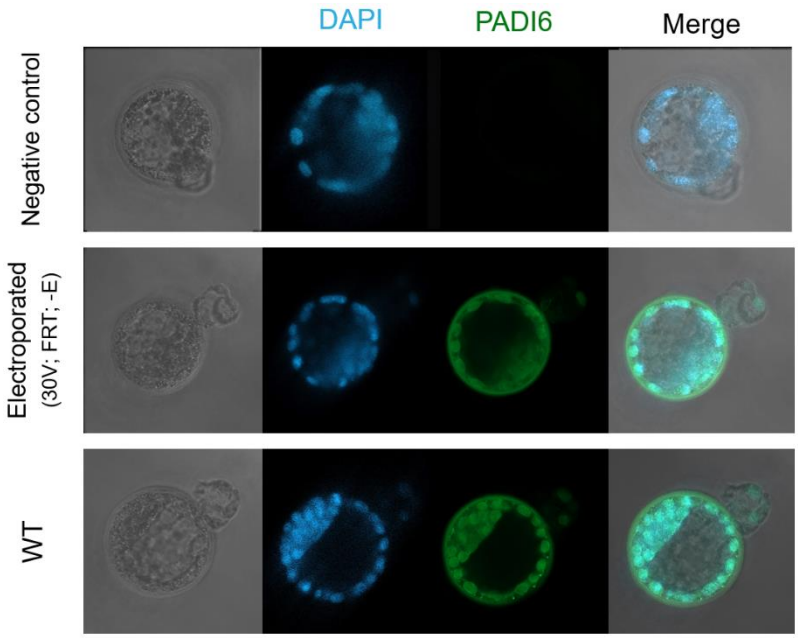

Figure S5: *Immunofluorescent staining (IF) image of PADI6 (green) expression in wild-type (WT), electroporated and negative control blastocysts.*

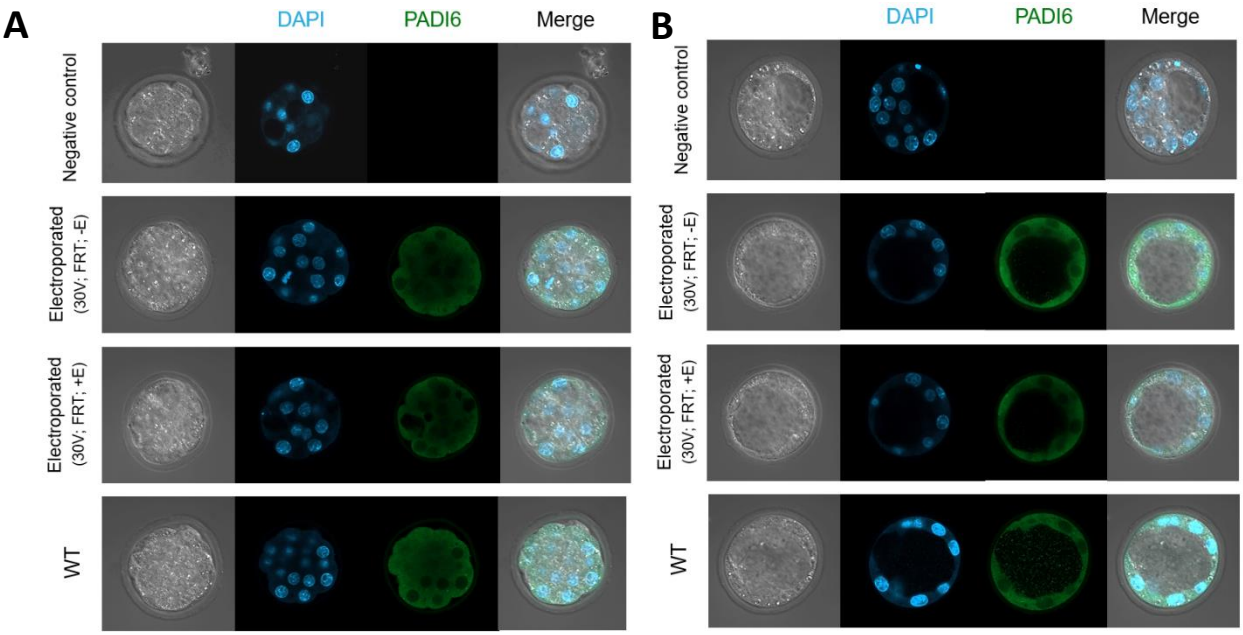

Figure S6: *IF image of* PADI6 *(green) expression in wild-type (WT), electroporated with and without enhancer and negative control (A) morulas and (B) blastocysts.*

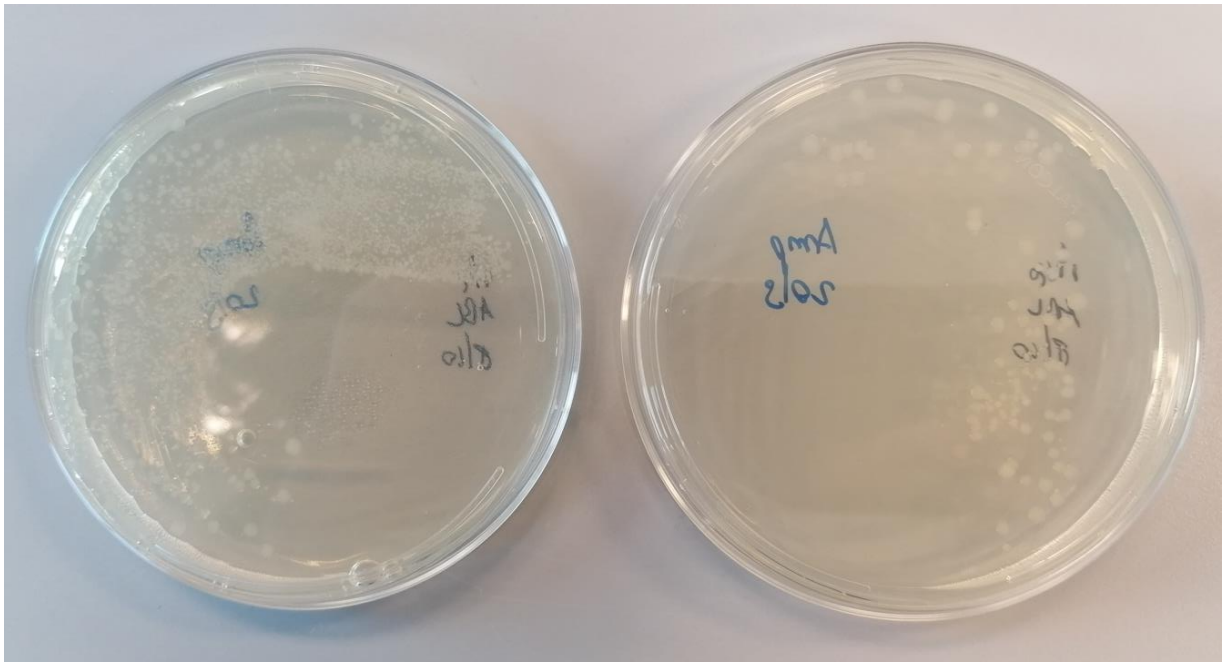

Figure S7: *Growth of the E.Coli bacteria which incorporated the plasmid containing the Padi6 cDNA and ampicillin (Amp) resistance gene on Amp positive agar plates.*

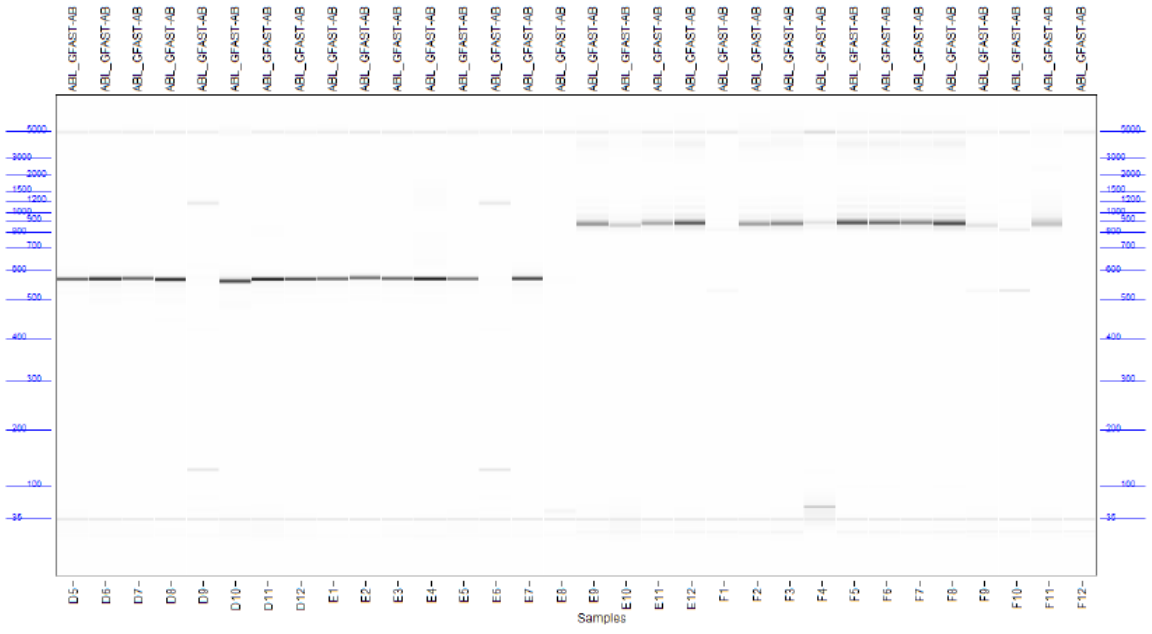

Figure S8: *Results of the fragment analyzation after colony-PCR of fifteen colonies grown on the Amp positive agar plates. D5-E7 consist the colony DNA of 15 colonies together with the primer couple used to check the first transition (F: TGTGTGGAATTGTGAGCGGA, R: TTCACAAGCAGGATGGCTCC), E9-F11 the colony DNA of the same 15 colonies together with the primer couple used to check the second transition (F: GGGAACGTGACCCTGTTTGA, R: TTGGGTAACGCCAGGGTTTT) and E8 and F12 containing a control sample.*

***Figure S9**: Sanger sequencing results of the colonies containing the wanted insert. In yellow the two unexpected mutations incorporated in the Padi6 cDNA causing change of amino acid (AA).*

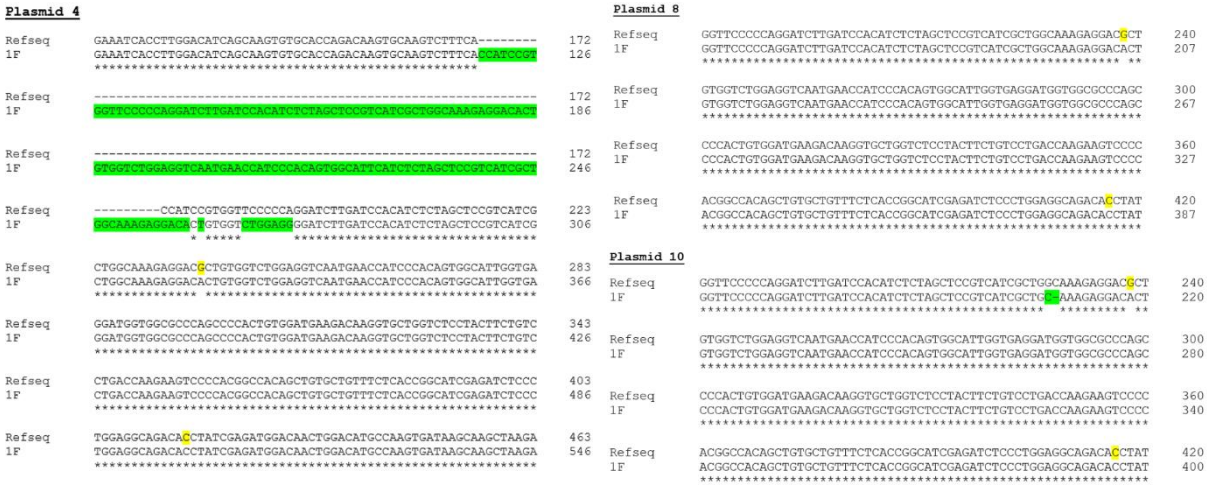

***Figure S10:** Sanger sequencing results of the colonies in which the first mutagenesis was successful. In yellow the mutations needed to be changed and in green new found mutations.*

Figure S11: *Sanger sequencing results of the colonies in which the second mutagenesis was successful. In yellow the mutations needed to be changed and in green new found mutations.*